AD-A196 686

UNCLASSIFIED

SECURITY CLASSIFICATION OF THIS PAGE (When Data Entered)

DTIC FILE COPY

(1)

REPORT DOCUMENTATION PAGE

READ INSTRUCTIONS BEFORE COMPLETING FORM

1. REPORT NUMBER: AFIT/CI/NR 88- 21
2. GOVT ACCESSION NO.:
3. RECIPIENT'S CATALOG NUMBER:

4. TITLE (and Subtitle): SYNOPTIC SCALE SENSITIVITY OF TIROS-N MOISTURE CHANNELS IN THE TROPICS
5. TYPE OF REPORT & PERIOD COVERED: MS THESIS
6. PERFORMING ORG. REPORT NUMBER:

7. AUTHOR(s): KEITH GORDON BLACKWELL
8. CONTRACT OR GRANT NUMBER(s):

9. PERFORMING ORGANIZATION NAME AND ADDRESS: AFIT STUDENT AT: TEXAS A&M UNIVERSITY
10. PROGRAM ELEMENT, PROJECT, TASK AREA & WORK UNIT NUMBERS:

11. CONTROLLING OFFICE NAME AND ADDRESS:
12. REPORT DATE: 1988
13. NUMBER OF PAGES: 124

14. MONITORING AGENCY NAME & ADDRESS (if different from Controlling Office): AFIT/NR, Wright-Patterson AFB OH 45433-6583
15. SECURITY CLASS. (of this report): UNCLASSIFIED
15a. DECLASSIFICATION/DOWNGRADING SCHEDULE:

16. DISTRIBUTION STATEMENT (of this Report): DISTRIBUTED UNLIMITED: APPROVED FOR PUBLIC RELEASE

DTIC ELECTE AUG 0 3 1988 S D H

17. DISTRIBUTION STATEMENT (of the abstract entered in Block 20, if different from Report): SAME AS REPORT

18. SUPPLEMENTARY NOTES: Approved for Public Release: IAW AFR 190-1
LYNN E. WOLAVER 12 JULY 88
Dean for Research and Professional Development
Air Force Institute of Technology
Wright-Patterson AFB OH 45433-6583

19. KEY WORDS (Continue on reverse side if necessary and identify by block number):

20. ABSTRACT (Continue on reverse side if necessary and identify by block number): ATTACHED

DD FORM 1 JAN 73 1473 EDITION OF 1 NOV 65 IS OBSOLETE

PII Redacted

UNCLASSIFIED

SECURITY CLASSIFICATION OF THIS PAGE (When Data Entered)

ABSTRACT

Synoptic Scale Sensitivity of TIROS-N Moisture Channels in the Tropics. (December 1987)

Keith Gordon Blackwell, B.S., University of Wisconsin-Madison

Co-Chairmen of Advisory Committee: Dr. James P. McGuirk
Dr. Aylmer H. Thompson

Water vapor radiance data obtained from a satellite-borne radiometer were evaluated for synoptic information content and accuracy over the tropical eastern Pacific Ocean.

An upper moist layer was defined in terms of precipitable water by integrating sounding data downward from 300 mb. The varying pressure of this upper moist layer was correlated with collocated 6.7 and 7.3 μm water vapor brightness temperatures (BT)s.

A persistent cluster of elevated BTs was observed over the subtropical Pacific adjacent to the western flank of a series of moisture bursts. Collocated rawinsonde soundings and satellite BTs consistently showed excellent agreement within this region, indicating extreme dryness in the middle and upper troposphere. The anomalous lack of upper tropospheric moisture, the tight clustering of abnormally large BTs, and the close proximity to a large area of active convection suggests these elevated BTs occur only as an occasional synoptically induced feature.

Vertical motions were estimated through the temporal change of the upper moist layer "topography". Although high correlations were

obtained between satellite BTs and upper moist layer pressures, minute quantities of upper tropospheric moisture above 300 mb produced large changes in BTs. The inability of conventional rawinsondes to measure moisture in the cold, tropical upper troposphere often leads to discrepancies between rawinsonde-derived and satellite-inferred moisture profiles. These discrepancies were quantified and shown to result in an unsatisfactory estimation of vertical motion computed from the local change in BTs.

Estimation of the influence of horizontal moisture advection on local BT changes resulted in maximum values of the same order of magnitude as the maximum observed BT changes. However, comparisons of these magnitudes at individual grid points showed little similarity. Thus, vertical motion estimates had the potential to be strongly modulated by horizontal advection. However, the consistently weak correlations at individual grid points indicated uncertainty as to whether changes in channel 11 and 12 BTs were influenced more by horizontal rather than vertical advection of moisture.

COPY INSPECTED 6

Accession For
NTIS GRA&I
DTIC TAB
Unannounced
Justification
By
Distribution/
Availability Codes
Avail and/or
Dist Special
A-1

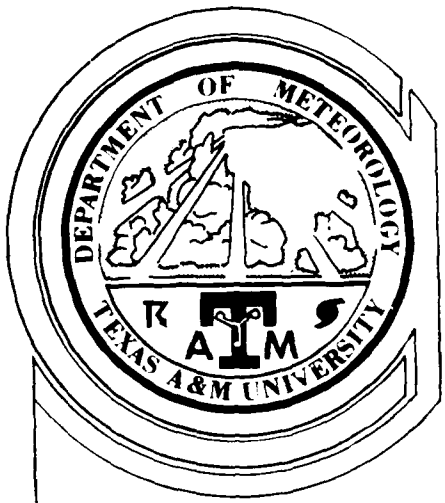

TEXAS A&M UNIVERSITY

DEPARTMENT OF METEOROLOGY

SYNOPTIC SCALE SENSITIVITY OF TIROS-N MOISTURE CHANNELS IN THE TROPICS

A Thesis

by

KEITH GORDON BLACKWELL

Submitted to the Graduate College of
Texas A&M University
in partial fulfillment of the requirements for the degree of

MASTER OF SCIENCE

December 1987

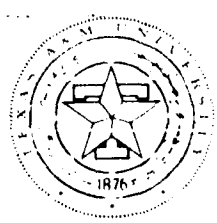

SYNOPTIC SCALE SENSITIVITY OF TIROS-N MOISTURE CHANNELS IN THE TROPICS

A Thesis

by

KEITH GORDON BLACKWELL

Submitted to the Graduate College of
Texas A&M University
in partial fulfillment of the requirements for the degree of

MASTER OF SCIENCE

December 1987

Major Subject: Meteorology

SYNOPTIC SCALE SENSITIVITY OF TIROS-N MOISTURE CHANNELS IN THE TROPICS

A Thesis

by

KEITH GORDON BLACKWELL

Approved as to style and content by:

James P. McGuirk
(Co-Chairman)

Aylmer H. Thompson
(Co-Chairman)

Rudolf J. Freund
(Member)

James R. Scoggins
(Head of Department)

December 1987

ABSTRACT

Synoptic Scale Sensitivity of TIROS-N Moisture Channels in the Tropics. (December 1987)

Keith Gordon Blackwell, B.S., University of Wisconsin-Madison

Co-Chairmen of Advisory Committee: Dr. James P. McGuirk
Dr. Aylmer H. Thompson

Water vapor radiance data obtained from a satellite-borne radiometer were evaluated for synoptic information content and accuracy over the tropical eastern Pacific Ocean.

An upper moist layer was defined in terms of precipitable water by integrating sounding data downward from 300 mb. The varying pressure of this upper moist layer was correlated with collocated 6.7 and 7.3 μm water vapor brightness temperatures (BT)s.

A persistent cluster of elevated BTs was observed over the subtropical Pacific adjacent to the western flank of a series of moisture bursts. Collocated rawinsonde soundings and satellite BTs consistently showed excellent agreement within this region, indicating extreme dryness in the middle and upper troposphere. The anomalous lack of upper tropospheric moisture, the tight clustering of abnormally large BTs, and the close proximity to a large area of active convection suggests these elevated BTs occur only as an occasional synoptically induced feature.

Vertical motions were estimated through the temporal change of the upper moist layer "topography". Although high correlations were

obtained between satellite BTs and upper moist layer pressures, minute quantities of upper tropospheric moisture above 300 mb produced large changes in BTs. The inability of conventional rawinsondes to measure moisture in the cold, tropical upper troposphere often leads to discrepancies between rawinsonde-derived and satellite-inferred moisture profiles. These discrepancies were quantified and shown to result in an unsatisfactory estimation of vertical motion computed from the local change in BTs.

Estimation of the influence of horizontal moisture advection on local BT changes resulted in maximum values of the same order of magnitude as the maximum observed BT changes. However, comparisons of these magnitudes at individual grid points showed little similarity. Thus, vertical motion estimates had the potential to be strongly modulated by horizontal advection. However, the consistently weak correlations at individual grid points indicated uncertainty as to whether changes in channel 11 and 12 BTs were influenced more by horizontal rather than vertical advection of moisture.

DEDICATION

I dedicate this thesis to my wife Mary Ann for her endless patience and understanding over the past two years. She weathered my many ups and downs and spent countless, long evenings and weekends alone. This work could not have been accomplished without her support. I am truly grateful.

I also dedicate this thesis to my parents, Gordon and Elise, for their consistent support of my varied meteorological endeavors throughout the years.

ACKNOWLEDGEMENTS

I acknowledge my committee for their excellent support and guidance in my research. I thank Dr. James P. McGuirk for sharing his broad, professional expertise and for his help in re-directing the emphasis of this research. I would also like to thank Dr. Aylmer H. Thompson for his help in clarifying many important points in this research. I sincerely appreciate their attention and patience.

Special appreciation is given to Rob Liles, Bryan Batson, Donna Woolley, Nicole Streetman, and especially Eddie Rieger for their assistance.

Finally, I thank the United States Air Force, Air Force Institute of Technology for allowing the opportunity to obtain my M.S. in Meteorology.

This research was sponsored by the Marshall Space Flight Center, National Aeronautics and Space Administration through Contract NAS8-37284.

TABLE OF CONTENTS

CHAPTER		Page
I	INTRODUCTION	1
II	BACKGROUND	4
	A. Measurement Capability	4
	B. Upper Tropospheric Moisture Distribution	6
III	DATA	10
IV	OBSERVED BRIGHTNESS TEMPERATURE SIGNATURES	11
	A. Influence of Surface Contamination on Brightness Temperatures	11
	B. Brightness Temperature Frequency Distribution	14
	C. High Brightness Temperature Regions	18
V	BRIGHTNESS TEMPERATURE/RAWINSONDE RELATIONSHIP	25
	A. Rawinsondes	25
	B. Brightness Temperature Interpolation	27
	C. Brightness Temperature/Sounding Correlation	29
VI	ESTIMATING TROPICAL SYNOPTIC VERTICAL MOTIONS	37
	A. Regression	38
	B. Satellite-Derived Vertical Motion Estimates	40
	C. Verification of Vertical Motion Estimates	46
	1. Adiabatic Method	46
	2. Outgoing Longwave Radiation Signatures	50
	3. Velocity Potential Fields	66
	D. Effect of Horizontal Moisture Advection	70
VII	MOISTURE SAMPLING ERRORS	77
	A. Comparisons of PWTP, BT and Sounding Profiles	77
	B. Calculated versus Observed BTs	95
VIII	SUMMARY AND DISCUSSION	114
REFERENCES		119

TABLE OF CONTENTS (Continued)

Page

VITA 124

LIST OF TABLES

TABLE Page

1 Number of rawinsonde soundings within specified distance and ±6 h of *one* or more satellite brightness temperature(s) for 21-29 January 1979. 29

2 Number of rawinsonde soundings within specified distance of *two* or more satellite brightness temperatures for 21-29 January 1979. 30

3 Channel 12 and channel 11 maximum correlation coefficicients (r) and corresponding PW for 100 km radius increments for 21-29 January 1979. 33

4 Comparison of vertical motion estimates produced by channel 11 (CH11) and channel 12 (CH12) water vapor brightness temperatures and estimates produced from soundings by the adiabatic method (Petterssen, 1956) for the 600-mb (AD600) and 400-mb (AD400) pressure levels. 49

LIST OF FIGURES

FIGURE		Page
1	TOVS weighting functions (normalized) for channel 11 (7.3 μm) and channel 12 (6.7μm).	13
2	Channel 12 brightness temperature (BT) frequency distribution.	15
3	As in Fig. 2 except for channel 11.	17
4a	Geographical distribution of channel 12 brightness temperatures higher than -15°C for 24 January 1979. . . .	19
4b	Unenhanced window channel GOES West satellite image for 0615 UTC 24 January 1979.	20
5	Johnston Island sounding for 0000 UTC 23 January 1979. . .	23
6	As in Fig. 5, except Matamoros sounding for 2100 UTC 26 January 1979 at 7°N/91°W.	24
7	Map of land- and ship-launched rawinsonde locations. . . .	28
8	Example of procedure used to calculate precipitable water thickness pressure (PWTP) for the upper 5 mm of precipitable water (PW).	31
9	Channel 12 correlation coefficients between BT and PWTP (pressure) for each 0.1 mm level in the upper 5 mm layer of PW.	35
10	As in Fig. 9 except for channel 11.	36
11	Scatter plot of 0.6 mm PWTPs versus channel 12 BTs overlain by the best fit linear (solid) and polynomial (dashed) regression curves.	39
12	As in Fig. 11 except for 0.9 mm PWTPs versus channel 11 BTs.	41
13a	Twelve-hour vertical velocity estimates (cm s^{-1}) from channel 12 BTs for the period ending 0000 UTC 23 January 1979.	44
13b	As in Fig. 13a except for channel 11.	45
14a	OLR radiances from 0000 UTC 22 January 1979 overlying channel 12 vertical motion estimates (cm s^{-1}) for the 12-h period ending 1200 UTC 22 January 1979.	52

LIST OF FIGURES (Continued)

FIGURE		Page
14b	As in Fig. 14a except for OLR radiances from 1200 UTC 22 January 1979.	53
14c	As in Fig. 14a except for channel 11 vertical motion estimates.	54
14d	As in Fig. 14b except for channel 11 vertical motion estimates.	55
15a	OLR radiances from 0000 UTC 26 January 1979 overlying channel 12 vertical motion estimates (cm s^{-1}) for the 12-h period ending 1200 UTC 26 January 1979.	57
15b	As in Fig. 15a except for OLR radiances from 1200 UTC 26 January 1979.	58
15c	As in Fig. 15a except for channel 11 vertical motion estimates.	59
15d	As in Fig. 15b except for channel 11 vertical motion estimates.	60
16a	OLR radiances from 0000 UTC 28 January 1979 overlying channel 12 vertical motion estimates (cm s^{-1}) for the 12-h period ending 1200 UTC 28 January 1979.	61
16b	As in Fig. 16a except for OLR radiances from 1200 UTC 28 January 1979.	62
16c	As in Fig. 16a except for channel 11 vertical motion estimates.	63
16d	As in Fig. 16b except for channel 11 vertical motion estimates.	64
17a	Channel 12 vertical motion estimates (cm s^{-1}) for the 12-h period ending 0000 UTC 22 January 1979.	68
17b	As in Fig. 17a except for channel 11.	69
18a	Channel 12 twelve-hour values (cm s^{-1}) representing the effect of horizontal moisture advection by 400-500 mb layer-averaged winds for data sampled at 0000 UTC 28 January 1979.	72
18b	As in Fig. 18a except for 500-700 mb layer averaged winds.	73
19a	As in Fig. 18a except for channel 11.	75

LIST OF FIGURES (Continued)

FIGURE		Page
19b	As in Fig. 18b except for channel 11.	76
20a	As in Fig. 11 except for use of letter-plots and omission of regression curves.	78
20b	As in Fig. 20a except for channel 11 and 0.9 mm PWTP. . .	79
21a	Scatter plot of 0.6 mm PWTPs versus channel 12 BTs for Johnston Island (B=91275).	81
21b	As in Fig. 21a except for 0.9 mm PWTPs versus channel 11 BTs.	82
22	As in Fig. 5 except for 1200 UTC 28 January 1979.	84
23a	As in Fig. 21a except for Lihue, Hawaii (D=91165).	86
23b	As in Fig. 21b except for Lihue, Hawaii (D=91165).	87
24a	As in Fig. 21a except for Veracruz, Mexico (S=76692). . .	88
24b	As in Fig. 21b except for Veracruz, Mexico (S=76692). . .	89
25a	As in Fig. 21a except for the ship Matamoros (J=MATAM). .	90
25b	As in Fig. 21b except for the ship Matamoros (J=MATAM). .	91
26	As in Fig. 6 except for 2100 UTC 29 January 1979 at 16°N/95°W.	92
27	RTM channel 12 weighting function profiles for the Johnston Island soundings at 0000 UTC 23 January 1979 (a) and 1200 UTC 28 January 1979 (b).	97
28	As in Fig. 27 except for channel 11.	99
29	Same as Fig. 27 except for Lihue, Hawaii at 0000 UTC 22 January 1979 (a) and 1200 UTC 24 January 1979 (b).	100
30	As in Fig. 5 except for Lihue, Hawaii for 0000 UTC 22 January 1979 (a) and 1200 UTC 24 January 1979 (b).	101
31	As in Fig. 29 except for channel 11.	102
32	RTM channel 12 weighting function profiles for the Matamoros ship sounding at 2100 UTC 26 January 1979. . . .	105
33	As in Fig. 32 except for channel 11.	106

LIST OF FIGURES (Continued)

FIGURE		Page
34	As in Fig. 5 except for Pariz ship for 2100 UTC 26 January 1979 at 1°N/150°W.	108
35	As in Fig. 32 except for the Pariz ship sounding.	109
36	As in Fig. 33 except for the Pariz ship sounding.	110
37	As in Fig. 20a except for overlaid observed-BT/RTM-BT difference contours.	111
38	As in Fig. 20b except for overlaid observed-BT/RTM-BT difference contours.	112

CHAPTER I

INTRODUCTION

Accurate evaluation of the spatial and temporal distribution of atmospheric water vapor (WV) remains a problem over data-sparse areas. Rawinsonde measurements are by far the most reliable (Timchalk, 1986); yet rawinsonde information is virtually non-existent over oceanic areas.

Similarly, the eastern tropical Pacific Ocean is plagued by a great scarcity of data; however, this data limitation became less of a problem during the Global Atmospheric Research Program's (GARP) First GARP Global Experiment (FGGE) in 1979. FGGE's Special Observing Period 1 (SOP 1) provided an increase of meteorological observational data including additional land/ship launched rawinsonde reports and satellite-measured radiances.

Of the various wave bands sensed by the satellite-borne radiometers, the 6.7 μm and 7.3 μm wavelengths are very close and moderately close, respectively, to the wavelength which experiences the maximum absorption by WV in the troposphere. Therefore, 6.7 μm radiances are highly moisture sensitive, whereas the 7.3 μm band is moderately sensitive to moisture content of the troposphere. As a result of this sensitivity, these two wavelengths are used widely to detect variations of atmospheric moisture in time and space.

The style is that of the *Monthly Weather Review*.

Using NOAA satellite imagery of 6.7 μm and 7.3 μm WV channels, Weldon and Holmes[1] stated four common generalizations as to what might be interpreted. These generalizations, in part, consist of:

1. the humidity at a specific pressure level in the atmosphere;
2. the amount of moisture contained in a vertical atmospheric column;
3. a topography of the height of the significant moisture in the atmosphere; and
4. the relative humidity of the atmosphere.

They further state that although some of these generalizations have merit, none of them is totally correct. However, they indicate that the height topography is the most accurate generalization.

The objective of this research is to evaluate the accuracy and synoptic information content of quantitative WV radiance data in the tropics. The specific area of interest for this study is located over the tropical eastern Pacific Ocean. The area is bounded by latitudes 10°S and 30°N and longitudes 90°W and 180°. The period of study is 21-29 January, 1979. Special attention is focused on the relationship between the moisture-sensitive radiances (6.7 μm and 7.3 μm channels) and the changes in the topography of the moist layer as measured by conventional "ground truth" rawinsondes.

---

[1] From a manuscript titled: "Characteristics of Water Vapor Imagery." Manuscript available from NOAA/NESDIS, Washington, D.C. 20233.

This objective is accomplished through several steps.

1. Prepare maps of the temporal and spatial distribution of brightness temperatures (BTs) from each channel.
2. Establish a relationship between the TIROS N WV BTs and the altitude of the WV upper boundary by following a procedure similar to the one used by Stout et al. (1984).
3. Estimate vertical motions from temporal changes in BTs.
4. Evaluate these estimates using results obtained from other types of vertical motion estimation procedures.
5. Estimate the effects of horizontal moisture advection on BT changes.
6. Analyze moisture sampling discrepancies between rawinsonde and satellite.

CHAPTER II

BACKGROUND

A. Measurement Capability

The first WV remote sensing channels were aboard the early TIROS satellites launched in the 1960's. Due to their large areal scanning capability, satellites detect extensive horizontal variations in atmospheric moisture; however, vertical variations are not so obvious.

Several studies have focused on the vertical resolution of moisture sensitive satellite channels, especially the 6.7 μm band. Chesters et al. (1982) described 6.7 μm channel radiances as originating from only the top few millimeters of total precipitable water (PW) in an atmospheric column. Stout et al. (1984) indicated a strong relationship between 6.7 μm radiance and this top few millimeters of PW which they referred to as "the upper boundary of atmospheric water vapor." They stated that the intensity of the 6.7 μm radiation is determined to a large degree by the weighted mean temperature through this upper boundary layer. The variability of atmospheric temperature in the tropics is subtle (Smith, 1983) and actual tropical soundings deviate only slightly from the mean. Therefore, the weighted-mean temperature can be assigned to a unique pressure level derived from the mean tropical sounding. This level is called the pressure level of the WV upper boundary. Stout et al. (1984) acknowledged that radiosondes measure low amounts of moisture poorly and that the actual thickness of the layer is not known;

however, a calculation by Chesters et al. (1982) from globally distributed soundings indicates 80% of the weighting of the 6.7 μm channel occurs in a layer 300-400 mb thick centered usually near 430 mb. This concentration of signal allows the 6.7 μm satellite radiances to be used in the construction of "topographic" maps delineating the pressure of the WV effective upper boundary. In general, Weldon and Holmes emphasized that radiation reaching the satellite from WV does not arrive from a single surface or level, but from some layer of finite depth. For most practical purposes, WV is nearly opaque to 6.7 μm radiation only when the vapor is highly concentrated in nearly saturated warm air where the PW content is high. But in nearly saturated, cold, upper tropospheric air, WV is nearly transparent to the same radiation because of the air's extremely low PW content.

Stewart et al. (1985) found that, "...the radiance sensed by the 6.7 μm channel corresponds to a layer-average 'Planck' radiance emerging from a portion of the atmosphere whose location is determined by two factors: 1) the profile of the emissivity of the radiating water vapor; and 2) the profile of the transmissivity of the entire depth of water vapor above each radiating level." The emissivity profile varies with the vertical structure of the WV mixing ratio, while the transmissivity profile varies with the vertical structure of the integrated precipitable water. Therefore, radiation measured from space is representative primarily of the uppermost moist region (high emissivity) with dry air (high transmissivity) above. According to Planck's Law, the magnitude of

the radiance observed is proportional to the mean temperature of the atmosphere as weighted by the product of the emissivity and transmissivity profile (the temperature-profile weighting function). In addition, Stewart et al. state, "Since the mid to upper tropospheric region contributing to the 6.7 μm radiance usually exhibits a constant lapse rate in temperature, the brightness temperature observed is generally close to the atmospheric temperature at the pressure level where the weighting function (and moisture as seen from above) is a maximum." In a comparison of GOES-5 brightness temperatures to rawinsonde temperatures, Stewart et al. found a correspondence which justifies assigning the pressure altitude of the WV wind vector as the pressure where the observed BT matches the environmental air temperature. On the other hand, Weldon and Holmes observe a lack of correspondence between WV BTs and the temperature within moist layers.

In summary, most of the above research indicates a potential relationship between the variation in the height of mid- or upper-tropospheric moist layers and the changes observed in WV BTs.

B. Upper Tropospheric Moisture Distribution

Remsberg et al. (1984), using the 6.9 μm LIMS experiment on Nimbus 7, found that a pronounced WV minimum exists just above the tropopause in the lower tropical stratosphere, while values increase toward both poles. This minimum corresponds to approximately the 100 mb level.

Ramond et al. (1981) showed that the 6.3 μm radiance signature of the polar jet stream differs significantly from that of the subtropical jet. The band of maximum radiance associated with the former delineates the tropopause break; however, maximum radiances associated with the subtropical jet are indicative of maximum amplitudes in tropospheric subsiding motions. These results are relevant for estimating vertical velocities in the upper troposphere through the analysis of consecutive WV images from satellites. Ramond et al. also found a relationship between the WV radiance field and the temperature on a WV isosteric surface. He asserted that this relationship, associated with an isentropic hypothesis, may allow development of a method for retrieving mean vertical velocities in the upper troposphere away from the vicinity of polar frontal zones.

Poc et al. (1980), using 6.3 μm *METEOSAT* imagery over western Europe and the Mediterranean Sea, concluded that it is possible to infer a quantitative correlation between the radiance and the WV mass above a given pressure level. This level appeared to be as low as 600 mb. Roulleau (1978) conducted an analysis of Nimbus-5 THIR 6-7 μm observations over the Mediterranean Sea. In this analysis he showed the possibility of using imagery features over wet or dry regions as dynamical tracers in clear sky conditions. Rodgers et al. (1976) used Nimbus-4 THIR 6.7 μm observations to produce 500 mb humidity patterns deduced from conventional WV data. By assuming that the WV is conserved within an atmospheric volume, they compared the 6.7 μm radiances to the outputs of a 10-level diagnostic model and confirmed quantitatively that these radiances are indicative of

three-dimensional advection processes in cloud-free areas. Therefore, WV imagery may be used as a tracer to delineate tropospheric dynamics. They also found that subsidence may be inferred in the upper and/or middle troposphere in areas of weak horizontal dry air advection when the corresponding BTs increase. Steranka et al. (1973), using the same kind of data, suggested that the WV imagery could be used to derive dynamic features over data-sparse regions in cloudless areas. Relationships between high WV BTs and middle/upper tropospheric subsidence also have been suggested in several other studies. Parmenter (1972) analyzed 6.7 μm radiances from Nimbus-4 over the western United States. Similarly, Shenk and Rodgers (1978) studied 6.7 μm radiances associated with Hurricane Camille. Both studies found a relationship between high BTs and deep tropospheric subsidence. Stewart et al. (1985) found that bright white represents clouds in GOES 6.7 μm VAS imagery and gray features are areas of high WV concentration; however, dark regions indicate dryness associated with mid-level subsidence.

Stewart and Fuelberg (1986) used GOES 6.7 μm imagery over the south central United States and compared this imagery to radiosonde-derived data. They concluded that the subsidence associated with the jet stream trough/ridge pattern is a likely cause for the dry region constituting the dark, warm image streak. They observed that middle tropospheric vertical motions showed ascent over the area southeast of the jet axis that agreed with the precipitation and cloudiness observed. In contrast, northwest of the jet axis there was widespread subsidence corresponding with the developing dry image

pattern. Thus, the area of strongest subsidence corresponds to the warmest and driest region on the 6.7 μm image. They also discovered that changes in tne lower-tropospheric (surface-to-800 mb) layer had little effect on 6.7 μm BTs.

Petersen et al. (1984) describe the 6.7 μm band as directly monitoring WV in the middle and upper troposphere. They claimed that although the weighting function for the 6.7 μm channel peaks near 400 mb, this level at which the weighting function peaks can shift significantly downward, as far as the 700-mb level, if dryness extends through a large portion of the middle and upper troposphere.

Briefly summarizing, several studies associate high BT values with deep subsidence in the middle and/or upper troposphere. Thus, WV imagery may be used to infer mid-tropospheric vertical motions.

CHAPTER III

DATA

The data from FGGE SOP 1 consist of traditional observations, satellite information, and computer-generated analyses based on these data. The actual observations for FGGE SOP 1 are labelled FGGE IIb. The data set includes aircraft dropsondes, ship- and surface-launched rawinsondes, and satellite-derived BTs. The BTs used in this investigation were the moisture-sensitive channel 11 and 12 infrared (IR) radiances from the TIROS N polar orbiting satellite.

The computer-derived analyses from the European Centre for Medium Range Weather Forecasts (ECMWF) are labeled FGGE IIIb. They include pressure surface wind fields which are available on a 1 7/8° by 1 7/8° gridded field. For this study, the field was modified to a 3 3/4° by 3 3/4° gridded field of zonal (u) and meridional (v) components for 21-29 January 1979.

In addition to the FGGE data sets, infrared satellite imagery was used. This imagery was obtained from the Western Geostationary Operational Environmental Satellite (GOES West), located above the equator near 130°W.

Dropsondes were not used because of their inaccuracy in measuring mid-tropospheric moisture (Velden et al., 1984). Data from dropsondes were examined within the area of interest for this study. It was determined by inspection that errors existed similar to those found by Velden, et al.

CHAPTER IV

OBSERVED BRIGHTNESS TEMPERATURE SIGNATURES

A. Influence of Surface Contamination on Brightness Temperatures

The majority of satellite BTs available within the analysis area over the 9-day period of study were located over the ocean; however, a significant number also were located over the southwest United States, Mexico and Central America. Several of these continental locations were situated within areas of high terrain.

Using the U.S. Standard Atmosphere temperature and moisture profile, Smith et al., (1979) produced weighting function curves for 6.7 μm (channel 12) and 7.3 μm (channel 11) radiances (Fig. 1). Similar to Smith et al., Weldon and Holmes acknowledged that satellites sense 7.3 μm radiation at lower atmospheric levels than 6.7 μm radiation. In a test to determine the basic factors which influence moisture-sensitive radiation measurements, Weldon and Holmes compared the 6.7 μm and 7.3 μm weighting curves produced from a sounding characterized by a constant dew point depression of 10°C and a temperature profile matching the U.S. Standard Atmosphere. Using this sounding, they found only 2% of the total 6.7 μm radiation reached the satellite from below 700 mb; however, approximately 50% of the 7.3 μm radiation sensed by satellite was emitted from below 700 mb, with a 7% contribution from the Earth's surface. Thus, if the terrain is significantly elevated, not only may 7.3 μm measurements be influenced erroneously, but 6.7 μm BTs also may be contaminated, especially in drier tropospheric conditions. Thus,

over land, differences in terrain may affect the satellite radiances, especially 7.3 μm imagery.

To check for adverse terrain influences on the moisture channel BTs, all the BTs for each channel which were located within a region between 16°N and 30°N latitude and 90°W and 130°W longitude were divided into two groups. The first group, labelled "continental", contained 145 BTs from each channel, whereas the second "oceanic" group contained 180 BTs from each channel. This region from which the two groups were chosen was under the influence of the same synoptic weather system through most of the period. Thus, mid and upper tropospheric conditions throughout this region were assumed to be similar. The calculated means for channel 11 continental and oceanic BTs were -12.28°C and -12.31°C, respectively, and the means for channel 12 BTs were -27.37°C over land and -27.73°C over ocean.

Two statistical tests, the parametric T-Test and the nonparametric Wilcoxon Rank Sum Test, were performed on these groups of data. Both tests detected no significant difference in BT means between ocean and land in either channel; therefore, high terrain was not significantly influencing the BTs over Mexico and the southwest United States. This conclusion was anticipated because both IR satellite imagery and rawinsondes indicated an extensive layer of mid- and upper-tropospheric moisture associated with an active synoptic cloud system (Schaefer, 1985) blanketing this region. This thick layer of moisture in clouds either prevented acquisition of BTs in this area or significantly reduced the impact of surface radiation on the observed BTs. For drier conditions, topography may be a

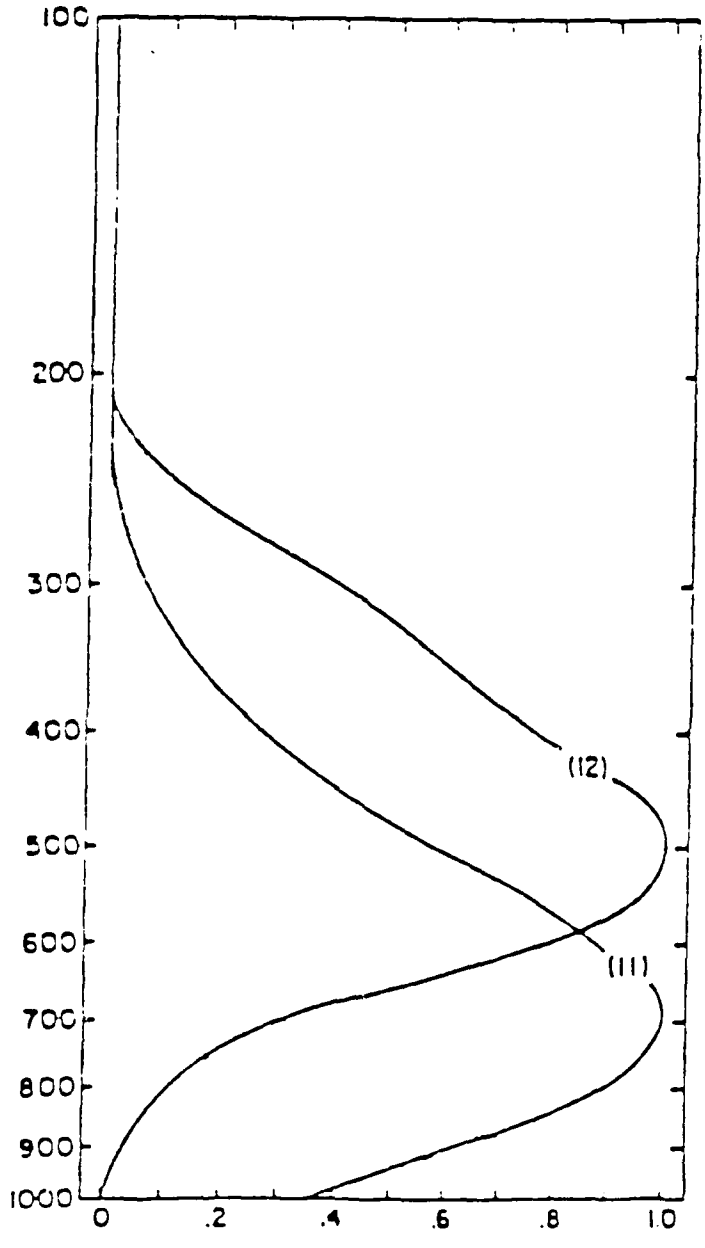

Figure 1. TOVS weighting functions (normalized) for channel 11 (7.3 μm) and channel 12 (6.7 μm). After Smith et al. (1979).

problem in this region.

B. Brightness Temperature Frequency Distribution

A distribution of frequency of occurrence of channel 12 BTs as a function of observed temperatures is shown in Fig. 2. Constructed from 3330 TIROS N 6.7 μm BTs recorded during the 9-day period from 21-29 January 1979 over the eastern Pacific, this distribution shows a skewed pattern in the direction of larger BTs. This pattern suggests a bimodal distribution in frequency of occurrence of BTs. Most BTs approximate a normal distribution about a mode of -27°C; a smaller group of higher BTs is clustered around -12.5°C.

To test for a non-normal pattern, with potential of bimodality, the calculated skewness of the channel 12 BT distribution was compared against the expected standard deviation of skewness computed from a sample normal distribution. The skewness for the BT distribution was nearly 10 times larger than the expected standard deviation of the skewness for a typical sample of this size taken from a true normal distribution; thus, this large skewness suggests the channel 12 BTs were not normally distributed. Although a bimodal distribution is highly skewed, one could not unequivocally conclude that this BT distribution had a bimodal character. However, this skewed distribution subjectively suggests that the pattern probably was bimodal in nature.

The majority of the BTs in the frequency distribution were lower than -15°C. Although these lower BTs are distributed nearly normally, there was a very broad peak frequency of occurrence between

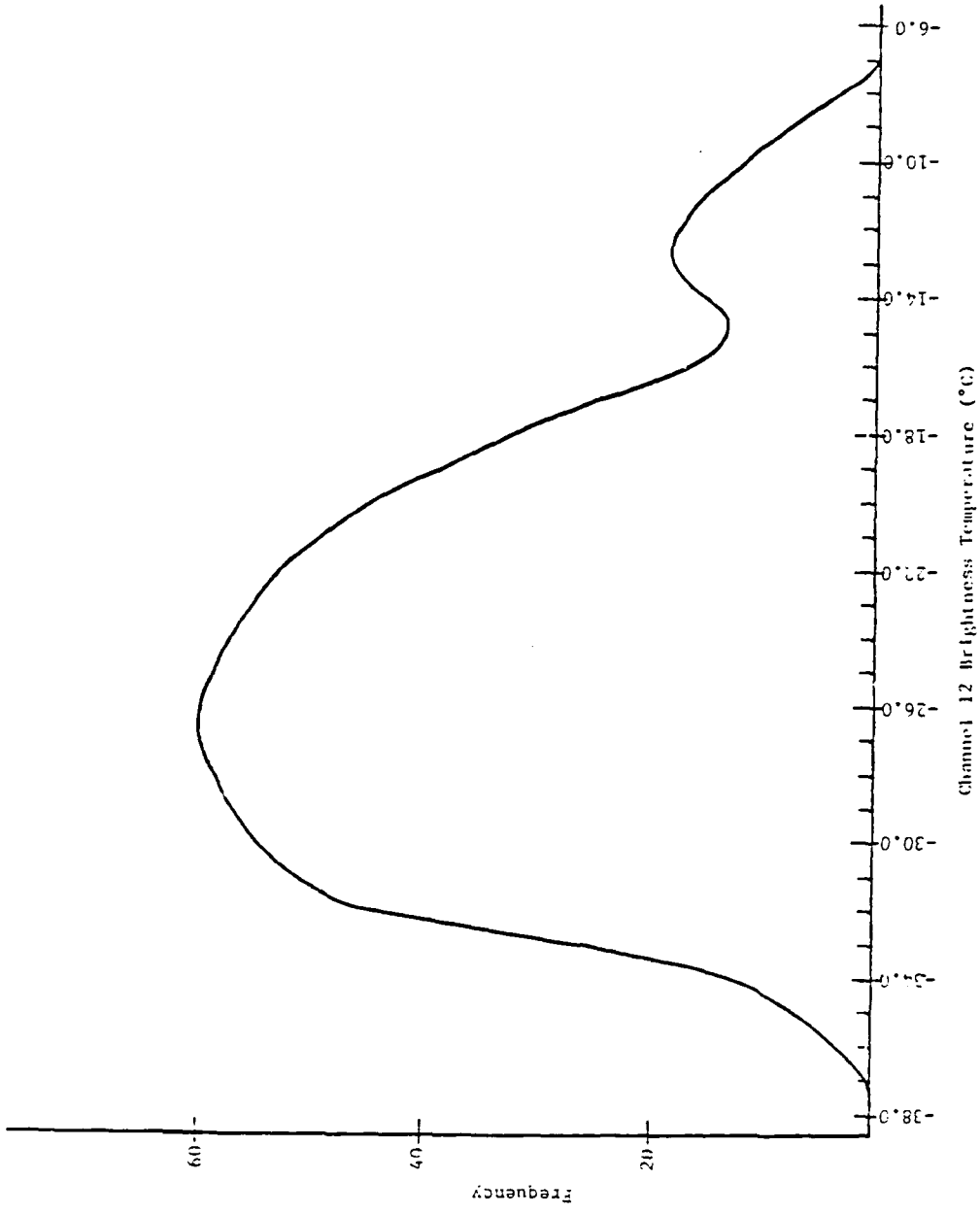

Figure 2. Channel 12 brightness temperature (BT) frequency distribution. Frequency is given as the number of occurrences per 0.3°C interval out of 3330 observations.

-20°C and -32°C. The smaller group of BTs higher than -15°C appeared to show evidence of another frequency maximum between -11°C and -13°C.

Unlike the channel 12 BTs, the frequency distribution (Fig. 3) for 3330 TIROS-N 7.3 μm channel 11 BTs during the same period of time showed a pattern approximating a normal distribution with very little evidence of skewness toward higher BTs. Therefore, the bimodal tendency shown in the channel 12 frequency distribution is not readily apparent in the channel 11 distribution.

As with channel 12, a test for evidence of a non-normal pattern within the channel 11 BT data was performed. The calculated skewness of the channel 11 BT distribution was compared to the expected variation of skewness for a sample normal distribution. Results from this comparison indicated the skewness for the BT distribution was only 1.5 times greater than the expected standard deviation of skewness; thus, channel 11 BTs approximated a normal distribution and showed very little evidence of bimodality.

The range of channel 11 BTs was smaller than that of the channel 12 BTs and extended from 3°C to -20°C. The broad frequency maximum evident in the channel 12 BTs in Fig. 2 also is evident in the channel 11 BTs shown in Fig. 3.

Evidence of a secondary frequency maximum in channel 12 BTs and the apparent absence of a secondary maximum in the frequency of occurrence of channel 11 BTs may be significant. Since the peak weighting of channel 12 occurs near the 500-mb level (see Fig. 1), this secondary maximum of high BTs observed in Fig. 2 may be the

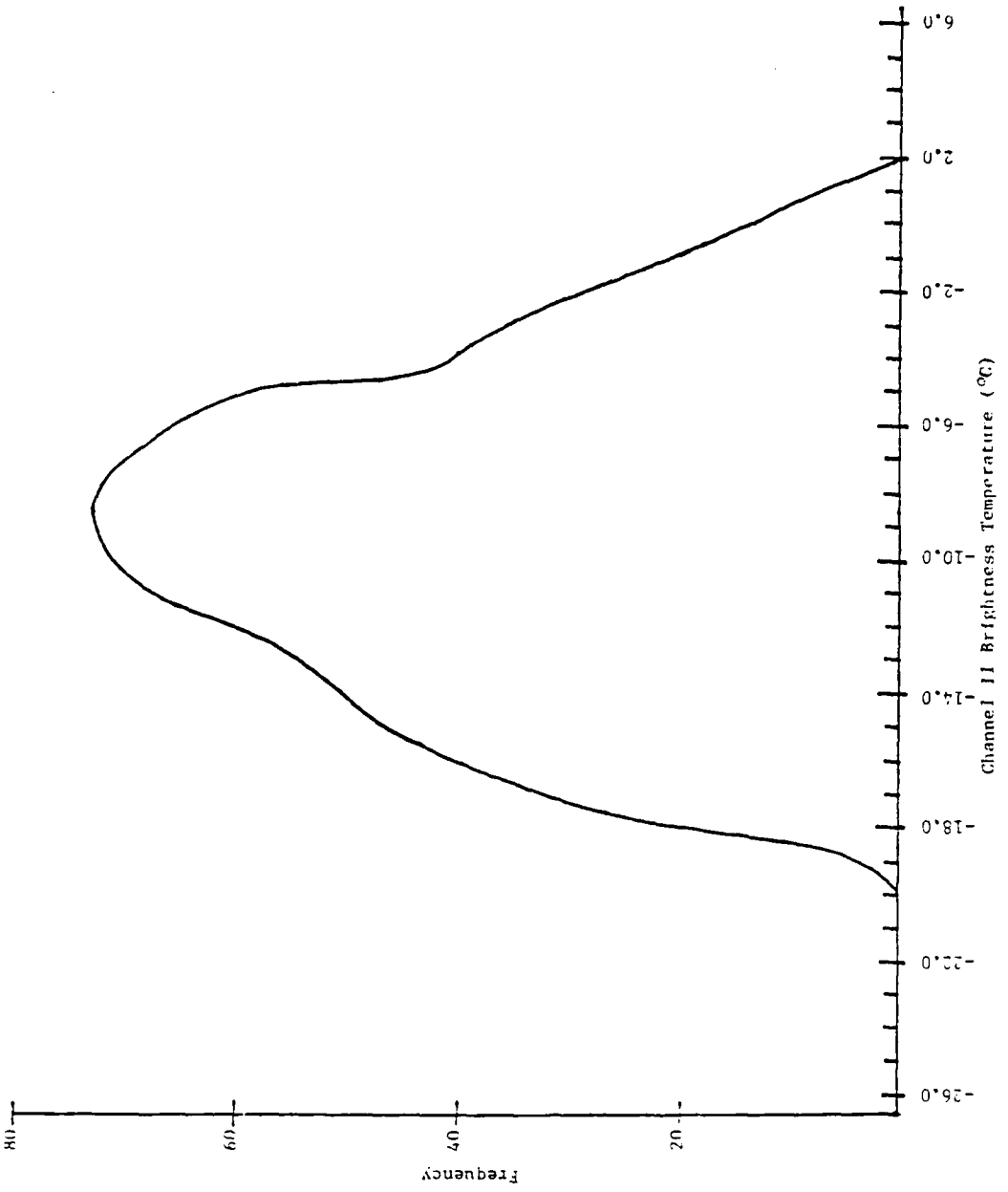

Figure 3. As in Fig. 2 except for channel 11.

signature of a synoptic feature in the upper troposphere. The next section focuses on the geographical distribution of the high channel 12 BTs observed within this secondary peak.

C. High Brightness Temperature Regions

Figure 4a shows the geographical distribution of channel 12 BTs observed on 24 January which were higher than -15°C. Corresponding unenhanced window channel GOES West IR satellite imagery of the eastern Pacific is shown in Fig. 4b. All of the BTs observed in the persistent cluster in Fig. 4a fell within the smaller frequency maximum in Fig. 2, and also fell within the near cloud-free region southwest of Hawaii. Without exception, this same pattern was observed each day throughout the period. From the 21st through 25th, these high BTs were clustered south and west of Hawaii and corresponded to large, mostly clear regions in the GOES West window channel imagery. Especially interesting was the location of these BTs directly adjacent to the western flank of a developing moisture burst (McGuirk et al., 1987), roughly bounded on the west by a line from 10°N/155°W to 25°N/145°W. The region of high BTs elongated eastward and diminished during the last few days of the period as the moisture burst moved toward the east and weakened (Schaefer, 1985).

The region south of Mexico (known as the Pacific dry zone) looked very similar in GOES West window channel imagery to the high BT region southwest of Hawaii; however, there was a noticeable lack of high BTs within this dry zone. This region south of Mexico remained free of any synoptic cloud systems throughout the entire 9-day period

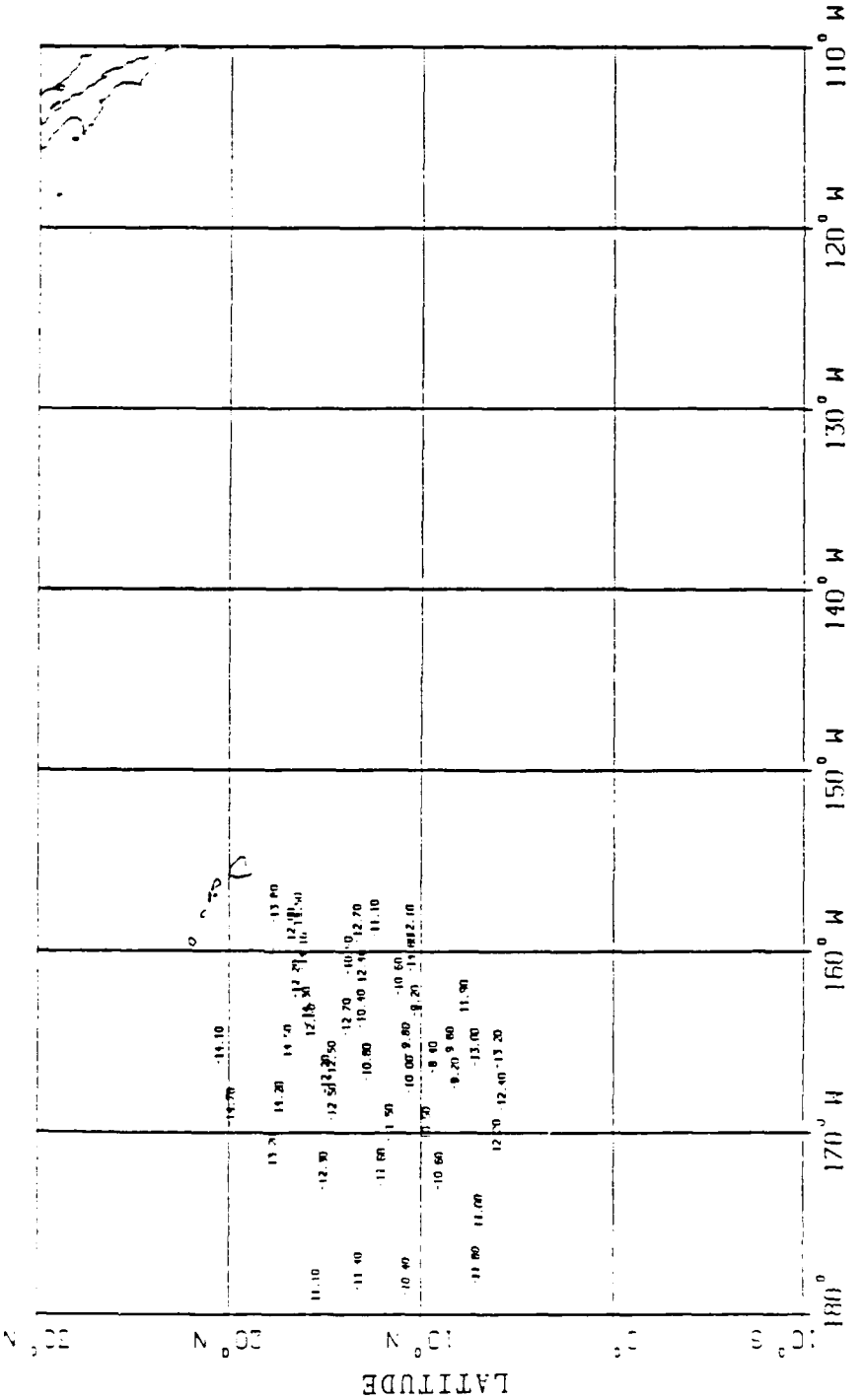

Figure 4a. Geographical distribution of channel 12 brightness temperatures higher than -15°C for 24 January 1979.

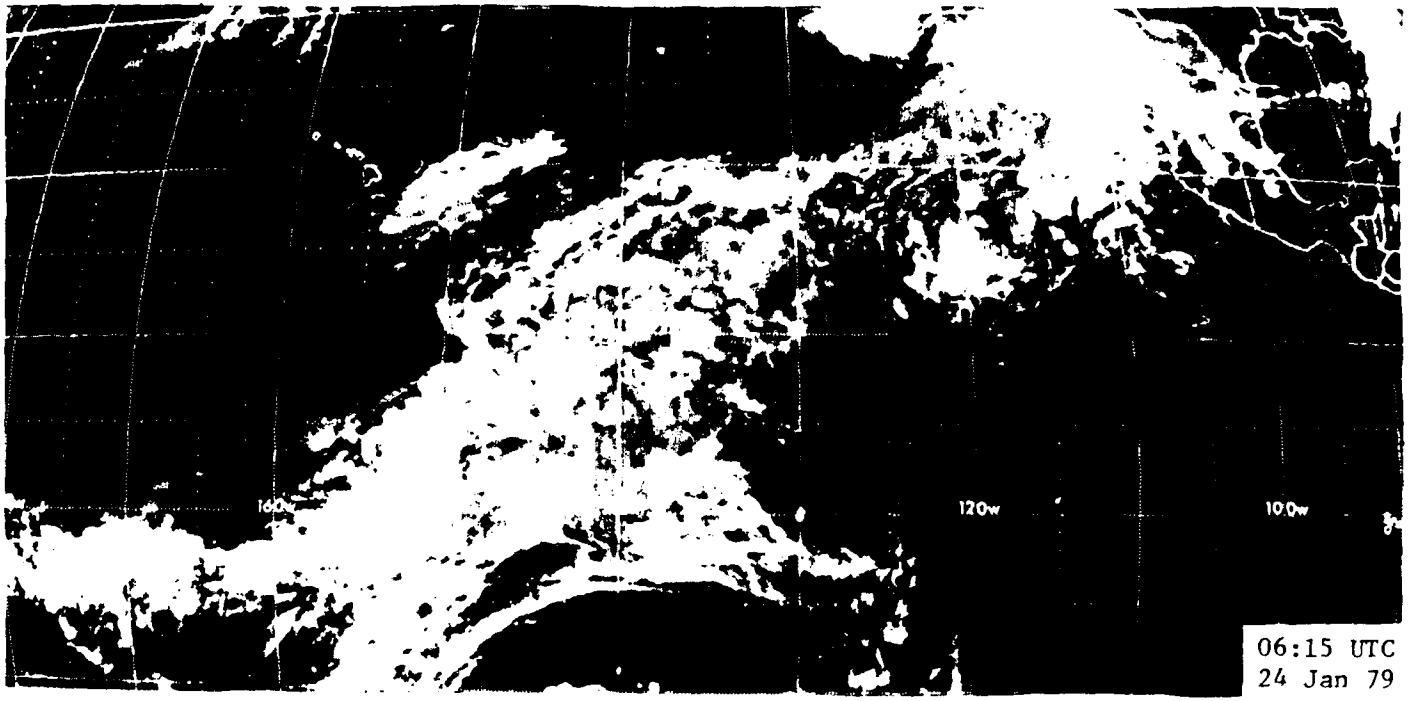

Figure 4b. Unenhanced window channel GOES West satellite image for 0615 UTC 24 January 1979.

and also remained virtually free of any BTs higher than -15°C which would be contained within the smaller channel 12 BT frequency maximum (Fig. 2).

Analysis of these findings suggests that the broad peak of the bimodal distribution in Fig. 2 may have been related to the typical occurrence of low BTs associated with a normal to very wet mid and upper troposphere in the tropics; however, the smaller frequency peak of high BTs appeared to be associated with an extremely dry mid and upper tropical troposphere. These extremely dry mid and upper tropospheric regions, corresponding to high BTs, have been verified below the 300-mb level by rawinsondes. Moisture profiles above this level were generally not available from conventional rawinsonde soundings. This small set of high BTs seems to be related exclusively to certain synoptic disturbances in the eastern Pacific.

A representative sounding within the region of large BTs is shown in Fig. 5. This Johnston Island sounding consisted of relative moistness below the 700 mb level, capped by a strong subsidence inversion. At pressures lower than 700 mb, the atmosphere was extremely dry with the dew point depression defaulting to 30°C at all levels. No moisture information was available for pressures lower than 250 mb due to the termination of moisture measurements for atmospheric temperatures less than -40°C. For comparison, a sounding from the scientific ship "Matamoros" in the Pacific dry zone (Fig. 6) displays many of the same characteristics. However, unlike the sounding from Johnston Island, the Matamoros sounding recorded dew point depressions greater than 30°C and moisture above the 100 mb

level. These dew point depressions were quality controlled below the 200 mb level by the operator. The significant differences between soundings were the thicker lower-tropospheric moist layer, the weaker subsidence/tradewind inversion, and the cooler, moister 300-250 mb layer and above recorded on the Matamoros sounding.

It is hypothesized that the large area of extremely high channel 12 BTs observed in western sections of the subtropical eastern Pacific (see Fig. 4a) may be associated with deep tropospheric subsidence as previously suggested by several researchers. Furthermore, it is hypothesized that the movement and the concentrated nature of these large channel 12 BTs relative to the active convection associated with a moisture burst may denote the subsidence branch of an intense, direct synoptic-scale circulation. This hypothesis is further substantiated by the observed shrinking of this BT area as the moisture burst weakens. Since channel 11 is more sensitive to moisture in the lower troposphere (see Fig. 1), the absence of a small, secondary frequency peak in the higher BT region of the channel 11 distribution (see Fig. 3) suggests the phenomenon producing the secondary channel 12 peak may be an anomaly restricted to the upper troposphere. This absence of a secondary channel 11 peak also suggests that the subsidence of dry air does not extend into the tropical boundary layer. This lack of subsidence into the boundary layer was further evidenced by numerous soundings within the high BT region which bore similar moist boundary layers and lower tropospheric profiles (500- to 1000-mb layer) to the Johnston Island sounding shown in Fig. 5.

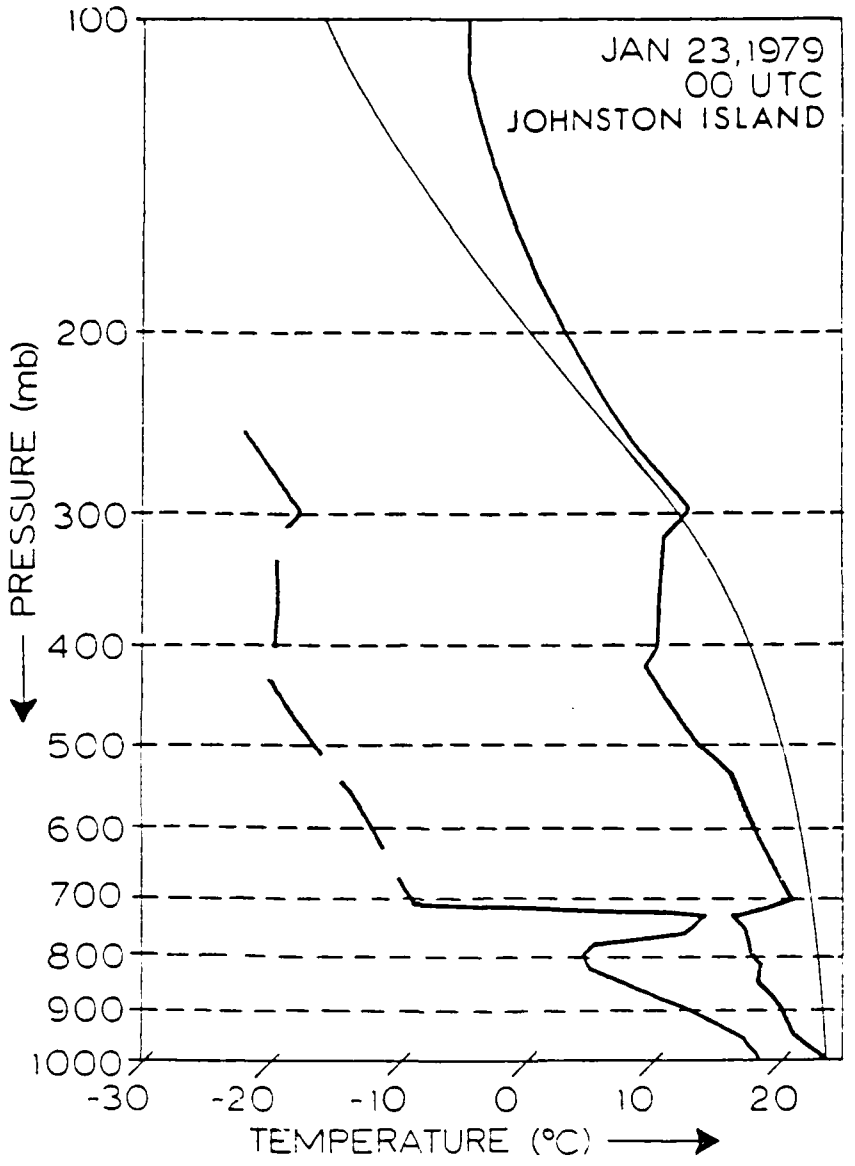

Figure 5. Johnston Island sounding for 0000 UTC 23 January 1979. The smooth curve in this skew-T log p plot represents the 24°C wet-bulb potential temperature. The jagged line on the right represents the temperature The jagged line on the left represents the dew point. Dashed regions on the dew point curve represent dew point depressions ≥ 30°C.

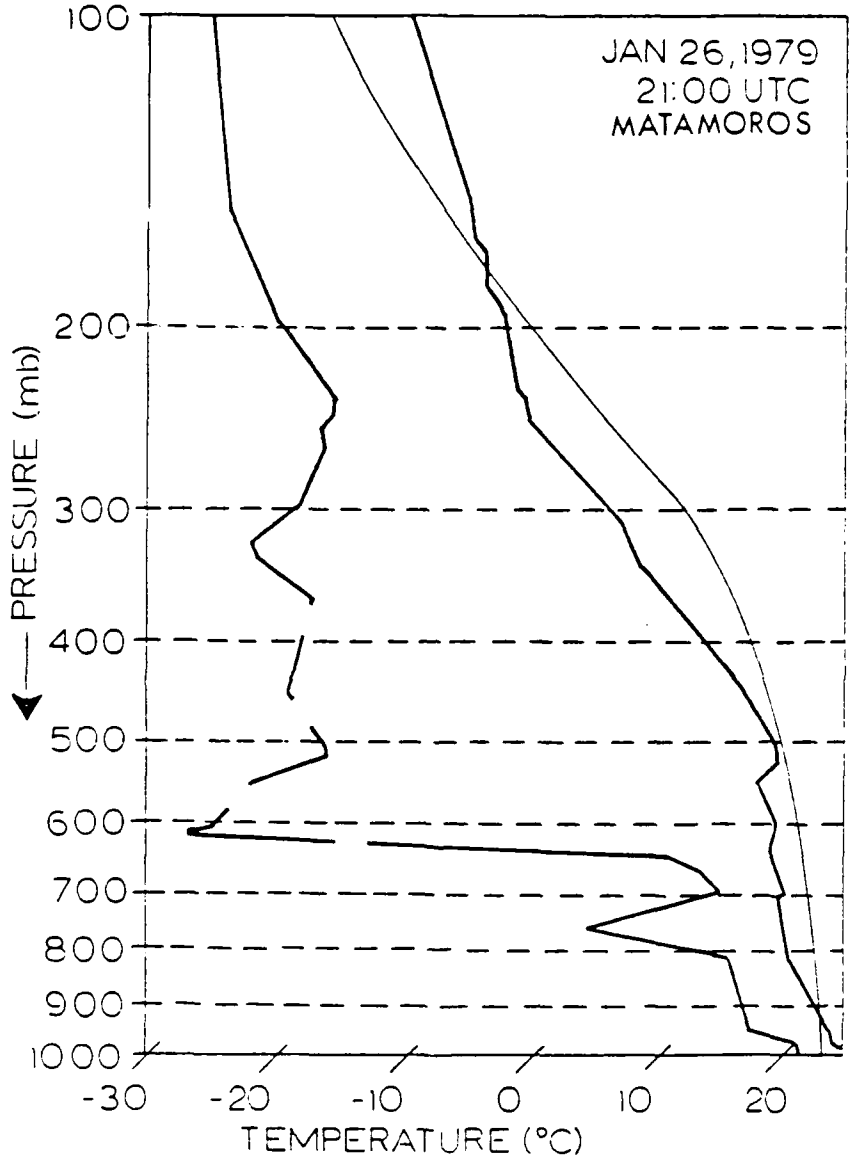

Figure 6. As in Fig. 5, except Matamoros sounding for 2100 UTC 26 January 1979 at 7°N/91°W.

CHAPTER V

BRIGHTNESS TEMPERATURE/RAWINSONDE RELATIONSHIP

An accurate topographical representation of the top of the moist layer depends on the ability of the TIROS-N moisture channels to locate accurately the pressure level corresponding to the top of this layer. It is hypothesized that the WV upper layer (boundary) can be inferred using WV satellite data. In order to find a relationship between satellite BTs and the top of the moisture in the troposphere, a connection must be established between BTs and some appropriate ground truth. The widespread use of conventional rawinsondes for vertical measurements of atmospheric temperature and moisture, together with their proven accuracy within a particular range of environmental conditions, provides the only "ground truth" data base to use for comparison. Thus, a correlation must be developed between BT and pressure from channel 12 and 11 BTs and the pressure level near the top of the moist layer as measured by collocated rawinsondes.

A. Rawinsondes

Moisture measurements from conventional rawinsondes are restricted to air temperatures warmer than -40°C and relative humidities above 20% (Federal Meteorological Handbook No. 3, 1981). Therefore, the raw rawinsonde data within the area of interest were checked for the average moisture cutoff pressure. This point varied from levels slightly above 300 mb in the tropics to just below the

300-mb surface in the subtropics. Consequently, all soundings with moisture measurements aborted at pressures greater than 300 mb were deleted. This procedure yielded 335 soundings with moisture measurements reaching to at least the 300-mb pressure surface.

The troposphere is very cold at pressures below 300 mb; therefore, this layer of air contains only small amounts of PW which are not measured accurately by rawinsonde. To determine the maximum amount of PW possible in the layer between 100 and 300 mb, the standard temperature profile at 15° north latitude (U.S. Standard Atmosphere Supplements, 1966) was used to compute moisture content for zero degree dew point depressions throughout this layer. From this assumed completely saturated layer, a rather small PW content of 0.50 mm was calculated with a 0.29 mm contribution from the layer between 250 and 300 mb. To obtain an idea of how moist the atmosphere actually was in this 50-mb thick layer, PW was calculated from approximately 100 soundings containing moisture measurements to the 250-mb level. The average measured PW total for this layer was only 0.09 mm; this total was just 31% of the maximum possible PW. Similar PW calculations for altitudes above the 250-mb level were not possible due to lack of moisture data. Based on the weighting function curves (see Fig. 1) from Smith et al. (1979), the possible influence on 6.7 μm and especially 7.3 μm BTs by upper tropospheric moisture appeared to be only minimal.

The data for the 335 soundings were checked for post-launch quality control, vertical resolution (especially in the mid- and upper-troposphere), and coding errors. More specifically, any

sounding would be deleted if it contained:

1. quality control marks which indicated the measured temperature and/or dew point depression at a pressure level was either suspect or incorrect;
2. a difference greater than 100 mb between reported pressure levels in the 300-800 mb layer; and/or
3. erroneous or highly questionable pressure, temperature, or dew point depression values.

For these three reasons, 28 soundings were determined to be unusable, leaving a sizeable total of 307 soundings for future utilization. Sounding locations are shown in Fig. 7. Except for Pariz, the scientific ships were constantly moving; therefore, their tracks are shown instead of a single location.

B. Brightness Temperature Interpolation

Satellite BTs rarely were collocated temporally and spatially with available sounding locations; therefore, a procedure was needed to estimate BTs at sounding locations from nearby BTs. Initially, a procedure similar to that used by Stout et al. (1984) was followed whereby any BT within 100 km and ±6 h of an available sounding was considered representative of the actual BT for that sounding location. However, as shown in Table 1, only 34 BTs were found within 100 km and ±6 h of available soundings over the entire 9-day period. A three- to four-fold improvement was obtained when the radius was increased to 200 and 300 km, respectively; however, collocation error, which appeared acceptable for BTs within a radius

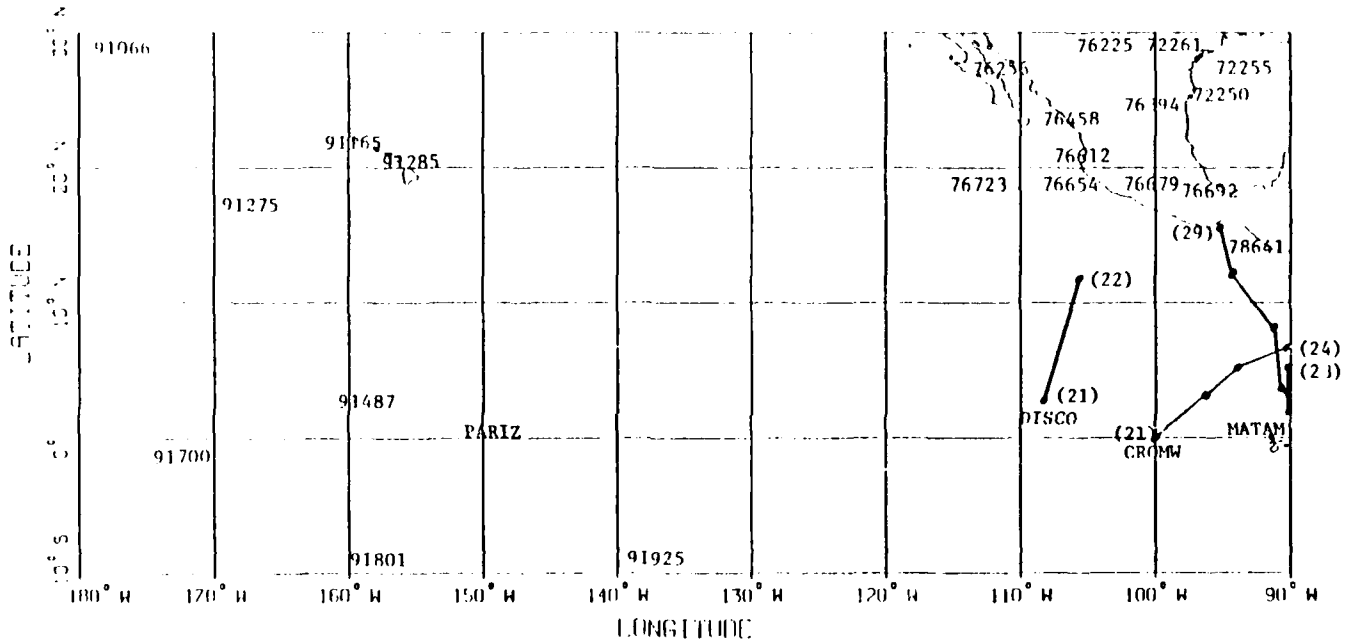

Figure 7. Map of land- and ship-launched rawinsonde locations. Tracks of ships are shown with dates at the start and end of each track. The five-digit numbers are international index numbers and the five-letter words represent ship names.

of 100 km, was deemed unacceptable for radii larger than 100 km.

Table 1. Number of rawinsonde soundings within specified distance and ±6 h of *one* or more satellite brightness temperature(s) for 21-29 January 1979.

Distance (km)	Number of Rawinsondes
100	34
200	84
300	127
400	159
500	177
600	184
700	197

A Barnes interpolation scheme (Barnes, 1973) was used whereby two or more existing BTs were employed to interpolate a new BT collocated with the location of an existing sounding. Table 2 shows the number of soundings which were within 100 km increments of at least two BTs. In order to sample a reasonably wide variety of atmospheric profiles, at least 100 collocated pairs were deemed necessary. The 400 km radius, containing 111 soundings, was the shortest distance meeting this criterion.

C. Brightness Temperature/Sounding Correlation

The upper 5 mm of PW for each sounding was calculated by integrating the specific humidity downward from 300 mb at each reported sounding level. Pressure levels were interpolated downward from the 300 mb level by a cubic spline interpolation procedure

(Gerald and Weatley, 1984). These interpolated pressure levels were assigned to each 0.1 mm increment within the 5.0 mm PW layer. The pressure level associated with each 0.1 mm PW increment was referred to as a PW thickness pressure (PWTP). An example and explanation of this procedure is shown in Fig. 8.

Table 2. Number of rawinsonde soundings within specified distance of *two* or more satellite brightness temperatures for 21-29 January 1979.

Distance (km)	Number of Rawinsondes
100	1
200	27
300	75
400	111
500	145
600	169
700	179

Correlation coefficients for channels 12 and 11 were computed between interpolated BTs and each 0.1 mm PWTP increment from 0.1 mm to 5.0 mm; this was simply a correlation between BT and pressure. Several different radii of influence were used. The correlation coefficients were computed for channel 12 and 11 BTs with a requirement of at least one observation within a radius of influence (ROI) of 100 km. The correlation coefficient for channel 12 peaked near 0.81 at the 0.4 mm PW thickness and near 0.79 at the 0.6 mm PW thickness for channel 11; however, as shown in Table 1, the sample size of 31 rawinsondes was small. Table 3 shows correlation

Figure 8. Example of procedure used to calculate precipitable water thickness pressure (PWTP) for the upper 5 mm of precipitable water (PW). From the observed dew point depressions in the first column, the specific humidity is integrated downward from 300 mb. The second column shows the PW for each layer calculated from the specific humidity in each of these layers. The accumulation of PW downward from 300 mb is shown at the base of each layer in the third column. The cumulative PW "thickness" is divided into 0.1 mm incrememts in the fourth column. Finally, the fifth column shows the pressure levels assigned by cubic spline interpolation to each 0.1 mm PW increment. These pressures corresponding to particular PW thicknesses are labelled PW thickness pressures (PWTPs).

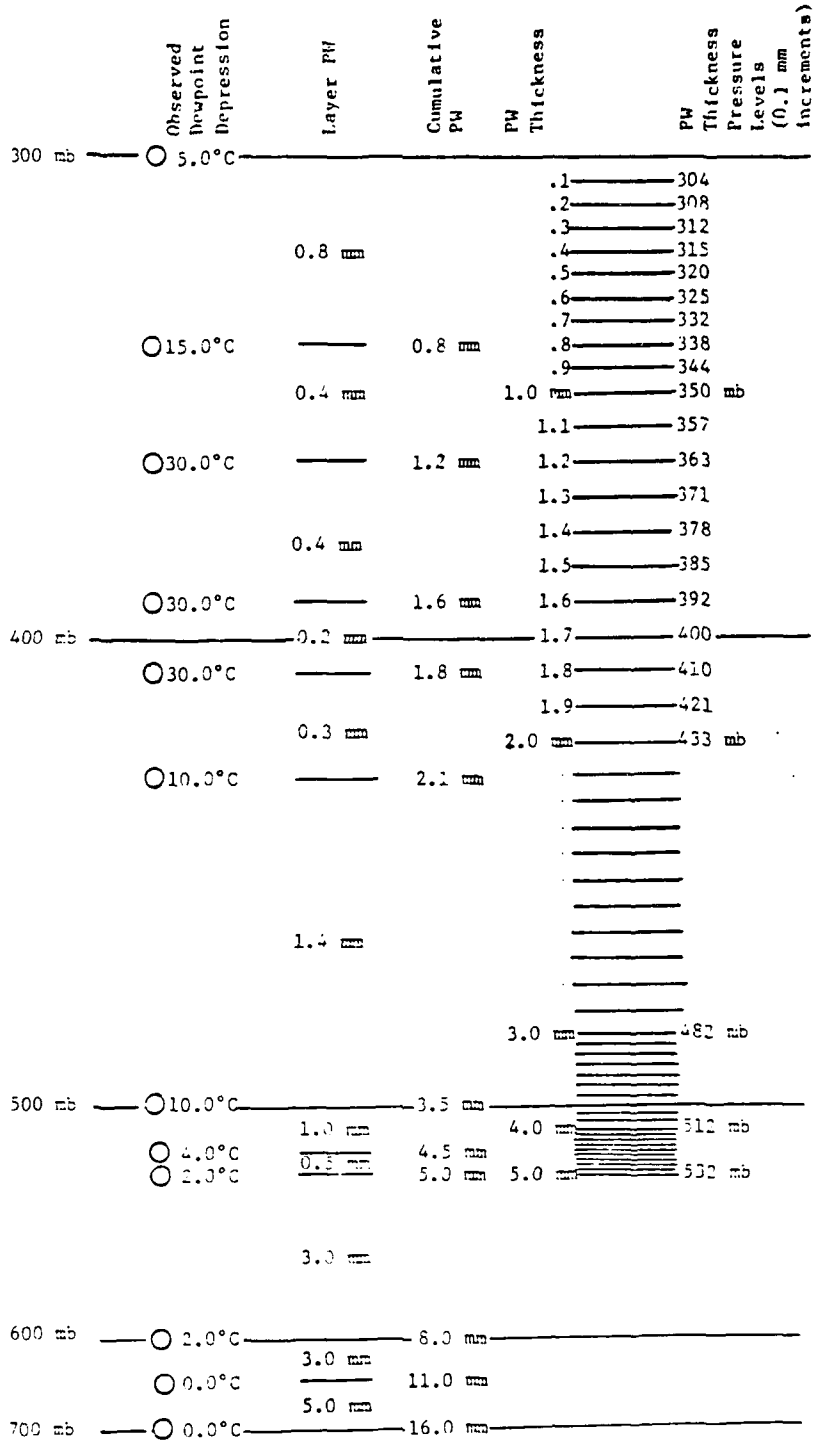
Observed Dewpoint Depression
Layer PW
Cumulative PW
PW Thickness
PW Thickness Pressure Levels (0.1 mm increments)
300 mb
5.0°C
0.8 mm
15.0°C
0.8 mm
0.4 mm
1.0 mm
350 mb
30.0°C
1.2 mm
0.4 mm
30.0°C
1.6 mm
400 mb
0.2 mm
1.7
400
30.0°C
1.8 mm
0.3 mm
2.0 mm
433 mb
10.0°C
2.1 mm
1.4 mm
3.0 mm
482 mb
500 mb
10.0°C
3.5 mm
1.0 mm
4.0 mm
512 mb
4.0°C
4.5 mm
2.0°C
0.5 mm
5.0 mm
5.0 mm
532 mb
3.0 mm
600 mb
2.0°C
8.0 mm
3.0 mm
0.0°C
11.0 mm
5.0 mm
700 mb
0.0°C
16.0 mm
.1 304
.2 308
.3 312
.4 315
.5 320
.6 325
.7 332
.8 338
.9 344
1.1 357
1.2 363
1.3 371
1.4 378
1.5 385
1.6 392
1.7 400
1.8 410
1.9 421

coefficients for both channels computed for several ROIs with a requirement of at least two observations within a given ROI.

Table 3. Channel 12 and channel 11 maximum correlation coefficicients (r) and corresponding PW for 100 km radius increments for 21-29 January 1979. *Two* or more satellite brightness temperatures were required within the indicated distance from a rawinsonde sounding.

Distance (km)	Channel 12		Channel 11	
	r	PW thickness	r	PW thickness
100	(not computed; sample size consisted of 1 observation)			
200	0.716	0.6 mm	0.792	1.2 mm
300	0.807	0.7 mm	0.843	0.9 mm
400	0.814	0.6 mm	0.841	0.9 mm
500	0.807	0.8 mm	0.832	0.9 mm
600	0.793	0.8 mm	0.820	0.9 mm
700	0.787	0.6 mm	0.819	0.9 mm

The 400 km ROI produced a channel 12 peak correlation coefficient of 0.81 at the 0.6 mm PW thickness (Fig. 9) and a channel 11 peak of 0.84 at the 0.9 mm PW thickness (Fig. 10). The 400 km ROI correlation profiles shown in Figs. 9 and 10 were typical of the other ROI values; however, the peaks in the correlation curves for the 400 km ROI were sharper than the peaks produced for other ROIs. Thus, the 400 km radius was chosen as the most suitable ROI, not only because of the sharper and more amplified peaks in the channel 11 and 12 correlation coefficients, but also because of the adequate number of soundings available. Consequently, a total of 111 sounding/interpolated BT comparisons were made. The high correlation established between BTs and the upper millimeter of PW observed in

the atmosphere appears to support the hypothesis stated at the beginning of this chapter that the WV upper layer (boundary) can be inferred using WV-sensitive BTs. Therefore, it seems worthwhile to study the significance of the change in the height of this moist layer as sensed from satellite.

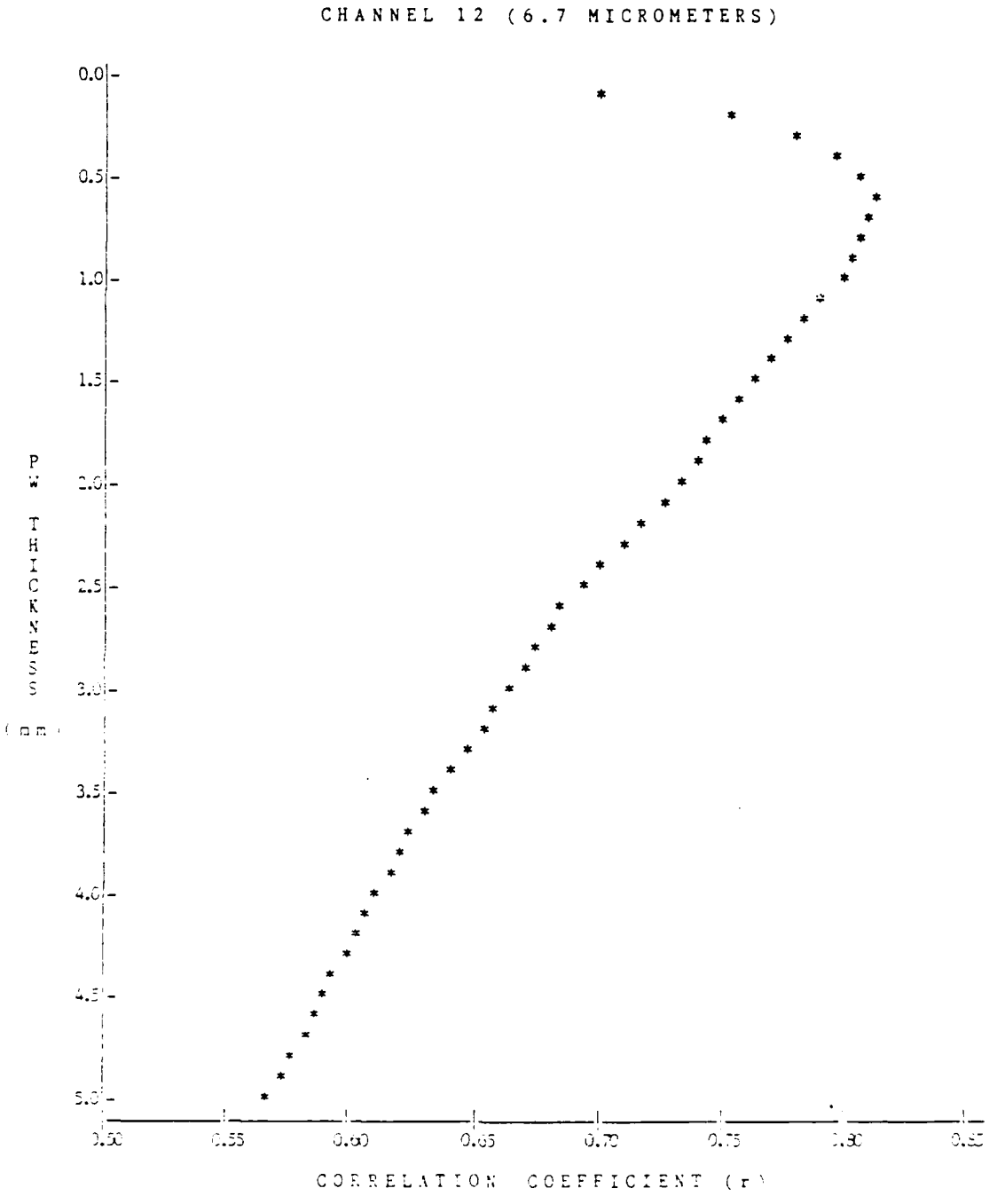

Figure 9. Channel 12 correlation coefficients between BT and PWTP (pressure) for each 0.1 mm level in the upper 5 mm layer of PW.

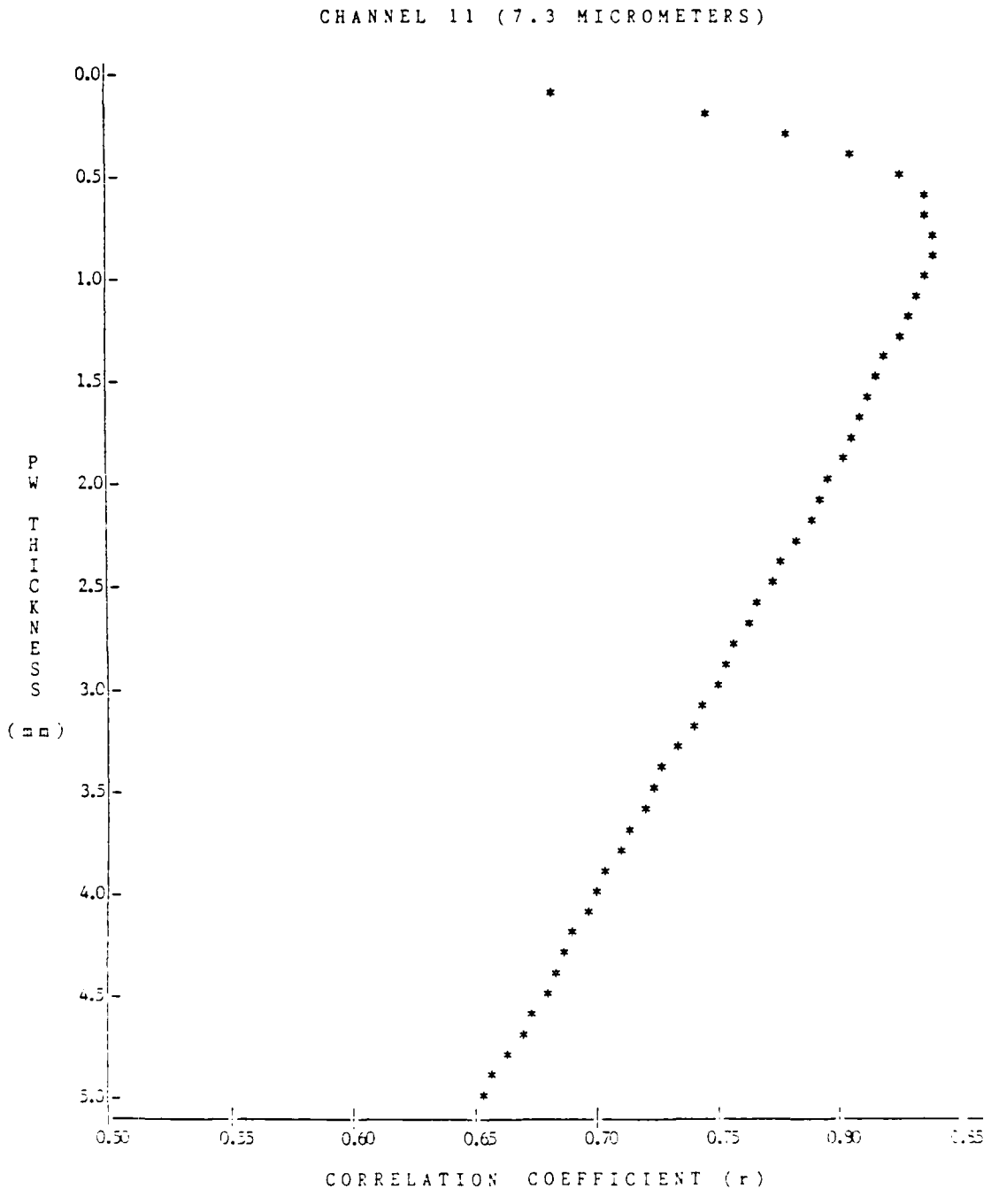

Figure 10. As in Fig. 9 except for channel 11.

CHAPTER VI

ESTIMATING TROPICAL SYNOPTIC VERTICAL MOTIONS

Vertical motions in the atmosphere are difficult to measure directly. Consequently, the most commonly used methods, the omega equation along with the kinematic, dynamic, and adiabatic methods, are indirect. Even in data-rich areas, these techniques are hampered by inadequate measurements of pressure, wind, and temperature. In addition, a special problem occurs in the tropics where divergent motions are diabatically generated by areas of organized deep convection.

Both horizontal and vertical advection of water vapor produce local changes in the channel 12 and 11 BTs. In a study of ECMWF-FGGE analyses for January and February 1979, Lin and Mock (1986) found a significant lack of model accuracy within 10° latitude of the equator. These results, along with the sparseness of rawinsonde locations over the eastern Pacific, precluded any reasonable estimates of horizontal moisture advection. Thus, if horizontal moisture advection and diffusion are neglected (Stout et al., 1984), it is hypothesized that local changes in the height of the upper moist layer detected by satellite over a 12-h period may be used to infer vertical motions. Although each calculated vertical motion will be a local estimate, regional clustering of these values may allow an estimate of synoptic-scale vertical motions.

Consequently, a best-fit regression equation must be obtained from the BT/PWTP relationship discussed in Chapter V which will allow

PWTPs ultimately to be computed strictly from WV BTs.

A. Regression

The relationships between the 0.6 mm PWTPs and channel 12 BTs, and the 0.9 mm PWTPs and channel 11 BTs were obtained by fitting linear and non-linear regression models to each data set, respectively. Since channel 12 and channel 11 moisture sensitivities are not equal, each association is studied separately beginning with channel 12.

The relationship between the 0.6 mm PWTPs and channel 12 BTs was obtained by performing linear and polynomial regression on the 111 collocated observations shown in Fig. 11. In a moist tropospheric sounding, the top of the moist layer should exist at a lower pressure (higher elevation) than in a drier sounding; therefore, wetter soundings should have a lower PWTP than drier soundings. The scatter plot in Fig. 11 appeared to support this relation by showing a tendency from low PWTPs and low BTs to high PWTPs and high BTs.

Fig. 11 also shows the best fit linear curve through the scatter plot. Although the correlation between these two parameters was very high ($r = 0.81$ with 66% of the PWTP variance explained by this curve), the root mean square (RMS) error of PWTP with respect to that estimated from collocated rawinsonde measurements was quite large (RMS error = 50 mb). This RMS error was nearly 15% of the observed 0.6 mm PWTP range. The potential significance of this large RMS error is discussed in Chapter VII.

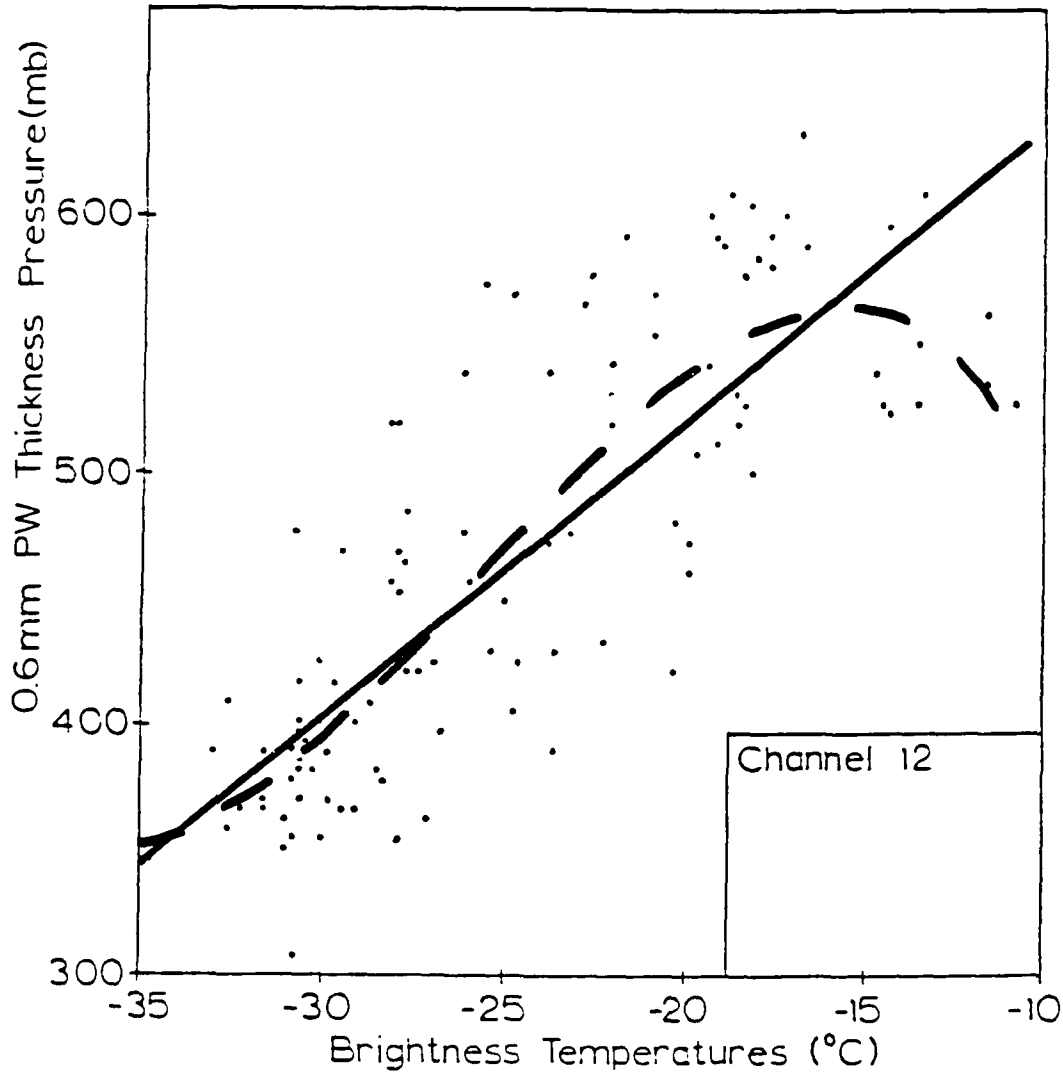

Figure 11. Scatter plot of 0.6 mm PWTPs versus channel 12 BTs overlain by the best fit linear (solid) and polynomial (dashed) regression curves.

Polynomial regression was attempted to improve the fit of the scatter plot and thereby reduce the RMS error. The curve produced by the cubic polynomial regression equation (see Fig. 11) was found to produce the best fit by explaining 71% of the 0.6 mm PWTP variance; however, the RMS error was reduced by only 4 mb. Thus, a significant increase in fit and corresponding reduction in the RMS error over the linear regression model was not indicated by polynomial regression methods.

As with the channel 12 data, a linear relationship appeared evident in the scatter plot of 0.9 mm PWTPs and channel 11 BTs (Fig. 12). The correlation between the 0.9 mm PWTPs and channel 11 BTs remained high (r=0.84); however, the RMS error of PWTP also remained large (53 mb). Again similar to the linear RMS error observed in the 0.6 mm PWTP/channel 12 relationship, this RMS error was 14% of the observed 0.9 mm PWTP range.

Polynomial regression was attempted to improve the fit of the 0.9 mm PWTP/channel 11 scatter plot. A quartic polynomial regression equation (see Fig. 12) produced the best fit of this scatter plot by explaining 78% of the 0.9 mm PWTP variance and by reducing the RMS error to 47 mb. Again, a significant increase in fit and reduction of the RMS error over the linear regression model was not observed.

B. Satellite-Derived Vertical Motion Estimates

Given the persistently high RMS errors observed in both linear and polynomial regression models and only a slight increase in polynomial as compared to linear correlation, the linear regression

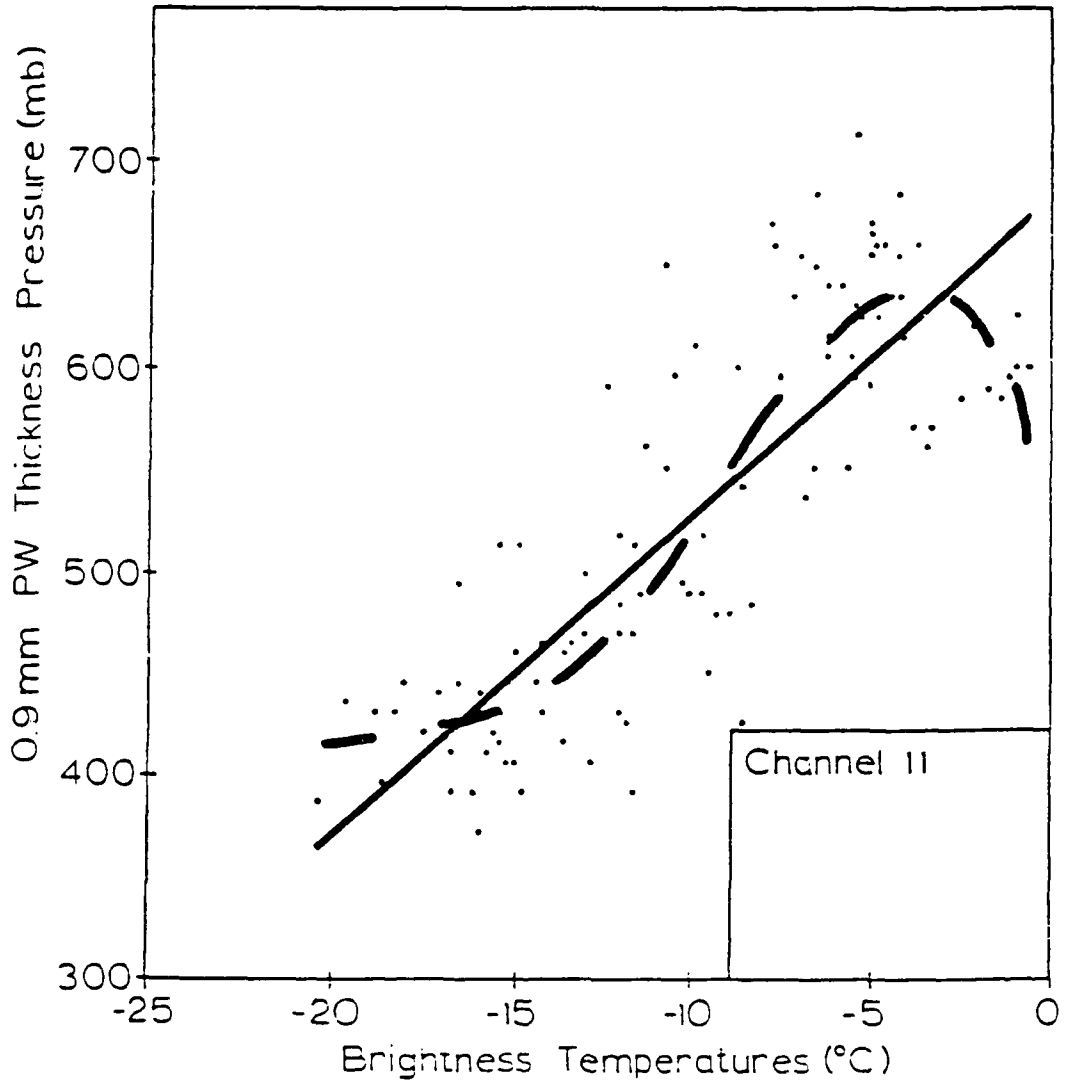

Figure 12. As in Fig. 11 except for 0.9 mm PWTPs versus channel 11 BTs.

equation for both channel 12 (1) and channel 11 (2), respectively, were used to compute the pressure at the top of the moist layer from satellite BTs:

$$PWTP = 763.181 + 11.352(BT_{12}) \quad (1)$$

$$PWTP = 673.193 + 15.343(BT_{11}) \quad (2)$$

with PWTP = pressure at the top of the moist layer (mb)

BT_{12} = channel 12 BT (°C)

BT_{11} = channel 11 BT (°C)

Available BTs for each channel were interpolated every 12 h onto an eastern Pacific grid with 3 3/4° spacing in latitude and longitude. The interpolation procedure was the same used for collocation, except grid point locations were used in place of rawinsonde locations. From these grid point BTs, a grid point pressure for each channel was computed from equations (1) and (2). From this pressure, a corresponding atmospheric height was directly assigned from the 15°N standard atmosphere (U.S. Standard Atmosphere Supplements, 1966) to each grid point. Temporally consecutive grids were overlain and the height differences derived from each channel were computed for appropriate grid points. Dividing these 12-h height differences by 43200 s/12 h, a vertical velocity (cm s^{-1}) was computed for each channel at each grid point. This procedure was repeated every 12 h from 21-29 January and resulted in 17 vertical motion analyses for each channel.

Figures 13a and 13b show eastern Pacific vertical motion estimates computed from channel 12 and channel 11 BT differences,

respectively, for the period 1200 UTC on 22 January 1979 to 0000 UTC on 23 January 1979. In this figure, the magnitude of the largest vertical velocity estimate observed was 3.6 cm s^{-1} and 3.0 cm s^{-1} for channel 12 and channel 11, respectively; however, most absolute magnitudes were less than 2.0 cm s^{-1}. These magnitudes agree favorably with those discussed by Holton (1979) and Stout et al. (1984).

A comparison of the channel 12 and 11 vertical velocities at each point in Fig. 13 showed fairly good agreement between the channels, especially when at least one of the channels had a vertical velocity over 1 cm s^{-1} at a particular grid point (see the north and central Gulf of Mexico). Yet, there were a few comparisons which violently disagreed in both sign and magnitude (see the extreme southern Gulf of Mexico). The different sensitivities of each channel through each tropospheric layer (see Fig. 1) may give a possible explanation for this observed behavior. If the vertical motion estimates from both channels favorably agree, then similar moisture changes may be occurring in both the lower (sensitive to channel 11) and upper (sensitive to channel 12) troposphere. When the estimates disagree, then moisture changes may be occurring in one tropospheric layer and not in the other.

Since channel 12 is more sensitive to WV than channel 11, one would expect the channel 12 derived vertical motions to be representative of vertical velocities at a higher level (lower pressure) in the troposphere than channel 11 derived motions. From the 3330 BTs comprising each channel's data set over the entire 9-day

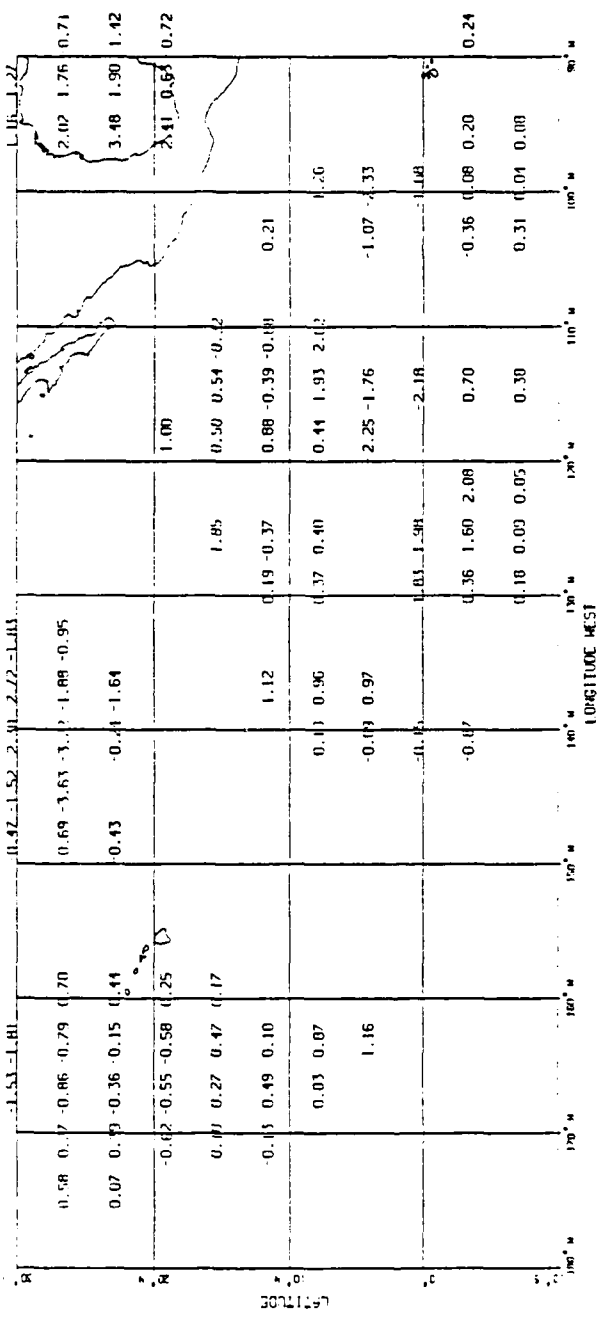

Figure 13a. Twelve-hour vertical velocity estimates (cm s^{-1}) from channel 12 BTs for the period ending 0000 UTC 23 January 1979.

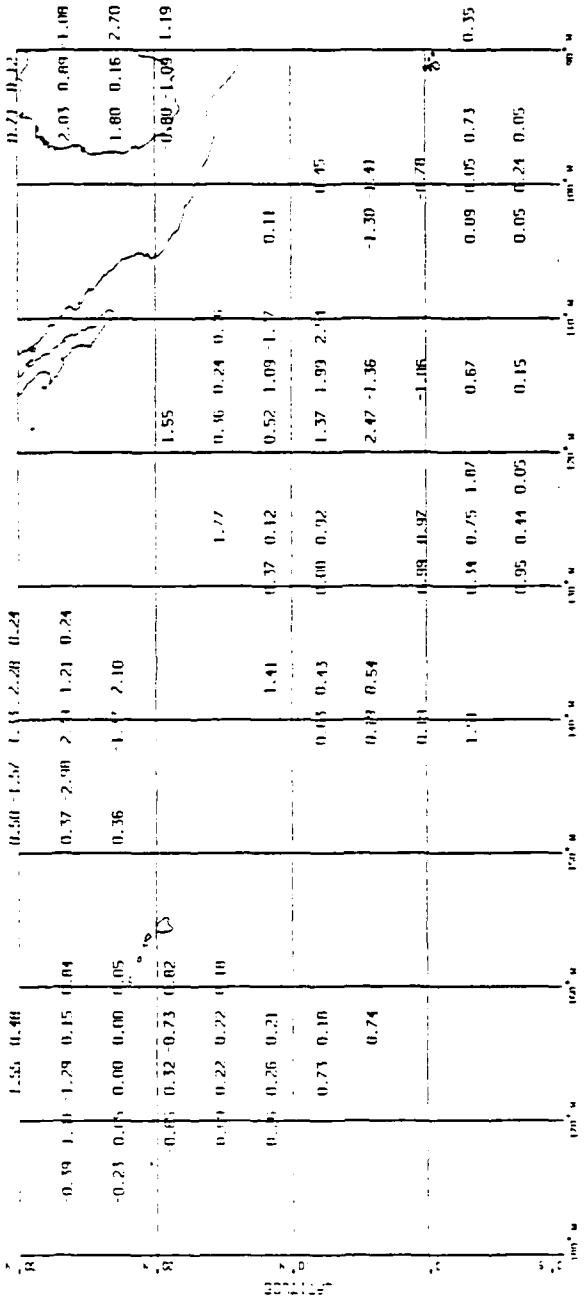

Figure 13b. As in Fig. 13a except for channel 11.

period, the mean BTs were computed to be -24.0°C and -8.9°C for channels 12 and 11, respectively. Mean pressure levels for each channel were obtained by inserting these BTs into equations (1) and (2). These pressure levels theoretically should represent the mean level of moisture being sensed by each satellite channel. The 491-mb mean pressure level computed for channel 12 agreed closely with the 500-mb peak in the channel 12 weighting function curve shown in Fig. 1. As expected, the channel 11 BT mean pressure of 537 mb was higher than that of channel 12; however, this channel 11 pressure was approximately 150 mb lower than the 700-mb peak observed in the channel 11 weighting function curve (see Fig. 1). Therefore, both channels evidently were sensing the tropical middle troposphere with channel 12 detecting moisture at a slightly higher elevation than channel 11.

C. Verification of Vertical Motion Estimates

As seen in Section B, the very realistic magnitude of the satellite-derived vertical motion estimates was encouraging. However, for an indication of their accuracy, these estimates were compared with estimates derived from other methods.

1. Adiabatic Method

Two collocated soundings launched 12 h apart were used to compute vertical velocities at the 400- and 600-mb pressure levels for this 12-h period. The method used was similar to the adiabatic method described by Petterssen (1956). The 400- and 600-mb pressure levels

were chosen for three reasons:

1. the limited number of mandatory pressure levels reported in a mid-tropospheric sounding;
2. the proximity of these pressure levels to the level of non-divergence in the tropics may make these estimates more representative of actual vertical motions at these levels; and
3. the 400-mb adiabatic vertical motion estimates should more closely approximate channel 12 derived estimates, and 600-mb adiabatic estimates should more closely approximate channel 11 derived estimates.

Since the computed adiabatic vertical motions were very sensitive to lapse rate fluctuations, relatively moist soundings with average dew point depressions less than 15°C for each 100-mb layer between the 300- and 700-mb pressure levels were excluded. The moister the atmosphere, the greater the probability of vertical parcel displacement occurring along an image curve which represents a lapse rate less than the dry adiabatic lapse rate. This reduced lapse rate may be caused by the presence of liquid water or ice, and the smaller the dew point depression, the greater the likelihood of water (in its liquid or frozen state) being present. Thus, the use of these dry soundings assured that the vertical displacement of air parcels used in this comparison approximated motion along a dry adiabat and any lapse rate fluctuations were considered insignificant.

The 400- and 600-mb adiabatic-derived vertical motions from 32 eligible sounding pairs are shown in Table 4 together with channel 12

and 11 satellite-derived vertical velocities. Although the overall magnitude of the adiabatic vertical motions approximated the magnitude of those motions derived from satellite BTs, the individual comparisons shown on each row of Table 4 did not agree very well. Several of the comparisons, were extremely poor; 56% of channel 12/400-mb adiabatic estimates and 38% of the channel 11/600-mb adiabatic estimates did not agree even in sign. Although both channels produced bad comparisons, channel 11 performed better than channel 12. However, the results of linear regression calculations (see Table 4) exemplified the absence of a satellite/sounding vertical motion relationship. Virtually no correlation existed. Correspondingly, the RMS errors for both sets of satellite-/sounding-derived vertical motion comparisons were large. For example, the RMS error of 2.1 cm s^{-1} computed from the channel 12/400-mb vertical motion relationship was 50% of the observed channel 12 vertical motion range and 22% of the observed 400-mb vertical motion range. The channel 11/600-mb vertical motion relationship produced a considerably smaller RMS error of 0.8 cm s^{-1}; however, due to the smaller range of observed channel 11 and 600-mb vertical motions, this RMS error still encompassed 21% and 23% of these vertical velocity ranges, respectively.

Table 4. Comparison of vertical motion estimates produced by channel 11 (CH11) and channel 12 (CH12) water vapor brightness temperatures and estimates produced from soundings by the adiabatic method (Petterssen, 1956) for the 600-mb (AD600) and 400-mb (AD400) pressure levels. Estimates produced for 32 locations in the eastern Pacific from 21-29 January 1979.

	Vertical Motions (cm s^{-1})			
Station	CH11	AD600	CH12	AD400
1	-0.3	-2.7	-0.3	-0.8
2	0.7	-1.4	0.8	0.1
3	-0.1	-2.5	0.9	-5.5
4	-0.5	-1.2	-0.7	-1.9
5	-0.1	-1.7	0.3	-2.4
6	0.4	-1.1	0.3	0.2
7	1.7	-1.2	3.2	0.3
8	0.6	-1.2	0.7	-0.6
9	-0.4	-0.6	-1.1	-2.1
10	0.6	-0.5	0.1	-0.6
11	-1.0	-0.7	-0.7	0.3
12	-1.5	-1.1	-1.0	-0.5
13	-0.1	-0.9	0.3	-0.2
14	-0.2	-0.7	0.3	1.2
15	0.9	-0.9	1.9	-1.1
16	0.1	-0.6	1.3	-2.1
17	-0.2	-0.1	0.9	-1.5
18	1.3	0.4	1.3	3.3
19	0.7	0.2	-1.1	0.5
20	0.6	0.5	-0.4	2.4
21	0.5	0.7	0.2	4.0
22	0.1	-0.4	0.2	-0.1
23	-0.4	-1.5	0.1	-4.6
24	-0.5	-0.8	-0.1	-0.8
25	-0.9	0.0	-0.2	2.7
26	-0.4	0.3	-0.1	2.9
27	0.7	0.3	0.8	0.4
28	0.3	-1.0	0.5	-3.2
29	0.1	0.0	-0.7	0.8
30	-2.1	-0.9	-0.6	-1.0
31	-0.7	-0.6	-0.1	-0.3
32	0.8	-0.2	0.4	0.1

Linear Regression Results

Channel 11/600-mb Adiabatic Method Vertical Motions
R^2: 0.044 RMS Error: 0.8 cm s^{-1}

Channel 12/400-mb Adiabatic Method Vertical Motions
R^2: 0.003 RMS Error: 2.1 cm s^{-1}

Summarizing, the adiabatic method vertical motion estimates calculated from 32 soundings with dry mid- and upper-tropospheric profiles compared poorly to the estimates produced from the channel 11 and 12 BTs. The signs from over half of the channel 12 estimates did not agree with the adiabatic estimates, while only a third of the channel 11 signs disagreed. Possible reasons for the unsatisfactory comparisons are discussed in Chapter VII.

2. Outgoing Longwave Radiation Signatures

A second verification procedure was performed using maps of Outgoing Longwave Radiation (OLR) satellite signatures over the eastern Pacific. Julian (1984) found an inverse relationship between OLR intensity and the divergence distribution of the upper and lower troposphere in the tropics. Furthermore, mass continuity suggests the divergence profile should be well correlated with vertical motion. Therefore, regions of low OLR values suggest areas of upward vertical motion while high OLR values indicate subsidence.

From this analogy, OLR radiance values were analyzed at 12-h intervals over the eastern Pacific; 12-h changes in these values were compared with the concurrent moisture-channel-derived vertical motion estimates. The OLR analysis for 0000 UTC on 22 January (Fig. 14a) indicated two regions of high OLR values separated by an elongated low OLR zone representing a moisture burst (Schaefer, 1985). By 1200 UTC on the 22nd, the high OLR values within these two regions southwest of Hawaii and south of Mexico had expanded in areal coverage (Fig. 14b) which suggested areas dominated by suppressed

cloudiness and subsidence. Similarly, the channel 12-derived vertical motions estimates (Figs. 14a or 14b) southwest of Hawaii exhibited a small area of fairly strong subsidence of 2-3 cm s^{-1} near 10°N between 160°W and 170°W. However, contrary to the OLR indications, moderate ascent of 1.0-1.5 cm s^{-1} was indicated to the north near 20°N; slight ascent was manifested also in the region south of Mexico adjacent to the Galapagos Islands. In addition, the channel 11-derived vertical motion estimates (Fig. 14c or 14d) showed the same conflicting pattern as the channel 12 estimates.

OLR analyses from 0000 UTC and 1200 UTC on the 26th (Figs. 15a and 15b) showed an expansion of the cloudless region southwest of Hawaii; therefore, general subsidence was expected through this region. Yet, both channel 12 vertical motions (Fig. 15a or 15b) and channel 11 vertical motions (Figs. 15c or 15d) showed general ascent over this area. Well defined subsidence was noted in both moisture channel vertical motion profiles up to 1000 km east of Hawaii; this subsidence coincided well with the moderately high OLR values found here. Further to the east, the channel 12 vertical motions showed moderate ascent of 1-3 cm s^{-1} just east of 140°W between 20°N and 30°N in spite of the collocated homogeneous region of moderately high OLR values and cloudless skies. A similar contradiction existed to the north of Hawaii between 20°N and 30°N. Further inconsistencies existed along 160°W between the equator and 10°N where both moisture channels showed upward vertical motions in excess of 3 cm s^{-1} while the OLR signature suggested subsidence developing in the region as OLR values rapidly rose. The region south of Mexico within the $\geq$ 280

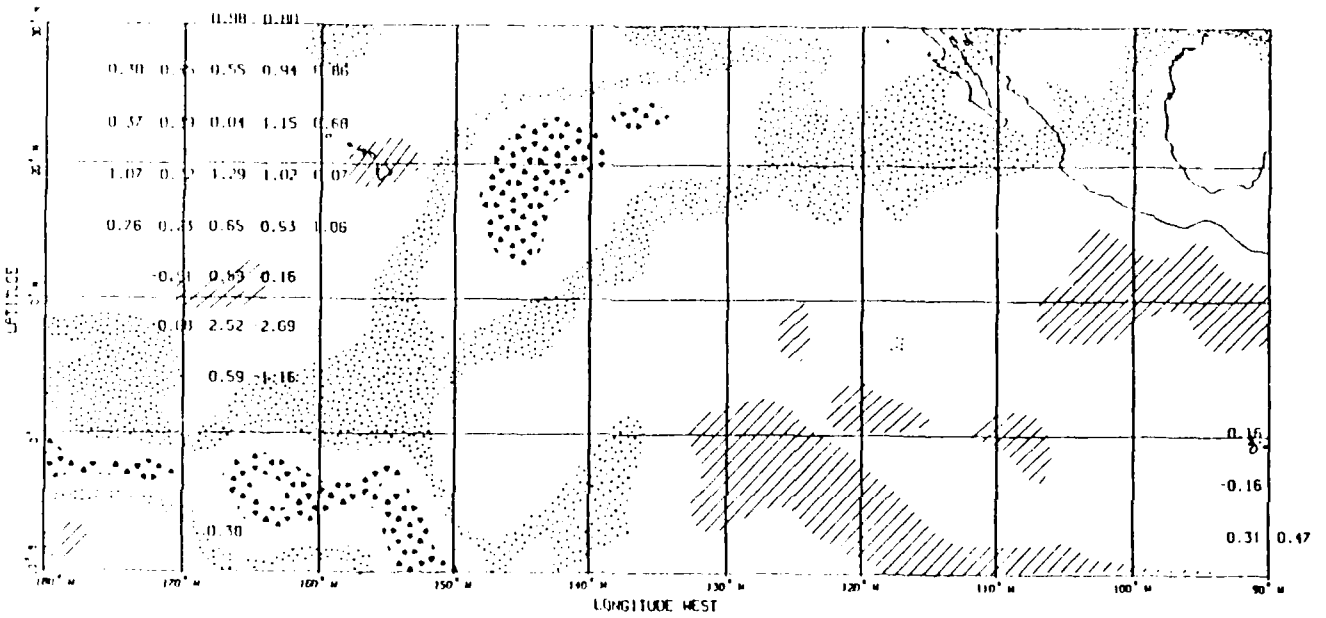

Figure 14a. OLR radiances from 0000 UTC 22 January 1979 overlying channel 12 vertical motion estimates (cm s^{-1}) for the 12-h period ending 1200 UTC 22 January 1979.

OLR = 200-240 watts m^{-2}

OLR ≥ 280 W m^{-2}

OLR ≤ 160 W m^{-2}

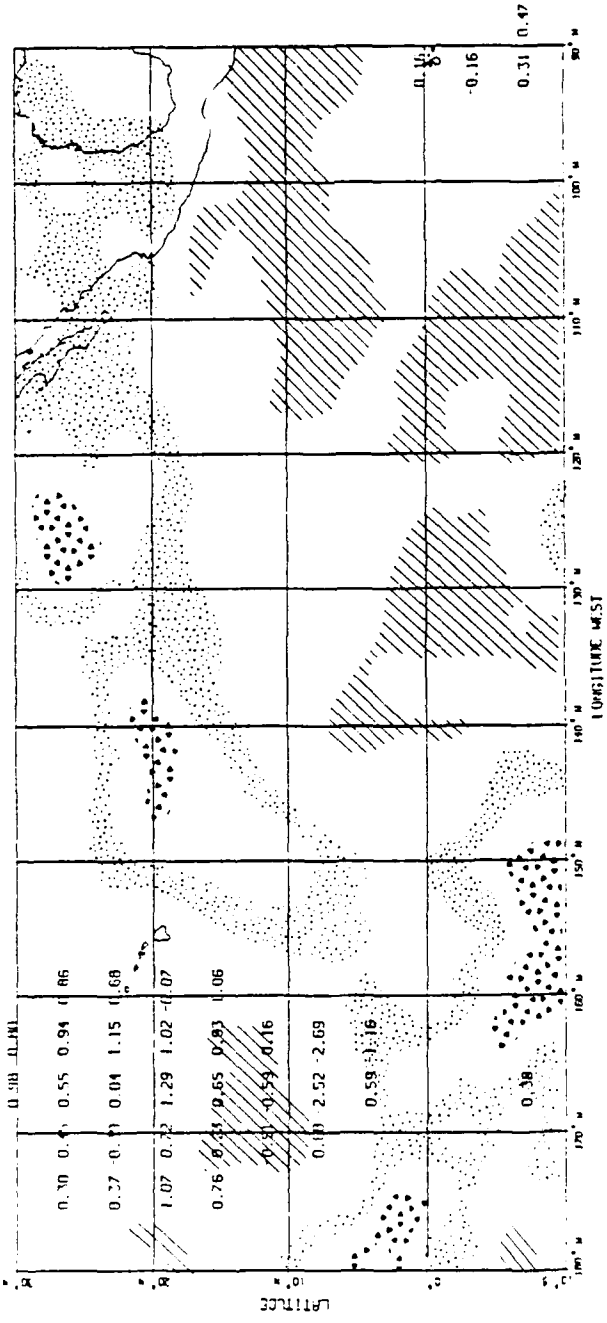

Figure 14b. As in Fig. 14a except for OLR radiances from 1200 UTC 22 January 1979.

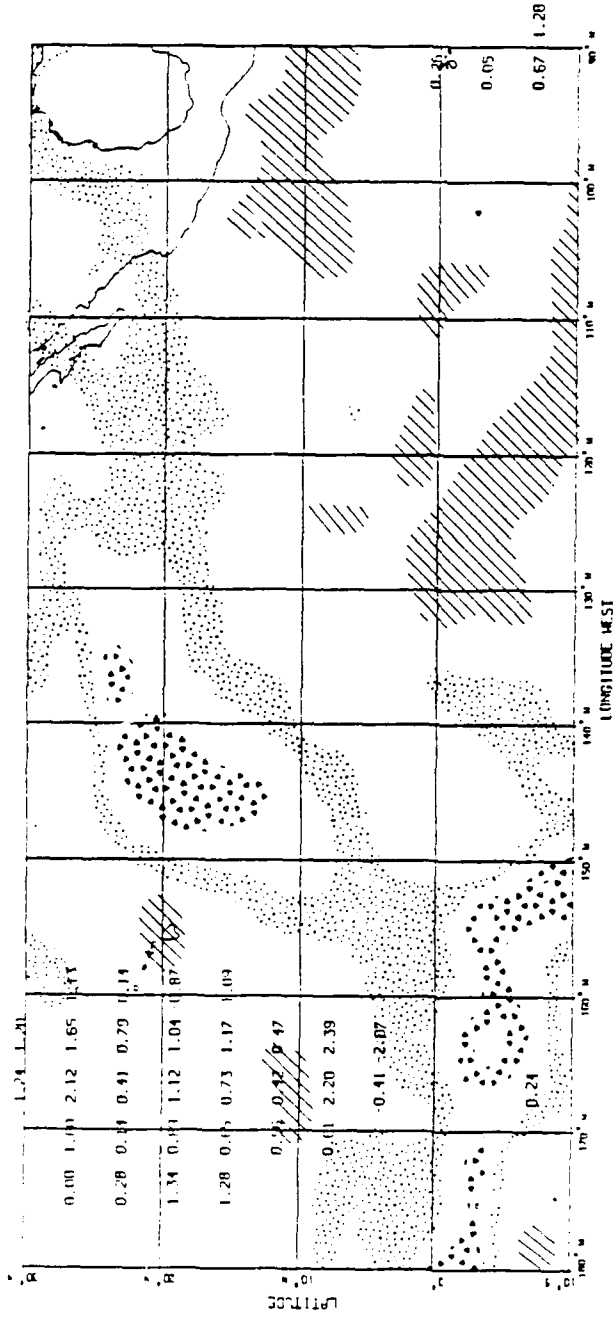

Figure 14c. As in Fig. 14a except for channel 11 vertical motion estimates.

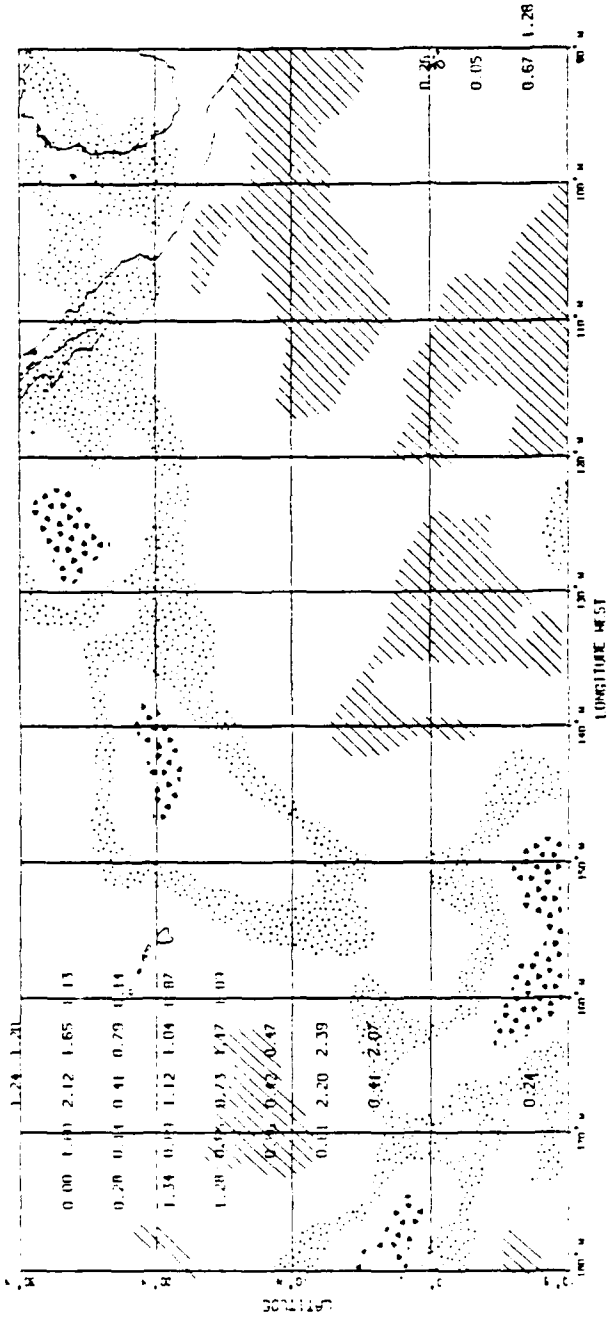

Figure 14d. As in Fig. 14b except for channel 11 vertical motion estimates.

W m^{-2} area changed little during this 12-h period and probably was indicative of continued subsidence. Weak subsidence was indicated by channel 12 vertical motion estimates throughout most of this area; however, channel 11 vertical motion estimates displayed a mixed pattern of weak ascent and descent. Of greater interest was the moisture channel vertical motion showing ascent in excess of 1 cm s^{-1} near 15°N/100°W while the OLR values indicated subsidence by sharply expanding northward.

A study of the channel 12 vertical motions (Fig. 16a or 16b) and channel 11 vertical motions (Fig. 16c or 16d) during the period from 0000 UTC to 1200 UTC on the 28th revealed an extensive region of moderate ascent near Hawaii between 10°N-20°N and 140°W-160°W. Upward vertical velocities on the order of 1.5-2.5 cm s^{-1} and 1.0-2.0 cm s^{-1} for channel 12 and 11, respectively, predominated within this area. However, as shown in Figs. 16a and 16b, a rapid eastward expansion of very high OLR values was occurring throughout this 12-h period. Infrared window channel satellite imagery at 1215 UTC on 28 January confirmed the lack of cloudiness in this region, thus supporting these observed high OLR values. General subsidence within this region seemed plausible; yet, moisture channel vertical motions indicated significant ascent. This represented the most flagrant disagreement in comparisons thus far.

Additional disagreement was seen along the southern coast of Mexico near 100°W and southeast of Hawaii near 4°N/138°W. In the former region, moisture channel ascent exceeding 1 cm s^{-1} was evident; however, significant subsidence was indicated in the OLR

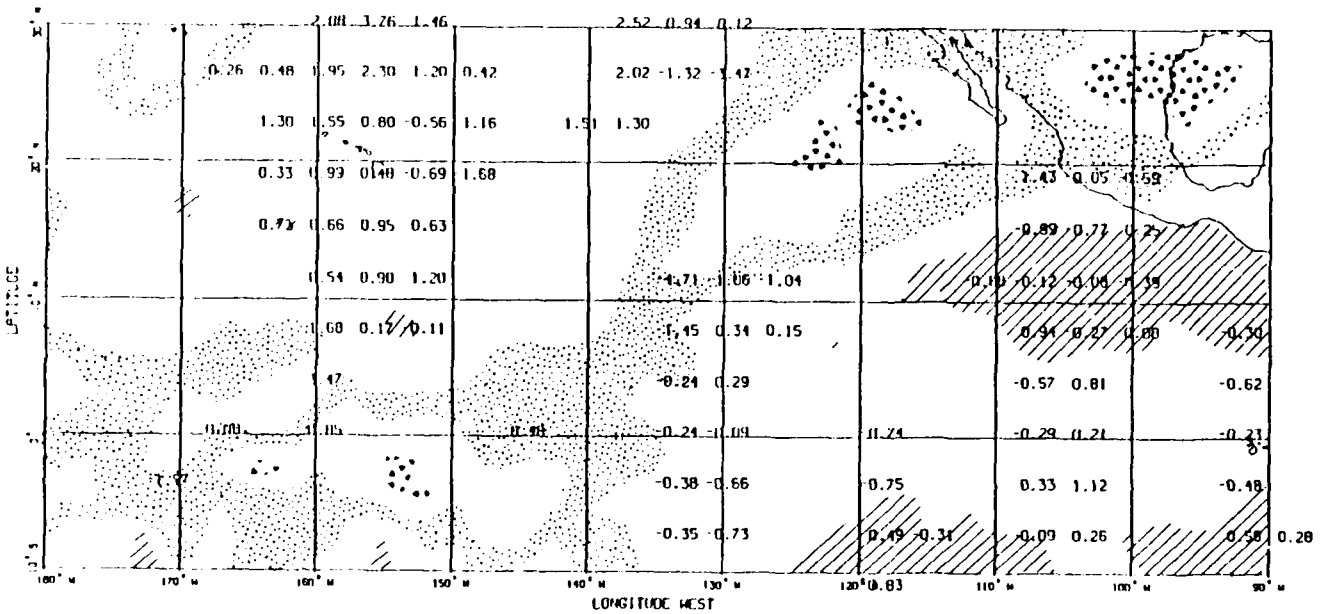

Figure 15a. OLR radiances from 0000 UTC 26 January 1979 overlying channel 12 vertical motion estimates (cm s^{-1}) for the 12-h period ending 1200 UTC 26 January 1979.

OLR = 200-240 W m^{-2}

OLR ≥ 280 watts m^{-2}

OLR ≤ 160 W m^{-2}

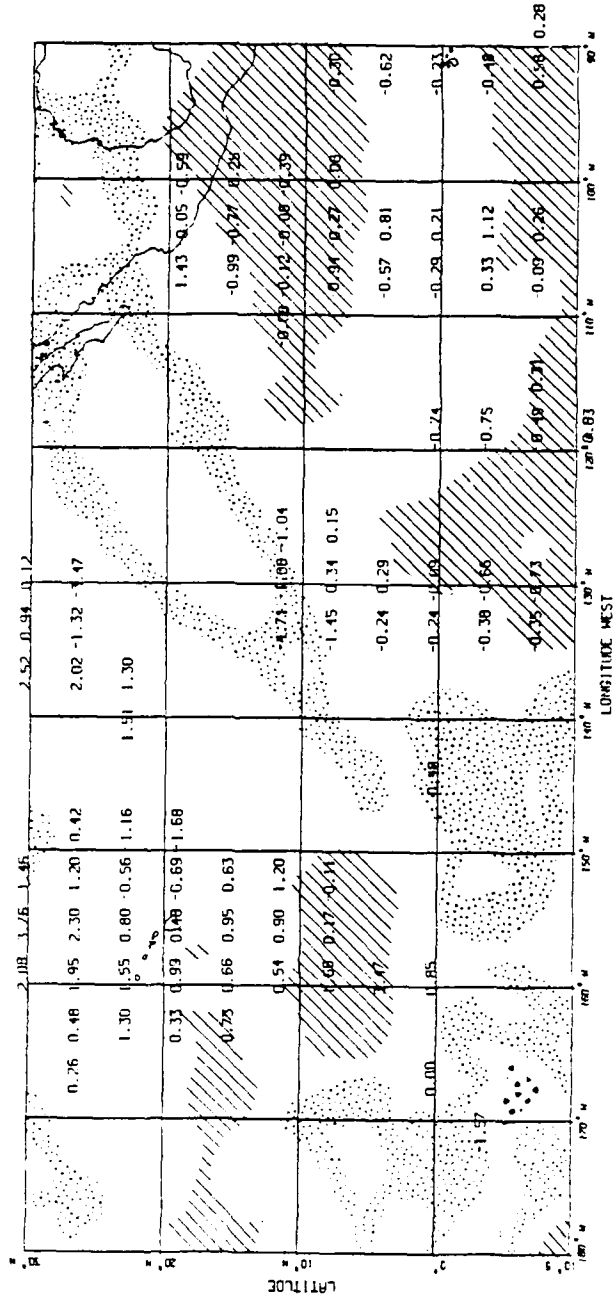

Figure 15b. As in Fig. 15a except for OLR radiances from 1200 UTC 26 January 1979.

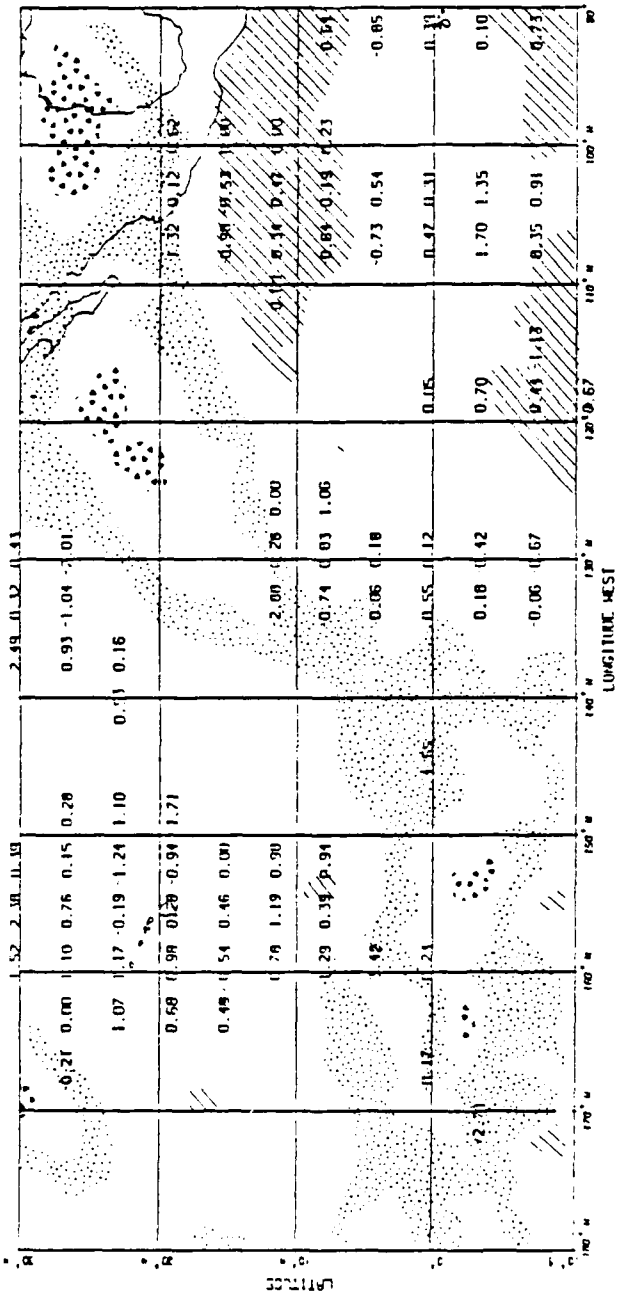

Figure 15c. As in Fig. 15a except for channel 11 vertical motion estimates.

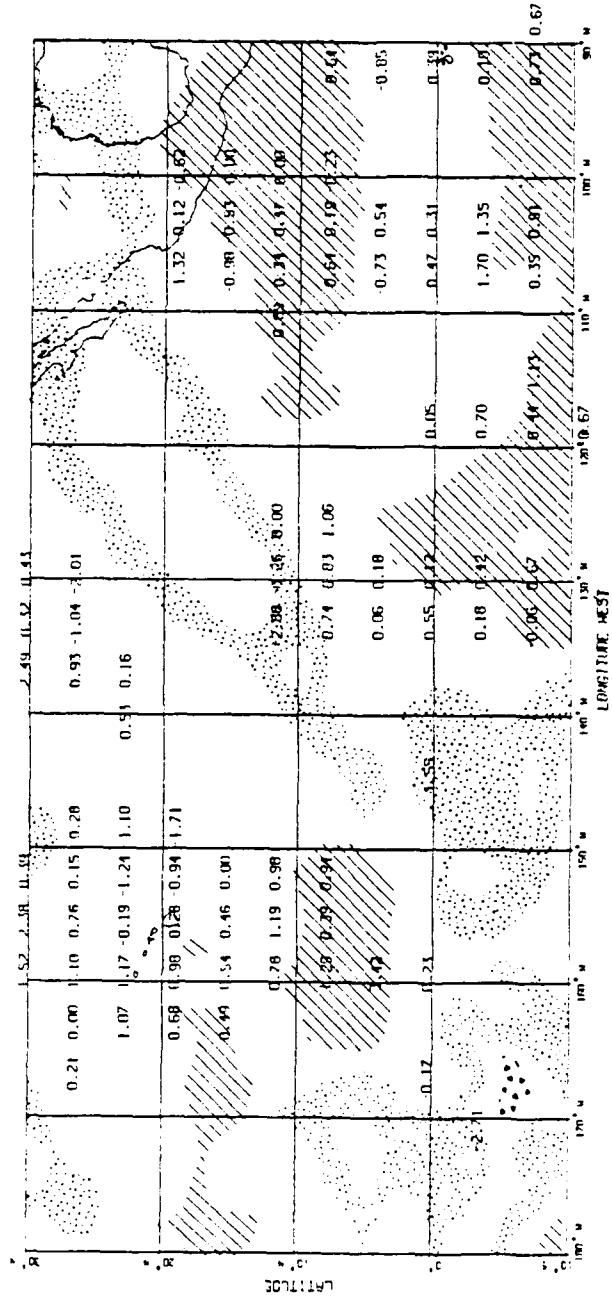

Figure 15d. As in Fig. 15b except for channel 11 vertical motion estimates.

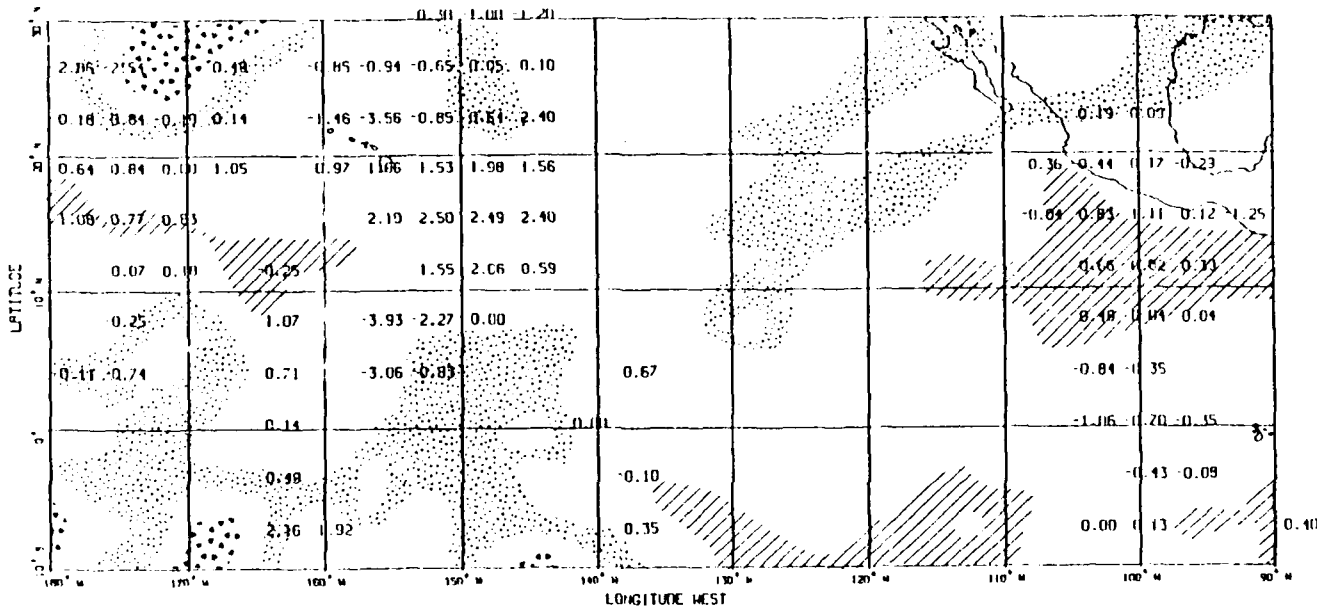

Figure 16a. OLR radiances from 0000 UTC 28 January 1979 overlying channel 12 vertical motion estimates (cm s^{-1}) for the 12-h period ending 1200 UTC 28 January 1979.

OLR = 200-240 watts m^{-2}

OLR ≥ 280 W m^{-2}

OLR ≤ 160 W m^{-2}

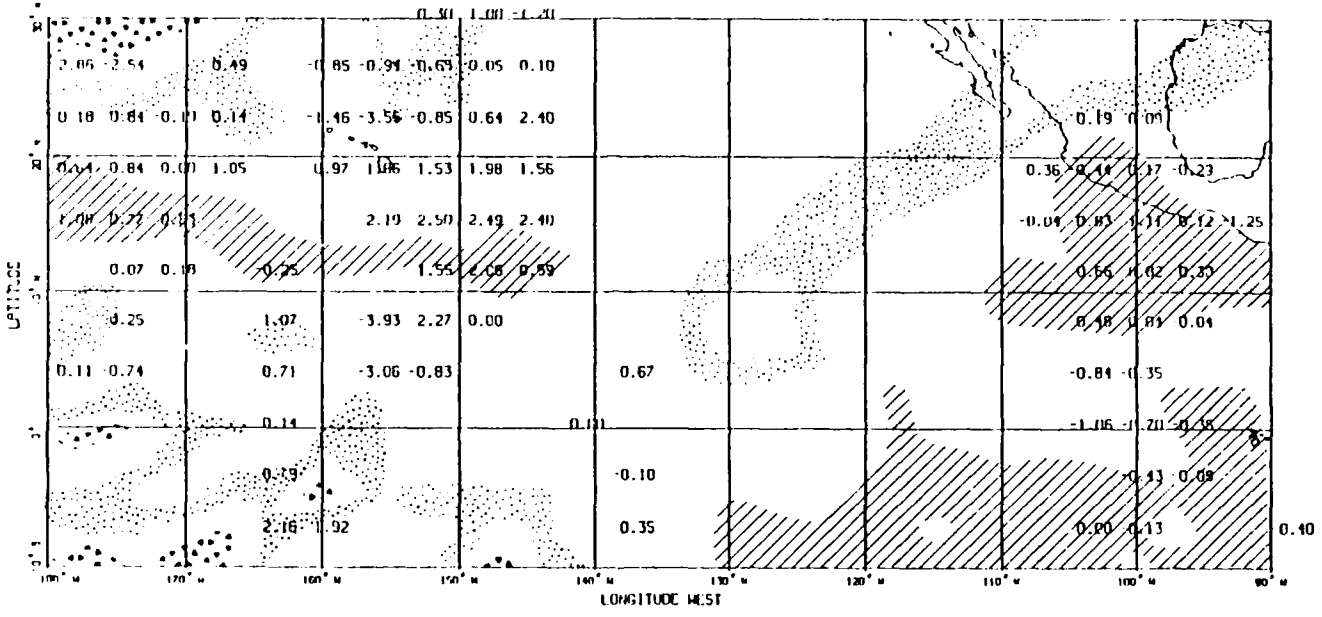

Figure 16b. As in Fig. 16a except for OLR radiances from 1200 UTC 28 January 1979.

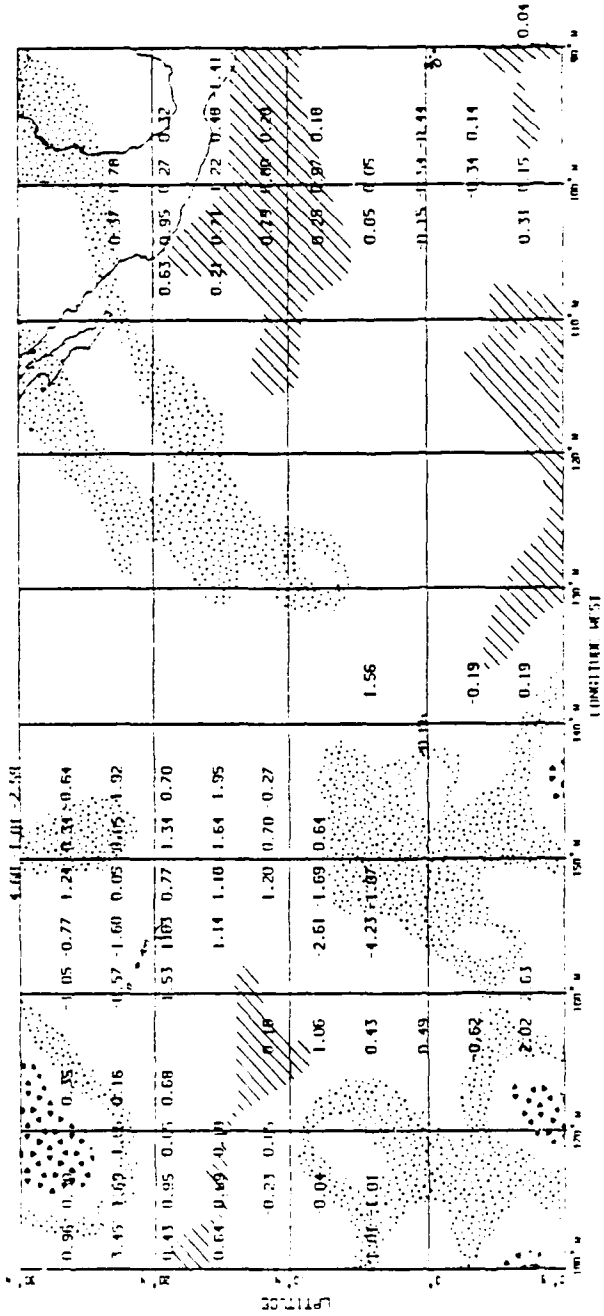

Figure 16c. As in Fig. 16a except for channel 11 vertical motion estimates.

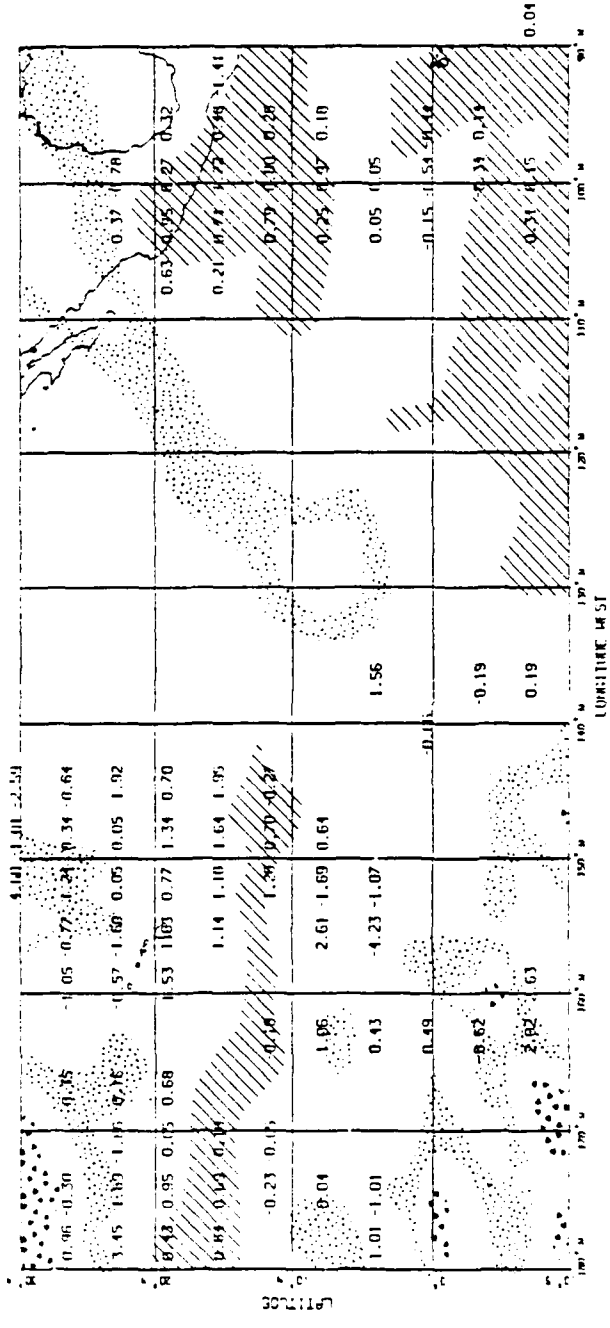

Figure 16d. As in Fig. 16b except for channel 11 vertical motion estimates.

analyses. These already high OLR radiance values rapidly increased to over 290 W m^{-2} and represented the largest values observed in the eastern Pacific during this 12-h period. Also displayed was the general weak ascent in the moisture channel vertical motions directly through the heart of this high OLR radiance region primarily north of 10°N between 90°W and 110°W. The latter region southeast of Hawaii showed persistent, fairly high OLR values; yet, the channel 11 vertical motion calculations presented an upward velocity of 1.6 cm s^{-1} while channel 12's was upward at a reduced velocity of 0.7 cm s^{-1}.

Further equatorward, intense subsidence was exhibited in the moisture channel vertical motions south of Hawaii between 3°N and 10°N. The analyses indicated OLR values changed very little and remained near 260 W m^{-2}; therefore, subsidence seemed reasonable within this higher OLR region. More agreement was found near 8°S between 160°W and 170°W where low OLR values supported the moisture channel vertical velocities of 2-3 cm s^{-1}. In addition, considerable harmony was shown in the region north of 20°N between 140°W and 160°W. Here, subsiding moisture channel vertical velocities up to -3.5 cm s^{-1} just north of Hawaii coincided with a persistent area of fairly high OLR values near 260 W m^{-2} while rapidly ascending moisture channel vertical motions occurred to the northeast of Hawaii in a region of rapidly falling OLR values associated with a synoptic cloud system.

In summary, vertical motion signatures from OLR analyses (Julian, 1984) were subjectively compared to collocated BT vertical motion

estimates. No systematic agreement was found. Particularly distressing were the BT estimates of 1-3 cm s^{-1} ascent within rapidly expanding regions of high OLR radiances which should denote deep tropospheric subsidence.

3. Velocity Potential Fields

In a study of the divergent wind component found in tropical wind fields, Snyder (1985) produced analyses of 850- and 200-mb velocity potential fields of the eastern tropical Pacific. These analyses were constructed at 12-h intervals covering the period 0000 UTC 21 January to 1200 UTC 22 January 1979. He consistently found that 850-mb centers of low velocity potential (divergence indicator) were overlain by 200-mb centers of high velocity potential (convergence indicator), and vice versa. Thus, in regions of 850-mb low velocity potential (LVP) overlain by 200-mb high velocity potential (HVP), subsidence should predominate.

Throughout this 36-h period, a region of HVP underlain by a region of persistent LVP dominated the subtropical Pacific around Hawaii. This region was roughly bounded by latitudes 15°N to 25°N and longitudes 155°W to 175°W. Therefore, similar to the OLR signatures previously discussed, these velocity potential fields strongly suggested persistent, strong subsidence within this region.

Channel 12 and 11 derived vertical motions (Figs. 17a and 17b) from the 1200 UTC on the 21st to 0000 UTC on the 22nd indicated weak subsidence primarily west of 170°W and/or south of 20°N; however, in direct conflict with the velocity potential field (not shown; see

Snyder, 1985), ascending velocities over 1 cm s^{-1} were observed directly north and northwest of Hawaii. Even worse, the 0000 UTC to 1200 UTC channel 12 and 11 vertical motions (Figs. 14a and 14c) on the 22nd showed a complete lack of agreement with the velocity potential field throughout the entire region north of 15°N and west of 160°W. Worse yet, some of the moisture channel ascending velocities exceeded 2 cm s^{-1}.

In summary, the poor correlation between vertical motion estimates derived using the adiabatic method and the vertical motion estimates derived from moisture channel data concurred with the absence of a systematic agreement with OLR and velocity potential analyses and the same moisture channel-derived vertical motion estimates. Since tropospheric moisture profiles derived from rawinsondes were used as "ground truth", it is hypothesized that the two moisture sensitive satellite channels used in this study may have detected moisture which is beyond the sensing capability of conventional rawinsondes. It is further hypothesized that horizontal moisture advection introduced a significant amount of error into the above comparisons. The hypothesis stated above pertaining to the sensing capability of rawinsondes is explored in the following chapter; the hypothesis pertaining to horizontal moisture advection is discussed in the next section of this chapter.

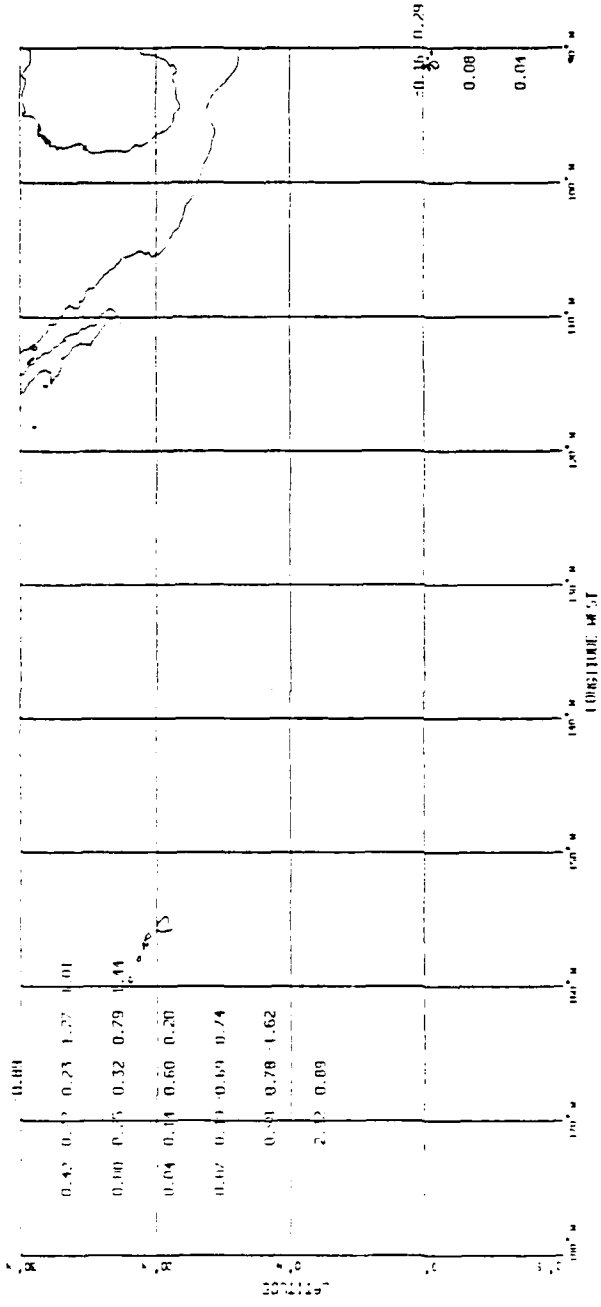

Figure 17a. Channel 12 vertical motion estimates (cm s^{-1}) for the 12-h period ending 0000 UTC 22 January 1979.

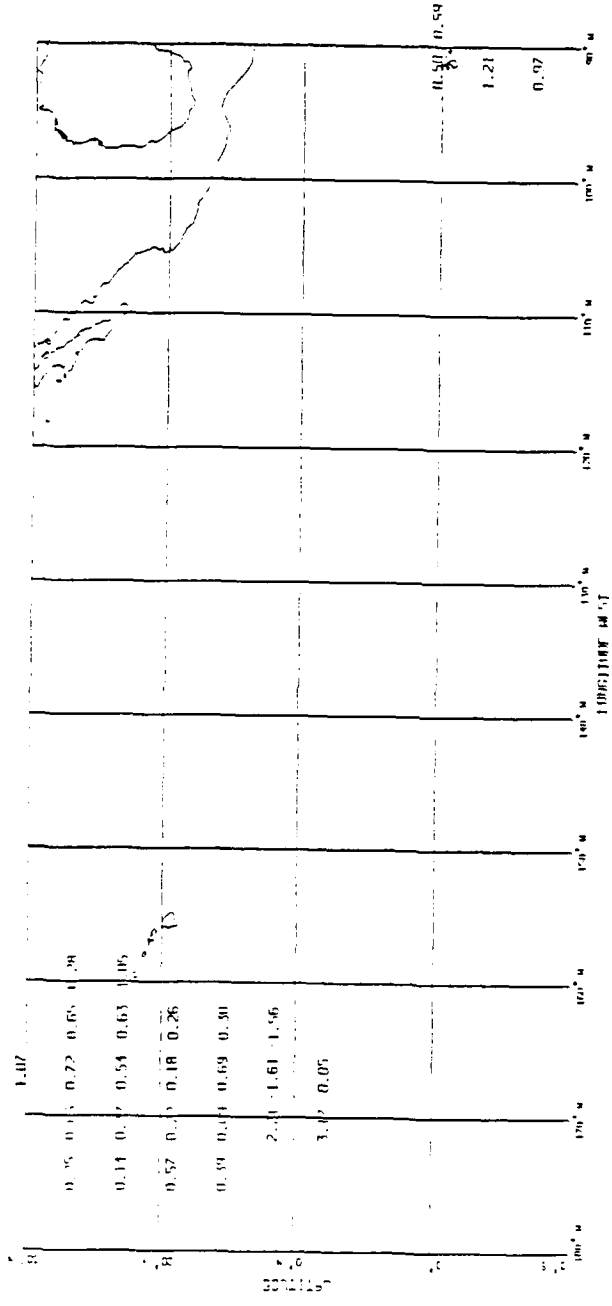

Figure 17b. As in Fig. 17a except for channel 11.

D. Effect of Horizontal Moisture Advection

Schaefer (1985) found large regions in the subtropical eastern Pacific which experienced 300-mb winds in excess of 48 m s^{-1} during the last ten days of January 1979. Although most of the 300-mb winds over the eastern Pacific were considerably lighter during this period, significant local changes in BTs may have occurred over a span of a few hours simply due to strong horizontal moisture advection.

A detailed study of the influence of horizontal moisture advection during this period was not accomplished due to the severe shortage of reliable data within this region. However, in a more subjective study, moisture was assumed to be conserved; therefore, the horizontal advection of moisture was used to estimate the vertical advection of moisture. This study was performed using available moisture channel BTs and ECMWF wind analyses.

Available BTs were gridded every 12 h by the Barnes procedure discussed in Chapter V. Where the data were sufficiently dense, zonal and meridional BT gradients were calculated. Next, temporally corresponding winds from the 400-, 500-, and 700-mb pressure levels were divided into their respective zonal (u) and meridional (v) components. From these velocities, the average wind components were computed for the 400-500 mb, and 500-700 mb layers. Thus, by multiplying these layer-averaged wind components by the appropriate BT gradients, BT changes due to local moisture advection effects were estimated at 12-h intervals. Finally, from these simulated BT changes, values representing the effect of horizontal moisture

advection were computed for each of the two pressure layers using equations (1) and (2) and the BT vertical motion method discussed earlier in this chapter.

Thus, this simulation was a crude test to determine whether the magnitudes of the values representing the effect of horizontal moisture advection were approximately the same as the magnitude of the BT vertical motion estimates computed earlier using the same two equations. If the magnitudes are approximately equal, it may be concluded that the observed channel 12 and 11 BT changes may have been influenced primarily by horizontal rather than vertical moisture advection.

Channel 12 BTs and the ECMWF wind analysis from 0000 UTC on 28 January were used in the above method to produce the values representing the effect of horizontal moisture advection shown in Fig. 18. The maximum magnitudes of these values were equivalent to the maximum magnitudes observed in the channel 12 BT vertical motion estimates computed earlier in the chapter. However, comparisons of these magnitudes at individual grid points showed little similarity. Channel 12 correlations between the values representing the effect of horizontal moisture advection and the BT vertical motion estimates were poor. These correlations, computed from BT changes produced by the 400-500 mb layer winds and the 500-700 mb layer winds, respectively, were 0.26 and 0.31.

Analogous to these channel 12 results, maximum magnitudes produced from the channel 11 BT/ECMWF wind analysis for 0000 UTC on the 28th (Fig. 19a and 19b) revealed values which were close to the

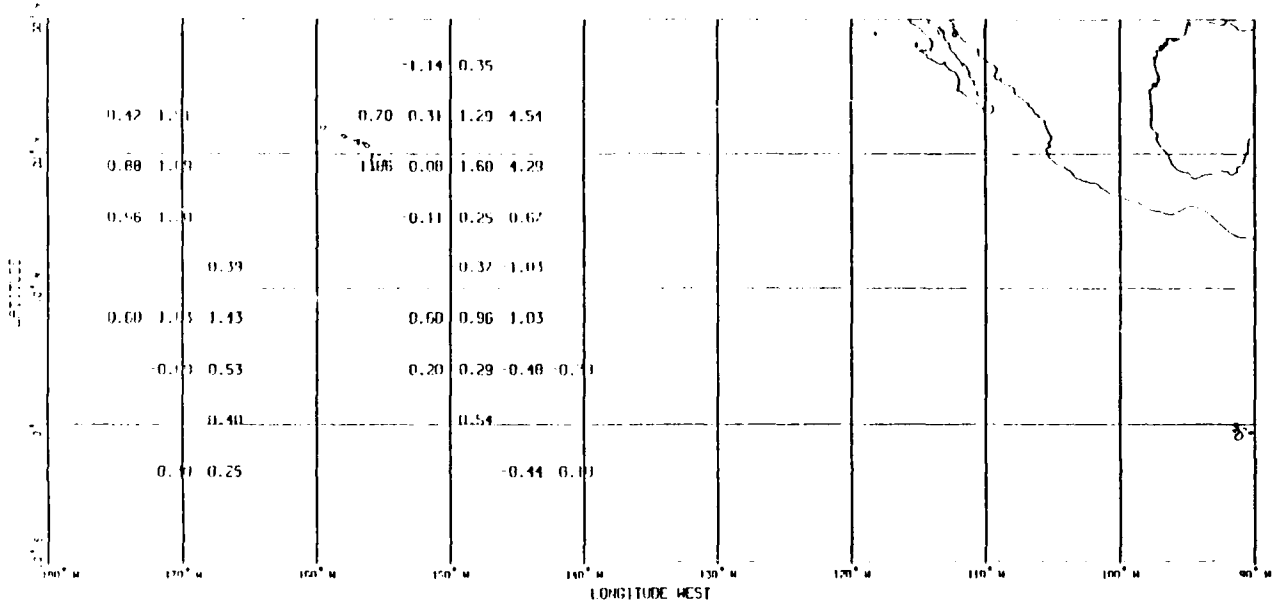

Figure 18a. Channel 12 twelve-hour values (cm s^{-1}) representing the effect of horizontal moisture advection by 400-500 mb layer-averaged winds for data sampled at 0000 UTC 28 January 1979.

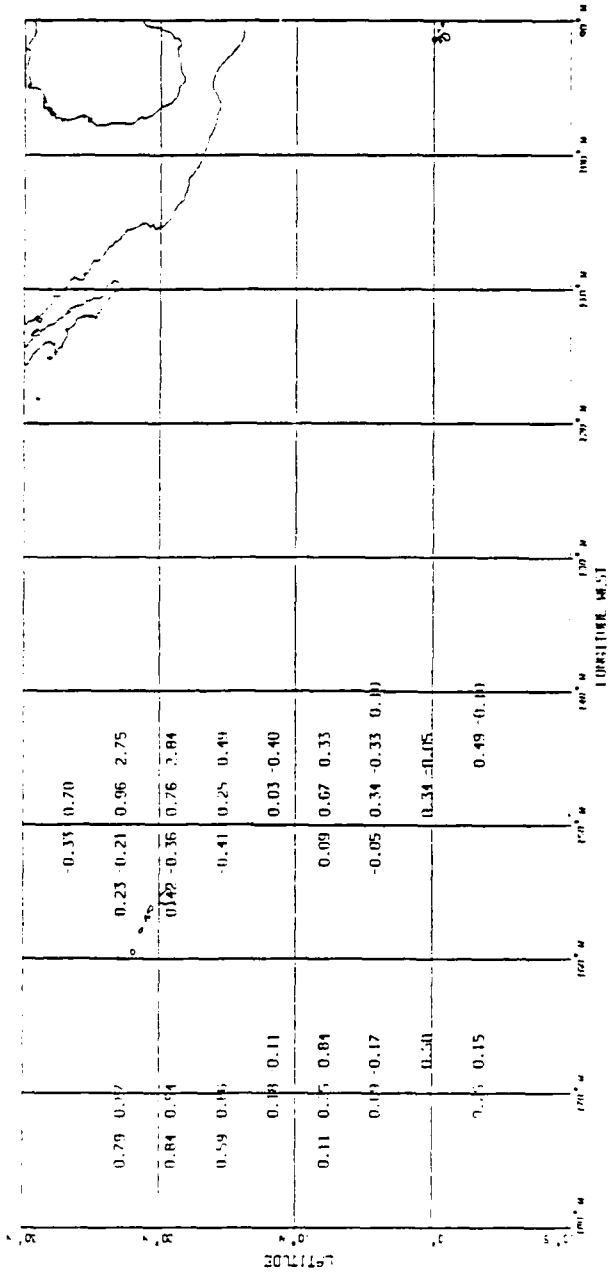

Figure 18b. As in Fig. 18a except for 500-700 mb layer averaged winds.

maximum magnitudes observed from the channel 11 vertical motion estimates. Yet, channel 11 correlations between these horizontal moisture advection values and the BT vertical motion estimates were worse than the channel 12 correlations. The channel 11 correlation computed from BT changes produced by the 400-500 mb layer winds was only 0.15, while the correlation obtained from BT changes produced by the 500-700 mb layer winds was limited to 0.28. Similar results for channels 12 and 11 were indicated for each period examined from 21-29 January.

In summary, much similarity was observed between the maximum magnitudes of the values representing the effect of horizontal moisture advection and the maximum magnitudes of the estimates produced from observed BT changes. This similarity in magnitudes indicated that horizontal moisture advection had the potential of being the dominant influence on observed BT changes. However, the consistently weak correlation at individual grid points between values produced from advection-BT changes and estimates produced from observed-BT changes indicated inconclusive results as to the actual influence of horizontal moisture advection on observed BT changes.

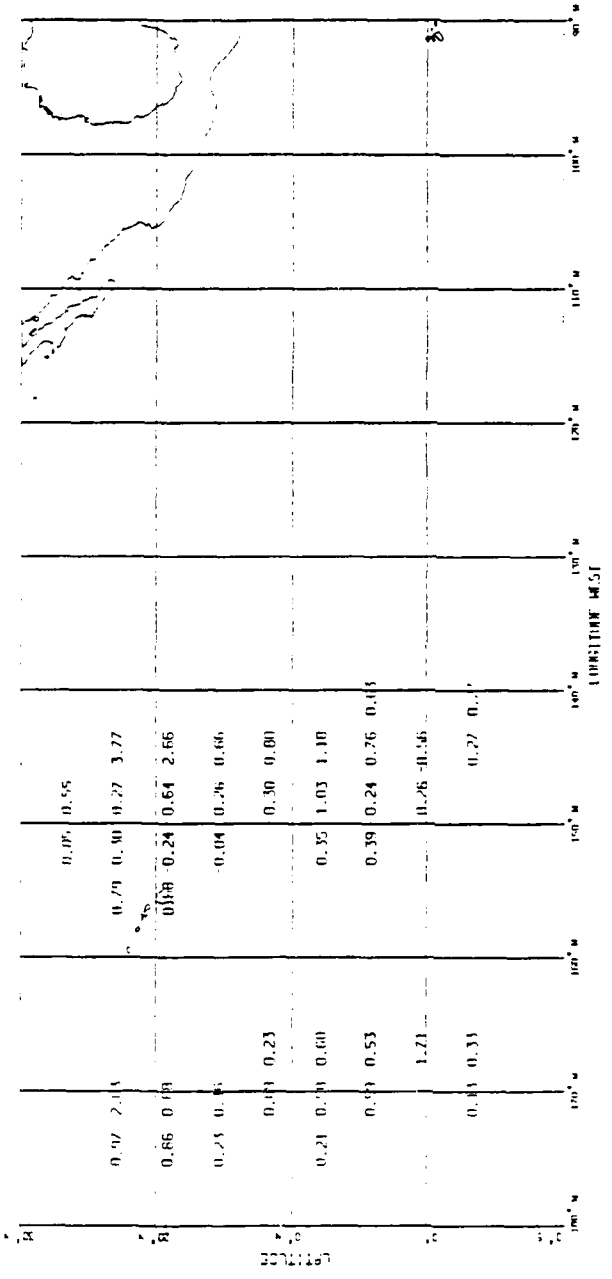

Figure 19a. As in Fig. 18a except for channel 11.

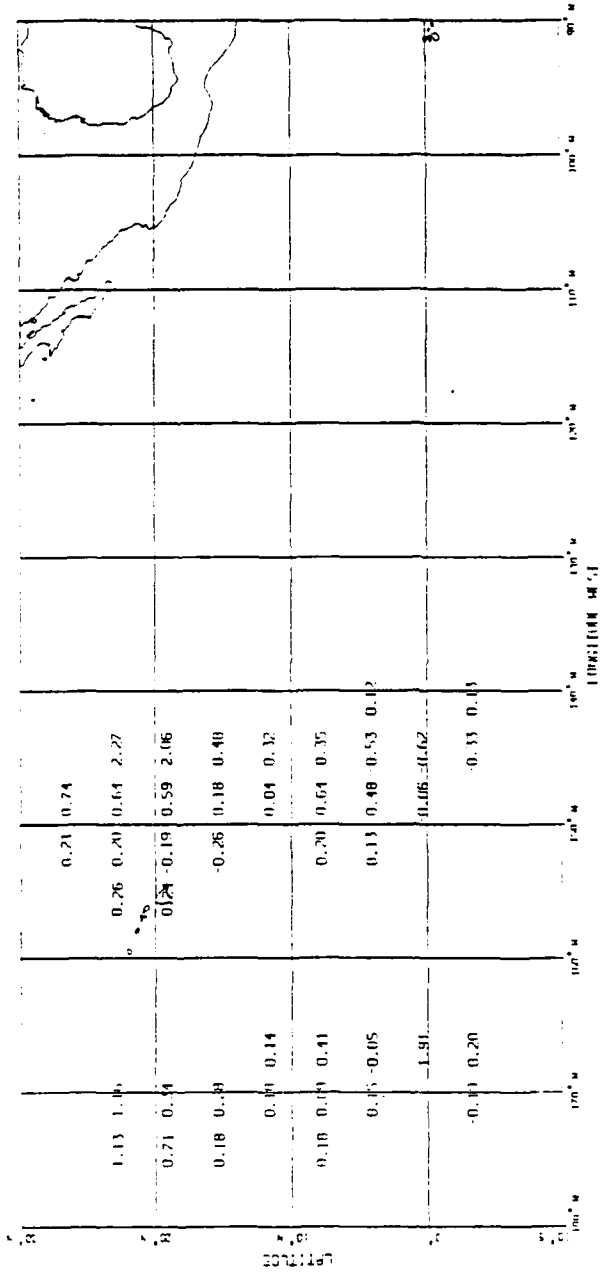

Figure 19b. As in Fig. 18b except for channel 11.

CHAPTER VII

MOISTURE SAMPLING ERRORS

The high linear correlation (in excess of 0.8) between rawinsonde PWTPs and satellite BTs for both channels supports the hypothesis, stated in Chapter VI, that local changes in the height of the upper moist layer detected by satellite may be used to infer vertical motions. But, as also seen in Chapter VI, horizontal moisture advection may be a cause of local BT changes. However, the large RMS error of BT-derived pressure levels with respect to PWTP levels estimated from collocated rawinsonde measurements suggests that collocated rawinsonde and satellite measurements may not be sampling the same moist layers in the middle and upper troposphere.

A. Comparisons of PWTP, BT and Sounding Profiles

If rawinsonde and satellite were actually sensing the same moist layers, then the rawinsonde/satellite plots of PWTP versus BT for each sounding location should form a line roughly parallel to the composite linear regression curve for all sounding locations. The channel 12 and channel 11 composite curves are shown in Fig. 11 and Fig. 12, respectively. Fig. 20a shows the 0.6 mm PWTP/channel 12 BT scatter plot; each individual station is represented by a specific letter. Similarly, specific letters represent individual stations in the 0.9 mm PWTP/channel 11 BT scatter plot shown in Fig. 20b.

Points marked "B" (Johnston Island) in Fig. 20a represented very dry soundings with most having less than 0.6 mm of PW above the

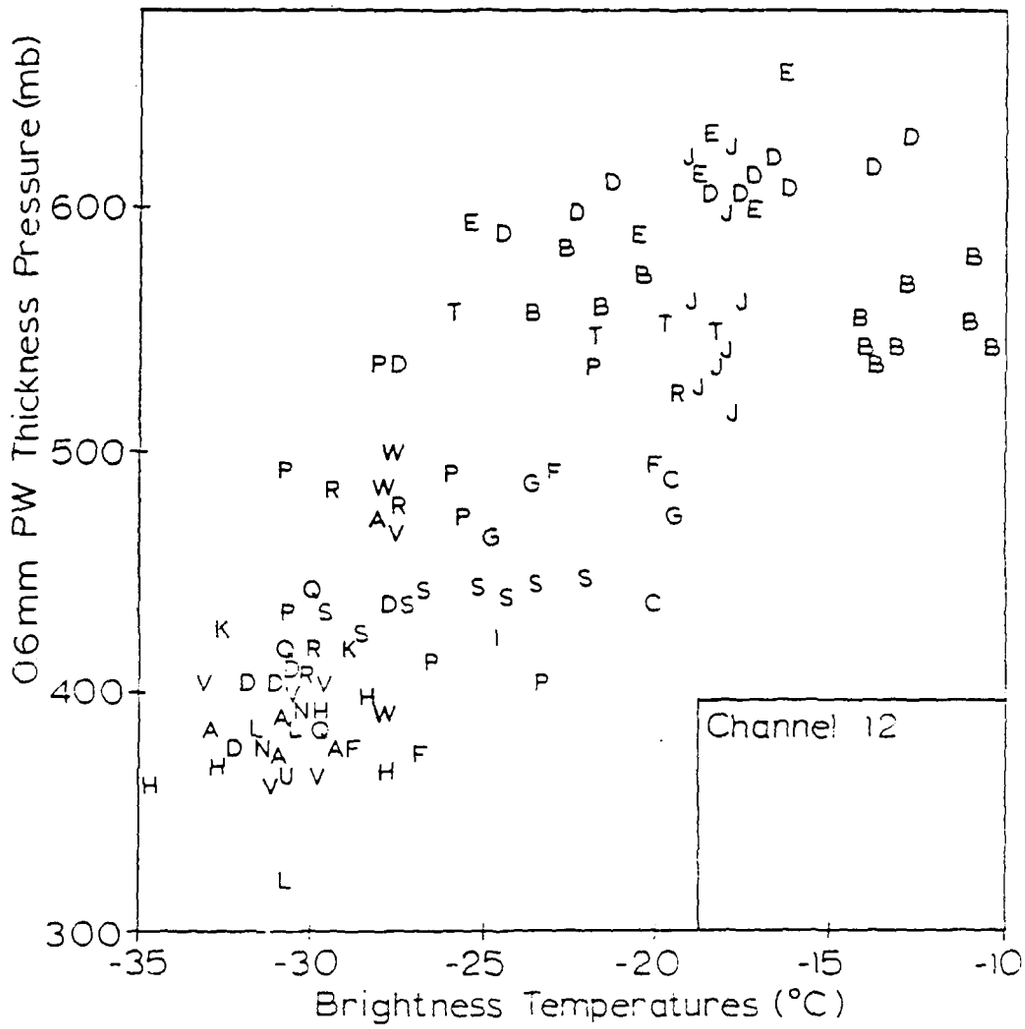

Figure 20a. As in Fig. 11 except for use of letter-plots and omission of regression curves. Each rawinsonde station is represented by a letter (A=91700, B=91275, C=91066, D=91165, E=91285, F=91487, G=CROMW, H=PARIZ, I=DISCO J=MATAM, K=76723, L=76225, M=76612, N=72261, O=76394, P=76679, Q=72255 R=72250, S=76692, T=78641, U=76256, V=76458, W=76654).

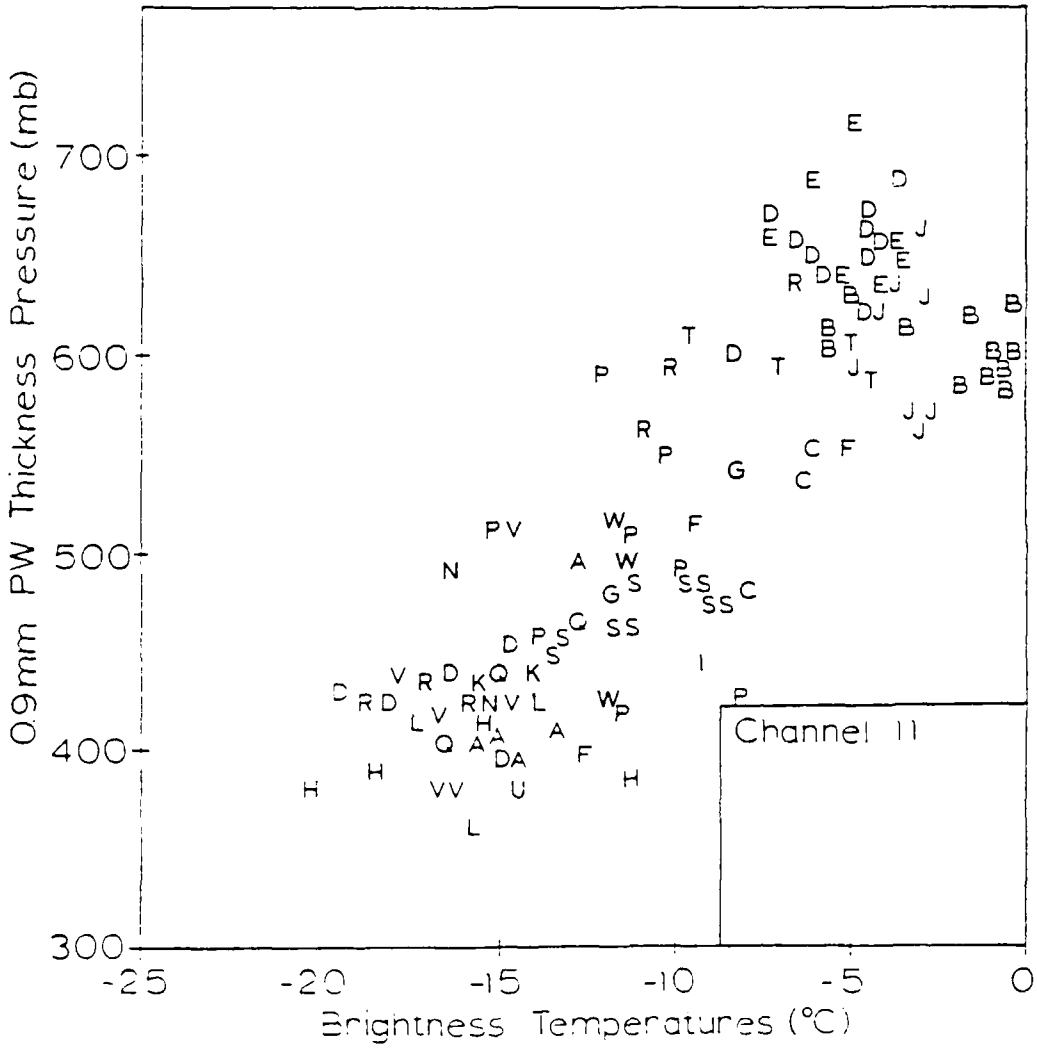

Figure 20b. As in Fig. 20a except for channel 11 and 0.9 mm PWTP.

550 mb surface. Fig. 21a shows the distribution of "B"s with respect to the linear regression curve for all data shown in Fig. 20a. The slope of the best fit curve for the data represented by the "B"s is different from the composite slope of the regression line of the data shown in Fig. 11 and Fig. 20a. The nearly horizontal orientation of a best fit line through this data plot suggests that the moisture profiles, as determined by rawinsonde for all 12 Johnston Island soundings, were very closely related. The 0.6 mm PWTPs for all the Johnston Island soundings varied by only 41 mb in range (12% of the total PWTP range shown in Fig. 20a); however, the collocated channel 12 BTs differed up to 14°C (56% of the total BT range in Fig. 20a).

Like Fig. 21a, the channel 11 BT/0.9 PWTP scatter plot (Fig. 21b) showed a similar lack of slope; however, there was less variation in channel 11 BTs than was observed in channel 12 data. This reduced variation suggests that the Johnston Island soundings may have closely resembled one another in channel 11 imagery. In contrast to channel 12 data, this smaller variation of channel 11 BTs also inferred that channel 11 BTs may have recognized mean-profile similarities in soundings better than channel 12 data.

Similar Johnston Island soundings are shown for 0000 UTC on 23 January 1979 (see Fig. 5) and for 1200 UTC on 28 January 1979 (Fig 22). The 24°C wet-bulb potential temperature curve is shown on both soundings as a reference. On the 23rd, a strong inversion existed near 700 mb, while the sounding on the 28th (Fig 22) showed the inversion at a lower elevation near 800 mb. Both soundings were

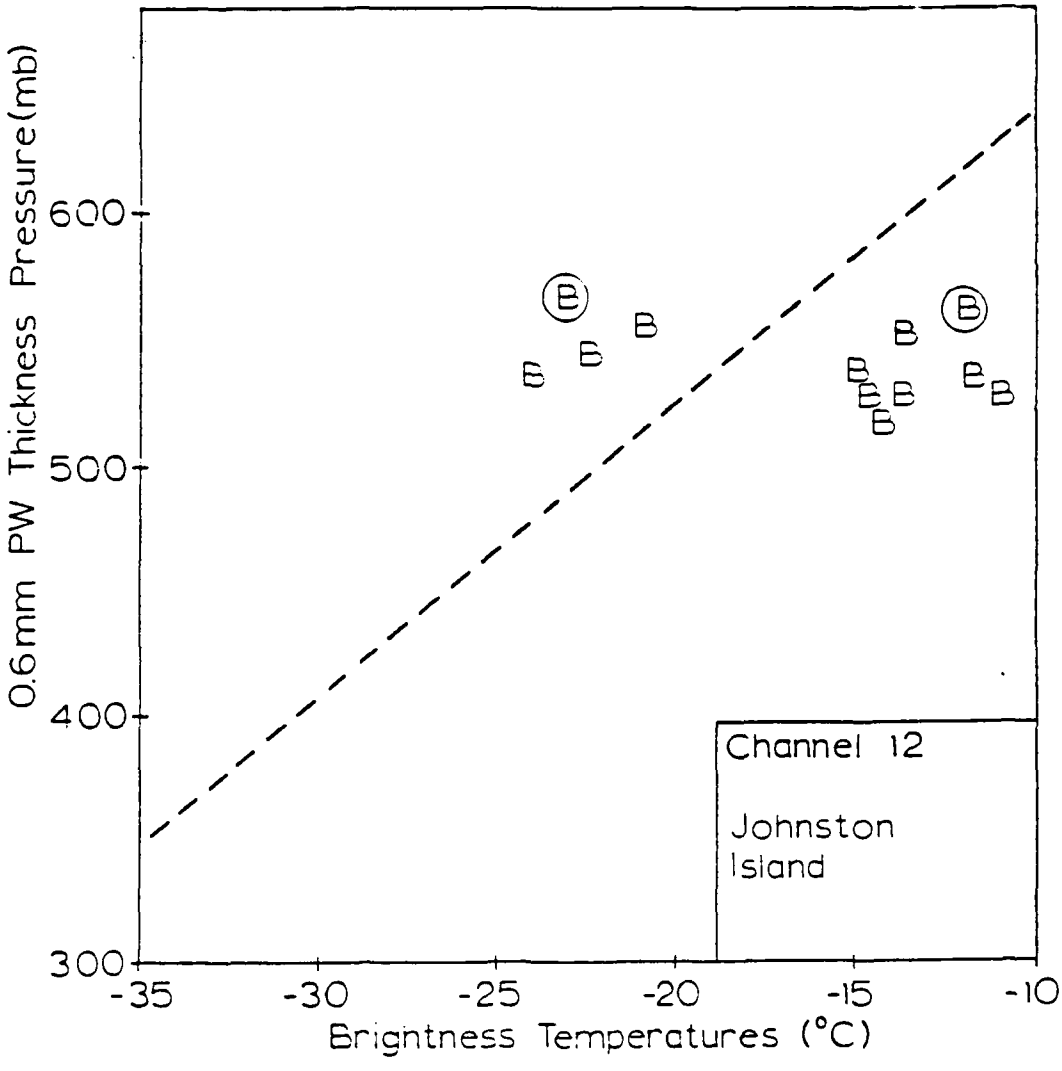

Figure 21a. Scatter plot of 0.6 mm PWTPs versus channel 12 BTs for Johnston Island (B=91275). Circled letters correspond to the two soundings discussed.

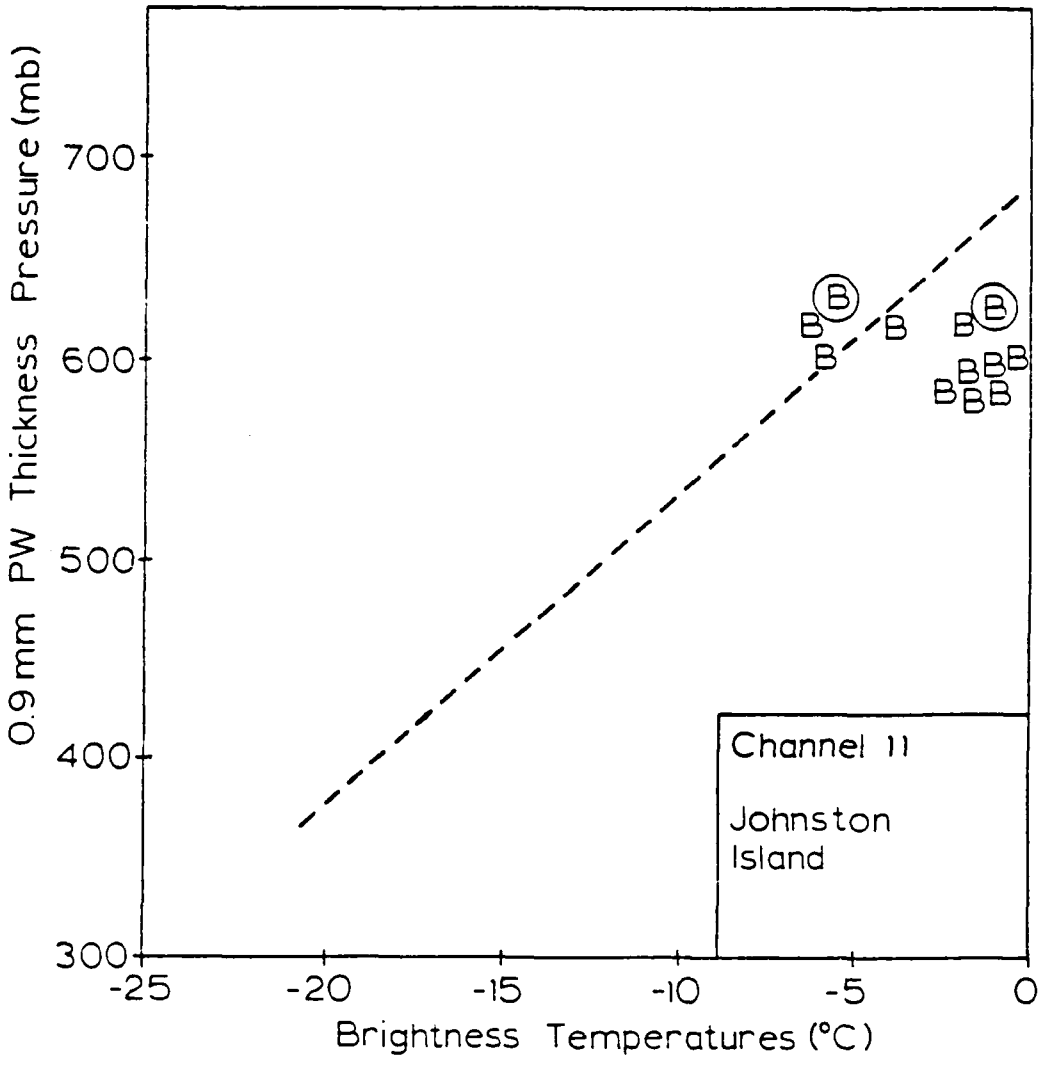

Figure 21b. As in Fig. 21a except for 0.9 mm PWTPs versus channel 11 BTs.

moist below and very dry (dew point depression defaulted to 30°C) above the inversion. Due to instrument limitations, dew point depressions, as measured by rawinsonde, which were greater than or equal to 30°C were recorded as 30°C. Therefore, actual dew point depressions likely were greater than 30°C; this larger actual dew point depression indicated the likely occurrence of a drier layer of air than that displayed in these soundings. More evidence of sounding similarity was shown by the rather insignificant 4 mb difference between their 0.6 mm PWTP's of 578 mb and 582 mb. Given these nearly identical rawinsonde soundings, one would expect only a small difference in collocated channel 12 BTs. Rather, the channel 12 BT difference between soundings was 12°C (46% of the BT range observed in Fig. 20a). Although the sounding on the 28th was colder in the 400-300 mb layer, the absence of detectable moisture in this layer significantly lessened the layer's influence on the collocated channel 12 BT.

Comparable to the small 0.6 PWTP variation between the two soundings noted in the previous paragraph, the 0.9 PWTPs varied by only 4 mb; however, unlike the channel 12 BTs, channel 11 radiance values differed by only 5°C, representing only 22% of the observed channel 11 BT range compared to 46% of the channel 12 range.

Analogous to the Johnston Island scatter plots shown in Figs. 21a and 21b, many other stations displayed slopes which were much different than respective composite slopes. The channel 12 and channel 11 PWTP/BT scatter plots for Lihue, Hawaii ("D") and Veracruz, Mexico ("S") are shown in Figs. 23a and 23b and in Figs.

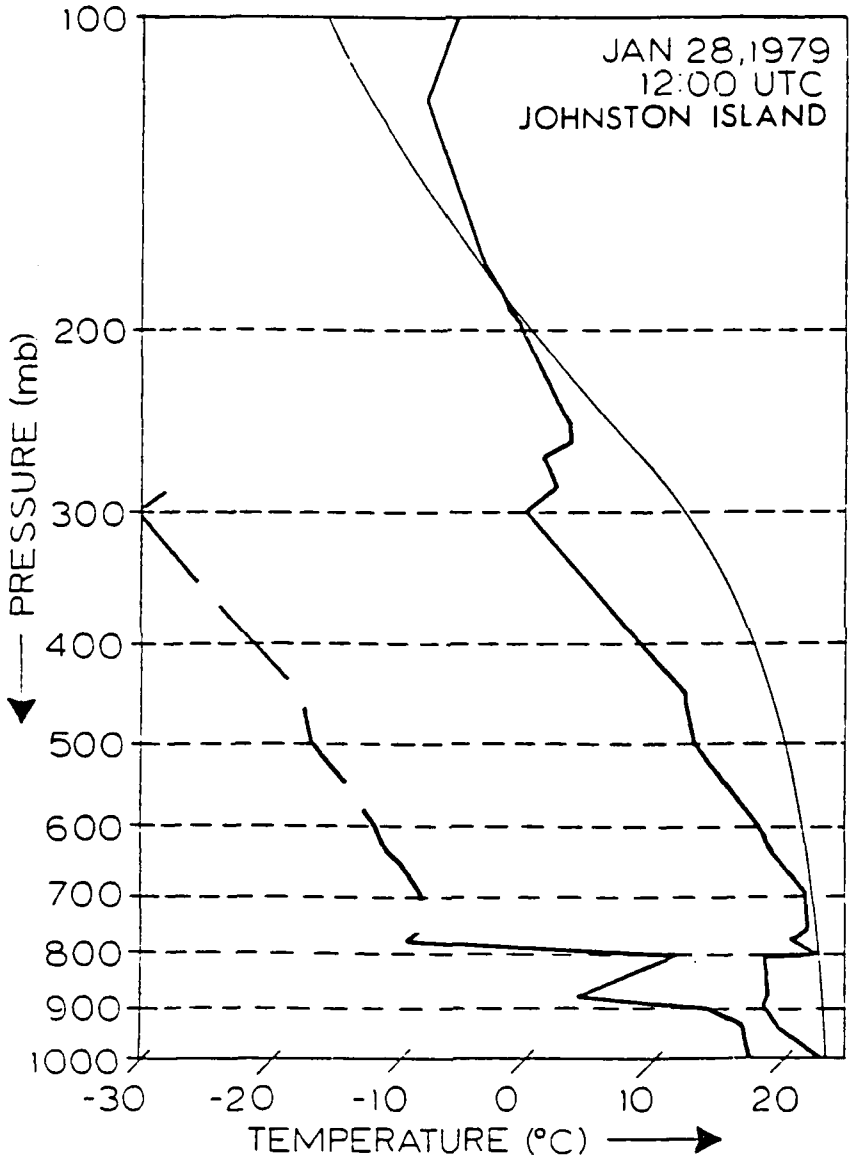

Figure 22. As in Fig. 5 except for 1200 UTC 28 January 1979.

24a and 24b, respectively. These closely resemble the trend noted in the Johnston Island plots.

A much different configuration was shown in the PWTP/BT scatter plots associated with soundings from the scientific ship Matamoros (Figs. 25a and 25b) in the Pacific dry zone south of Mexico (see Fig. 7). Unlike previous plots from Johnston Island, Lihue, Veracruz, and several other locations, the 0.6 mm PWTP/channel 12 BT (Fig. 25a) and the 0.9 mm PWTP/channel 11 BT (Fig. 25b) scatter plots from Matamoros displayed a nearly vertical slope which was much greater than the composite slope. Both of these plots showed considerable variation in PWTPs; yet, virtually no change in BTs.

Matamoros soundings from 2100 UTC on 26 January (see Fig. 6) and 29 January (Fig. 26) showed different moisture profiles in the middle and lower troposphere. This sounding difference was further demonstrated by the 93 mb PWTP difference derived from 0.6 mm PWTPs (620 mb on the 26th and 527 mb on the 29th). Likewise, from the same two soundings a 59 mb difference was calculated for the observed 0.9 mm PWTPs (629 mb on the 26th and 570 mb on the 29th). Given the channel 11 and 12 weighting function curves shown earlier in Chapter IV (see Fig. 1), these sizeable contrasts in middle and lower tropospheric moisture profiles seemingly warranted a significant disagreement in collocated channel 12 BTs and channel 11 BTs, respectively. Yet, almost no difference was observed. Channel 12 BTs and channel 11 BTs differed by less than 1°C.

The dew point depressions for the ship-launched rawinsondes were quality controlled by the operator between the surface and the 200 mb

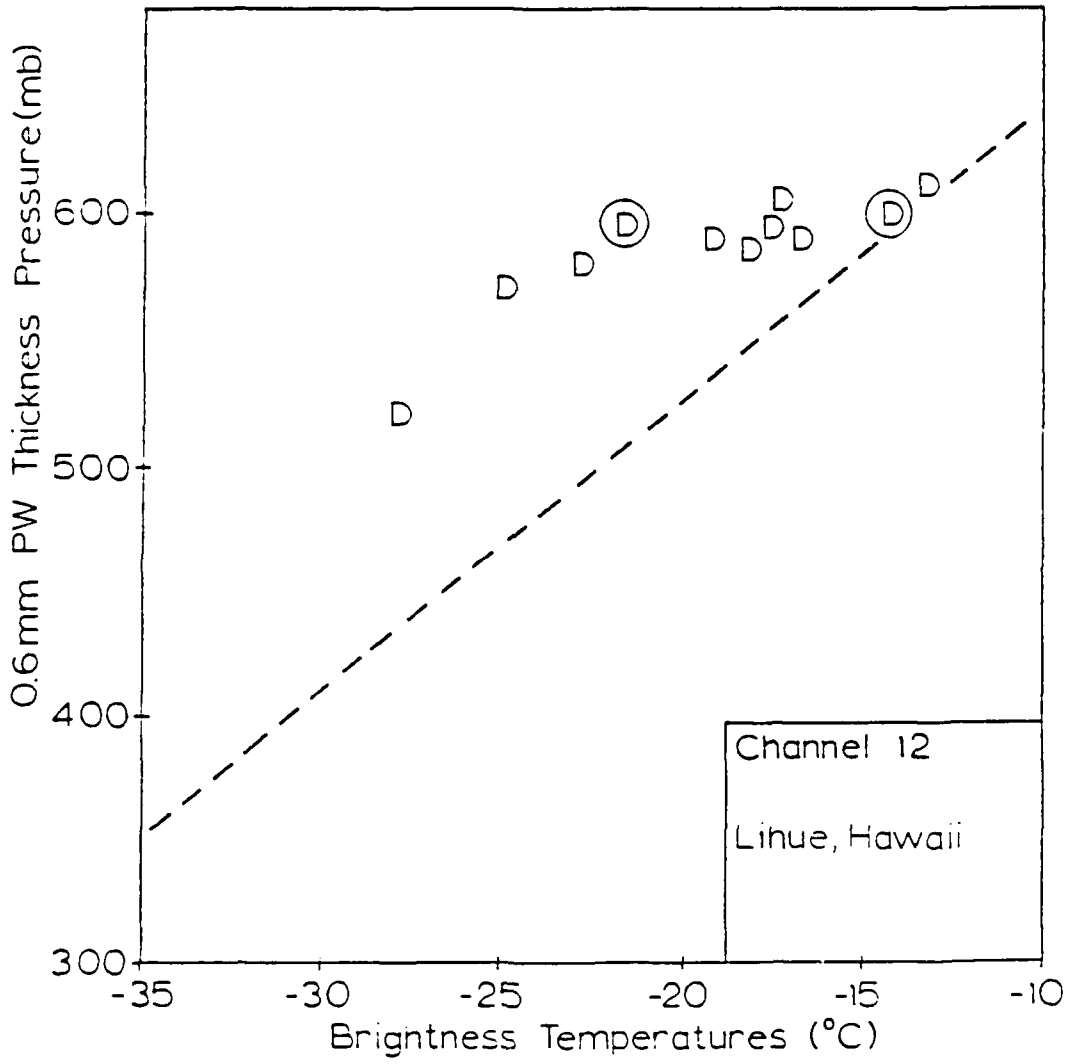

Figure 23a. As in Fig. 21a except for Lihue, Hawaii (D=91165).

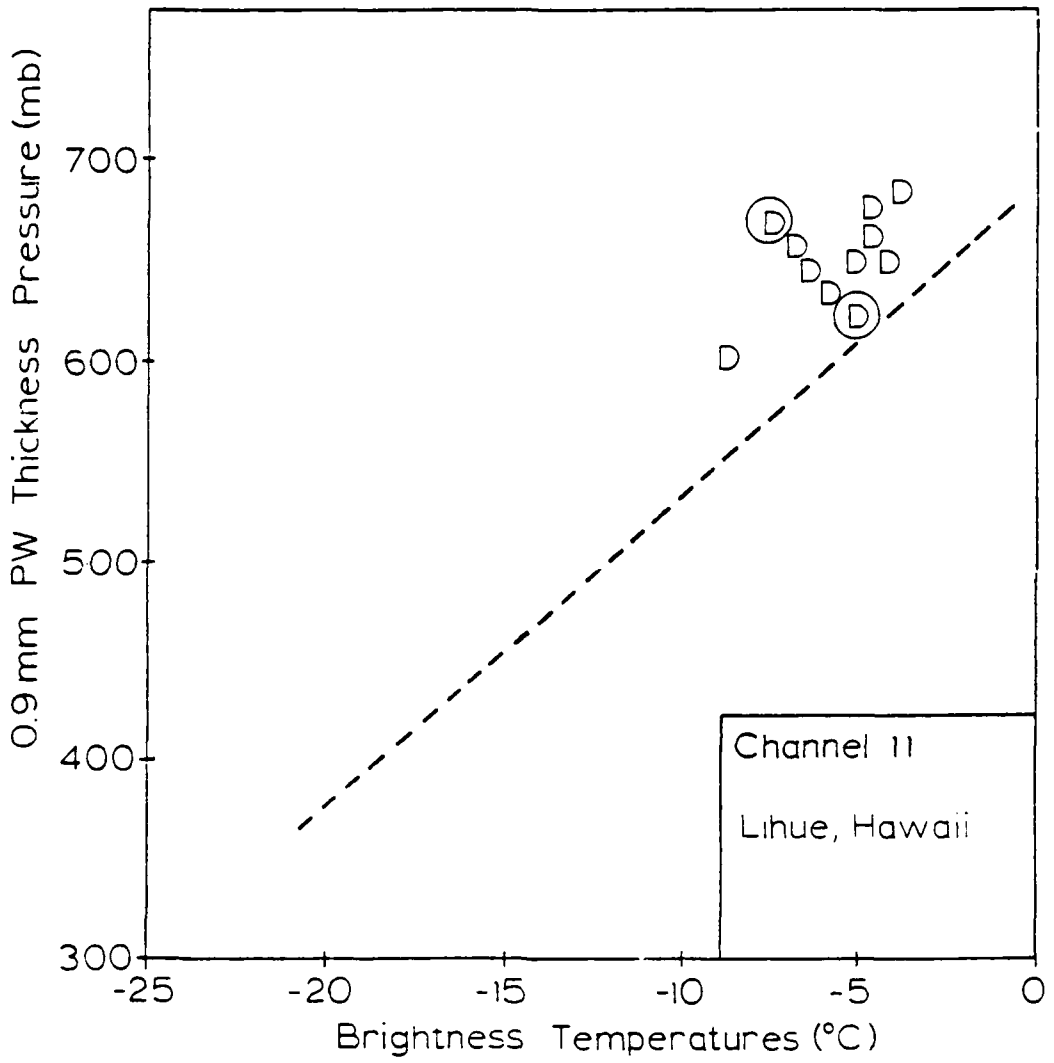

Figure 23b. As in Fig. 21b except for Lihue, Hawaii (D=91165).

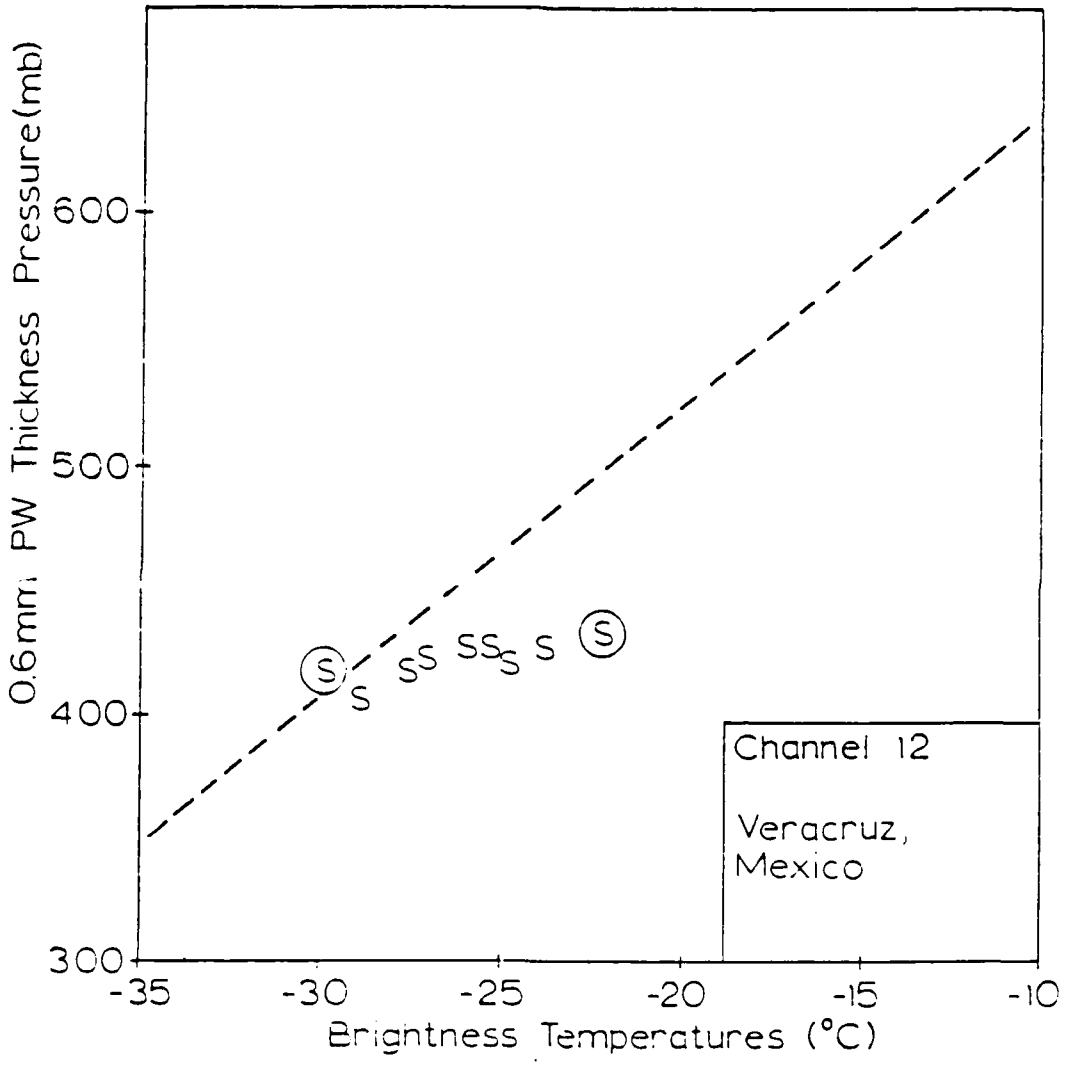

Figure 24a. As in Fig. 21a except for Veracruz, Mexico (S=76692).

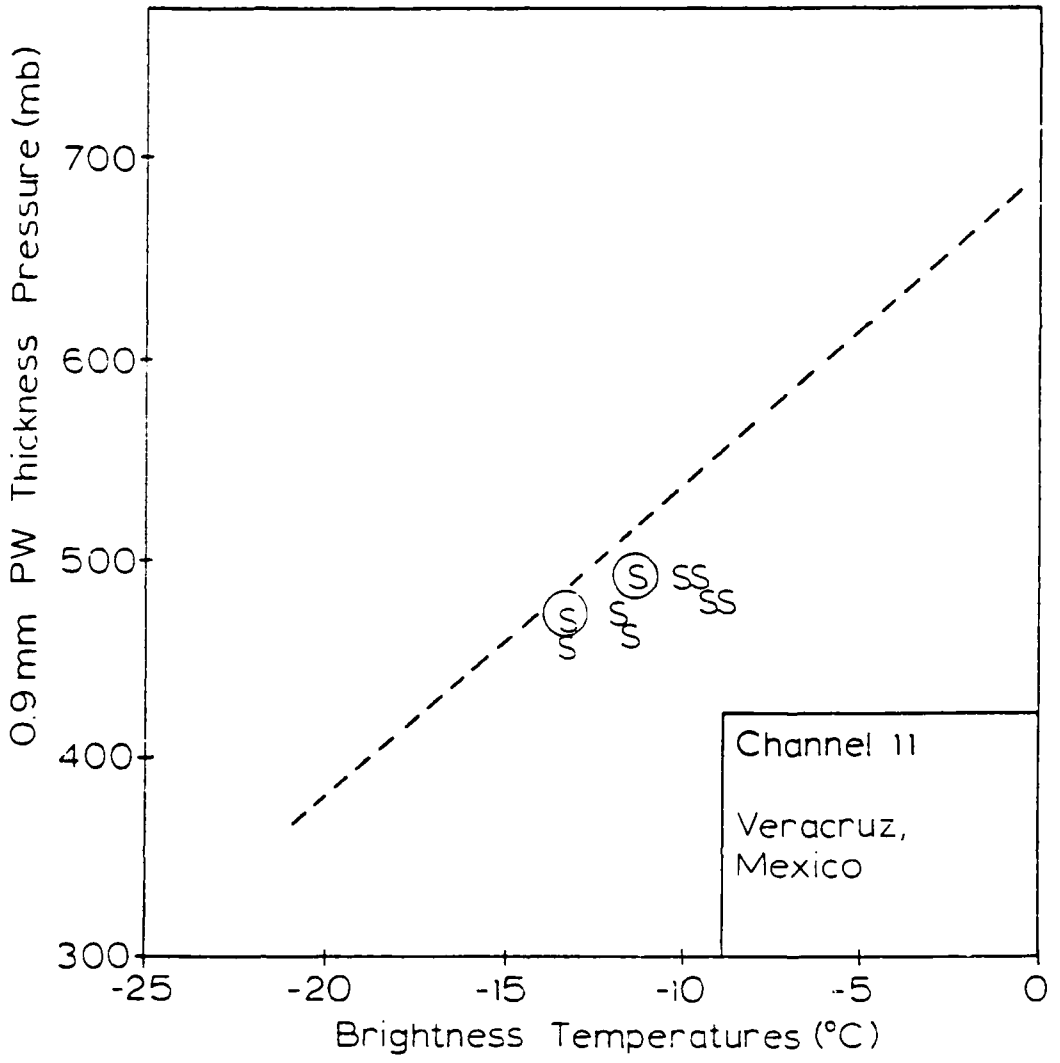

Figure 24b. As in Fig. 21b except for Veracruz, Mexico (S=76692).

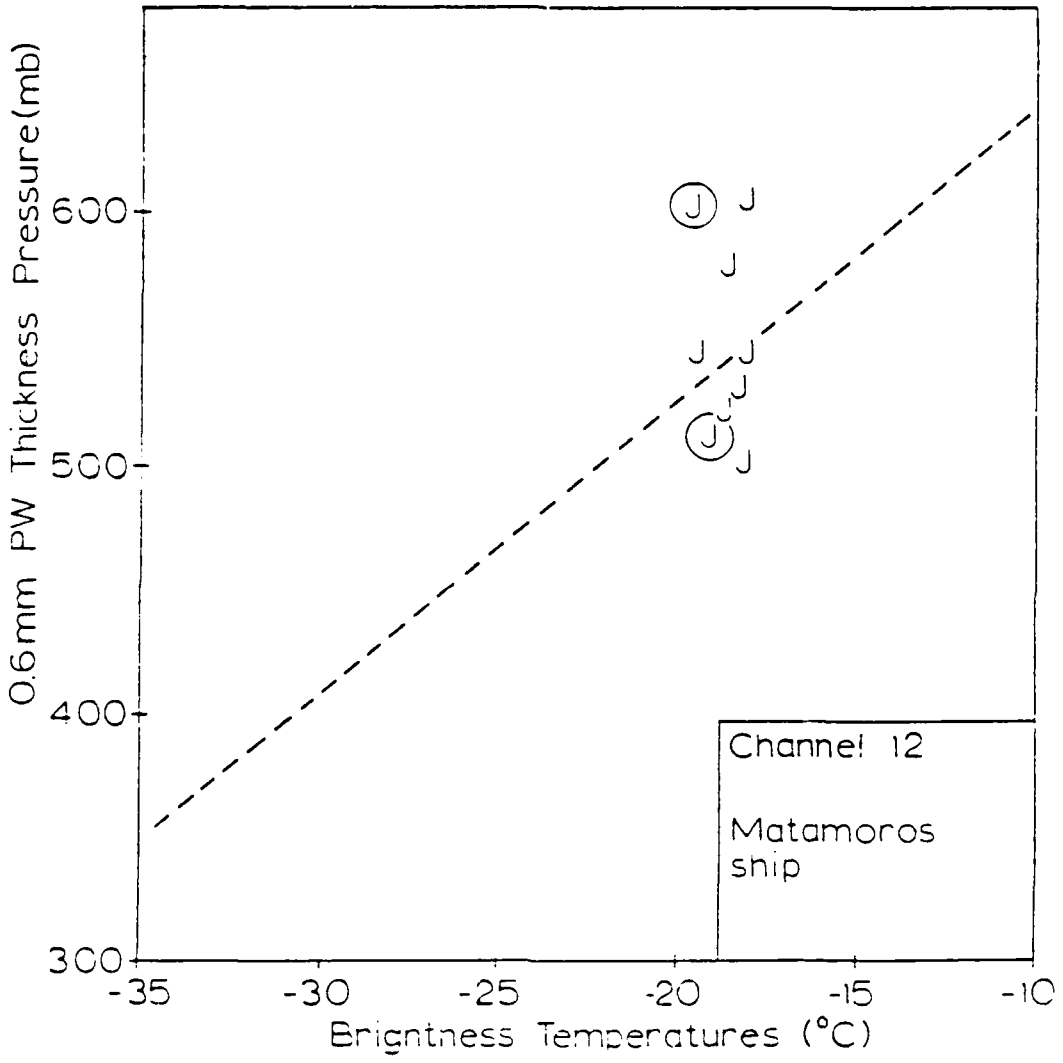

Figure 25a. As in Fig. 21a except for the ship Matamoros (J=MATAM).

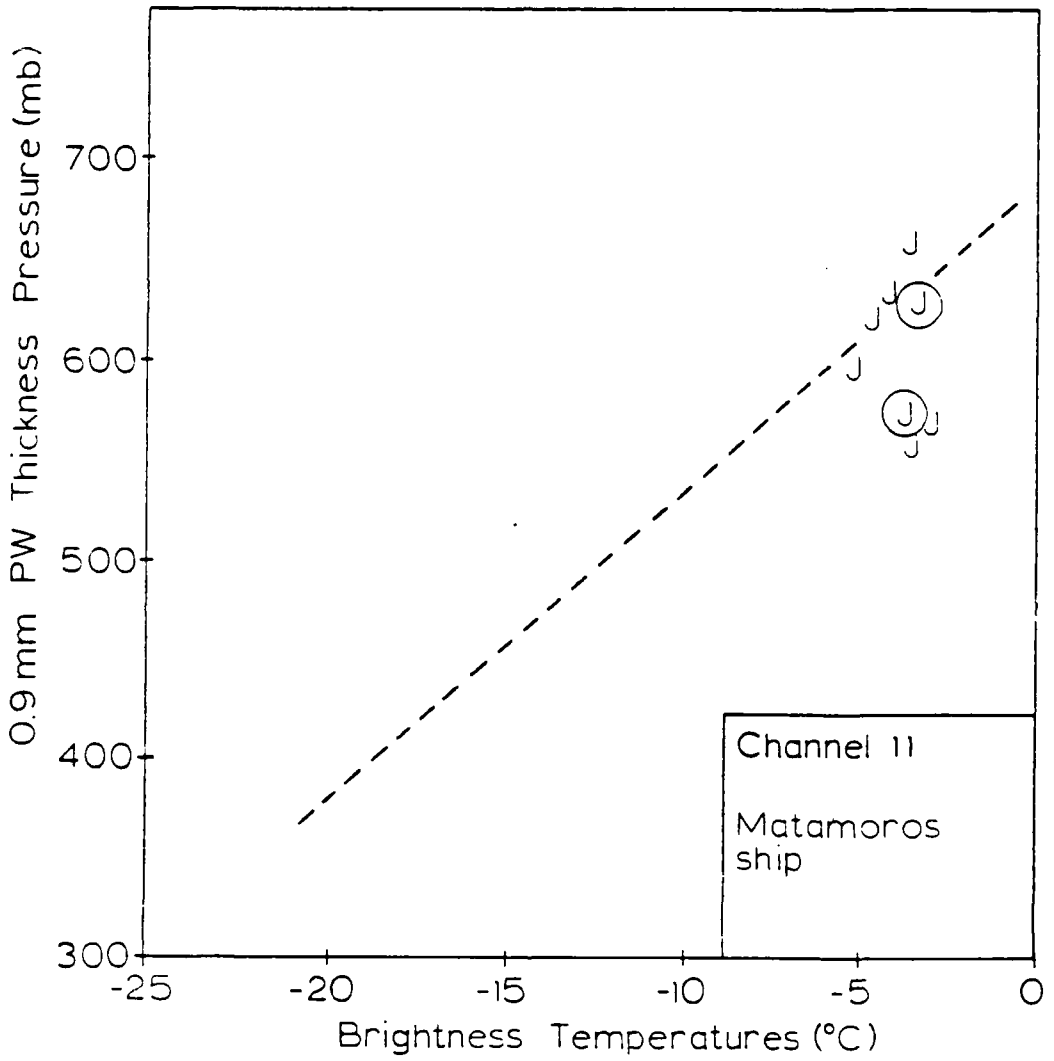

Figure 25b. As in Fig. 21b except for the ship Matamoros (J=MATAM).

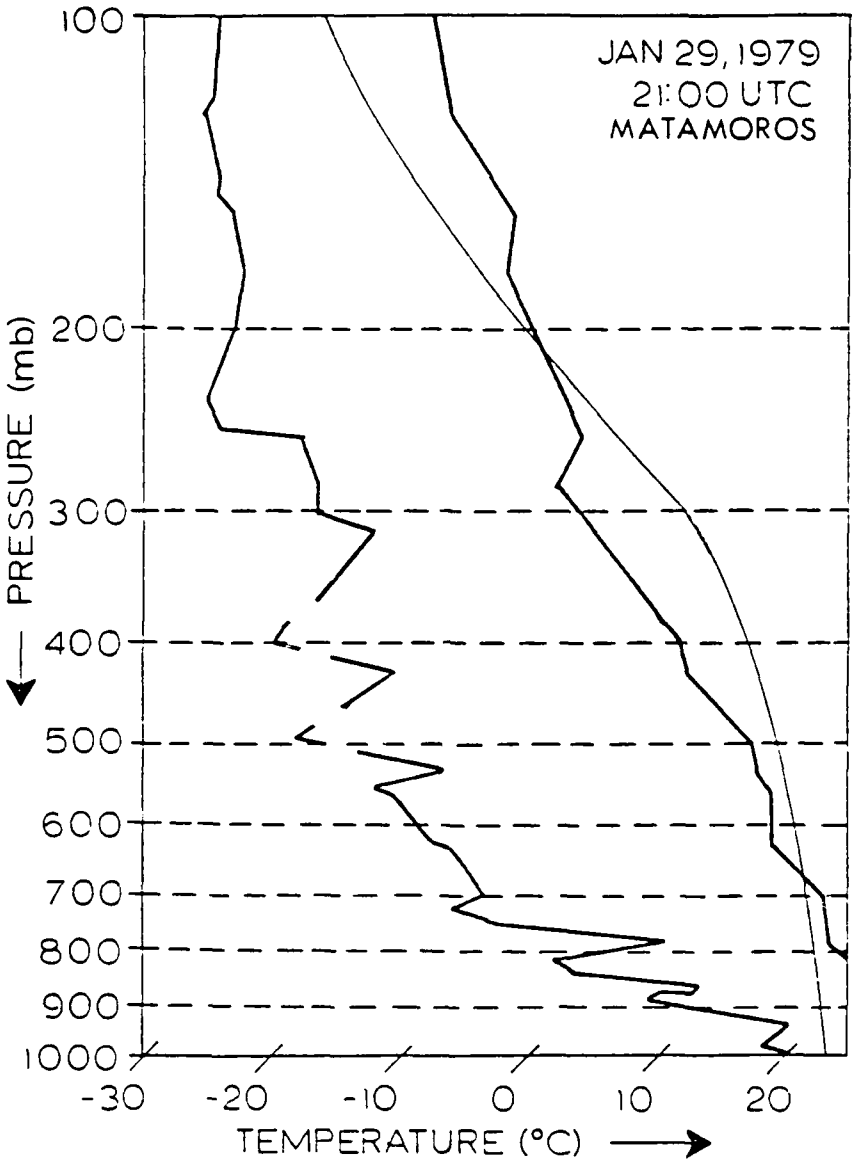

Figure 26. As in Fig. 6 except for 2100 UTC 29 January 1979 at 16°N/95°W.

level; yet, non-quality controlled dew point depressions were still reported above 200 mb with no indication of their reliability.

As stated above, the two Matamoros soundings indicated significantly different moisture profiles in the lower and middle troposphere. Assuming that the reported moisture profiles in these two soundings were fairly accurate between 200 and 100 mb, then the upper tropospheric moisture profiles above 300 mb showed some similarity; yet, this layer seemed slightly wetter in the sounding at 2100 UTC on the 26th than in the sounding at 2100 UTC on the 29th. Indeed, calculations performed on these two soundings for the layer between 300 and 100 mb indicated 0.038 mm PW at 2100 UTC on the 26th compared to 0.026 mm PW at 2100 UTC on the 29th.

In this comparison of Matamoros soundings, an interesting observation was made which was not possible with more conventional rawinsondes like the ones launched from Johnston Island. As stated in the previous paragraph, the Matamoros sounding at 2100 UTC on the 26th indicated a relatively moist layer above the 300 mb level, especially between 300 and 200 mb where the dew point depression averaged near 15°C. This layer was underlain by a very dry 650-300 mb layer in the mid-troposphere with an average dew point depression near 33°C. The opposite profile was observed in the mid and upper levels of the sounding at 2100 UTC on the 29th. The 300-200 mb layer was drier with an average dew point depression of 25°C while the 650-300 mb layer was slightly moister with an average dew point depression near 27°C.

Thus, conceivably the initially intense radiation (potentially high BT) passing upward through the 300 mb level in the Matamoros sounding profile on the 26th may have been reduced by the slightly more moist layer above the 300 mb level (lower potential BT). If the radiation-damping influence of the moderately moist atmospheric profile above the 300 mb level had not been present, the resulting BT on the 26th would have been several degrees higher than the observed BT of slightly over -19°C. As seen in the next section of this chapter, this conclusion is supported by a *r*adiation *t*ransfer *m*odel (RTM) which produced a BT of -8°C calculated from the 300-1000 mb layer shown in this same sounding. In contrast, the slightly moister middle troposphere observed in the Matamoros sounding on the 29th may have influenced upwelling radiation such that less intense radiation passed upward through the 300 mb level on the 29th than on the 26th. However, contrary to the 26th, this less intense radiation on the 29th was not influenced as much by the layer above 300 mb due to this layer's drier profile. Again, this was verified by the RTM which produced a -12°C BT from the 300-1000 mb profile; this RTM BT compared to an observed BT of -19°C on the 29th. Consequently, the paradox of a slightly higher channel 12 BT observed from the wetter mid-troposphere of the sounding on the 29th compared to a lower BT originating from the drier mid-troposphere on the 26th may be explained by significant upper tropospheric moisture influences.

Channel 11 BTs showed a weak trend in the opposite direction. Slightly lower BTs corresponded to the more moist mid-tropospheric sounding profile on the 29th while slightly higher channel 11 BTs

conformed to the drier sounding on the 26th.

In summary, the large inconsistencies observed when low and mid tropospheric sounding profiles derived from conventional rawinsondes were compared to collocated channel 12 and 11 BTs supports the hypothesis mentioned in Chapter VI: Moisture-sensitive radiation reaching the satellite may be emanating partially from moisture which is undetectable by conventional rawinsondes. Indeed, Lee et al. (1983) found that the evaluation of satellite-retrieved parameters was much less reliable at high altitudes due, in part, to the uncertainties involved with radiosonde upper air humidity reports. Therefore, it is subsequently hypothesized that minute amounts of PW in the extremely cold tropical troposphere at pressures below 300 mb, which are not detectable by conventional rawinsondes, have a significant impact on moisture sensitive satellite BTs. Given the greater discrepancies observed with channel 12 BT comparisons, it is further hypothesized that radiation in the frequencies detected by channel 12 is more seriously affected by this upper tropospheric moisture than channel 11 radiation.

B. Calculated versus Observed BTs

The hypothesis that small amounts of PW in the cold upper troposphere have a significant cooling effect on channel 12 and 11 BTs was explored by comparing observed BTs to model-derived BTs. BTs were calculated from actual soundings by means of the GLAS Physical Inversion *r*adiative *t*ransfer *m*odel (RTM) (Susskind et al., 1982). Thus, by comparing an RTM BT to the observed BT associated with the

original sounding, a computed BT may be compared to the observed BT.

The RTM-produced channel 12 weighting function curves from the Johnston Island soundings at 0000 UTC on 23 January 1979 (see Fig 5) and 1200 UTC on 28 January 1979 (see Fig. 22) are shown in Fig. 27. In layers where sounding moisture was represented by dashed lines (dew point depression defaulted to 30°C) in Figs. 5 and 22, the sounding moisture systematically overestimated the real moisture (dew point depression greater than 30°C). This overestimation of moisture was indicated roughly from the 800 mb and 700 mb level to the 300 mb level in the two Johnston Island soundings, respectively. Moisture at pressures less than 300 mb was set to zero since the rawinsonde moisture readings terminated at heights just above this level. Analogous to the soundings, the weighting function curves were similar, with both curves peaking near 500 mb. The collocated RTM and observed BTs at 0000 UTC on the 23rd were -10° and -11°C, respectively; thus, the correlation was excellent. However, the comparison at 1200 UTC on the 28th was extremely poor. As expected due to sounding similarity, the RTM BT remained high (-9°C) while the observed BT drastically lowered to -22.8°C, suggesting significant increase in actual moisture above 300 mb.

Similar to channel 12, the channel 11 weighting function curves (Fig. 28) for the same Johnston Island soundings (see Figs. 5 and 22) showed a great deal of resemblance with peaks occurring within 75 mb of each other. Like channel 12, the RTM and observed channel 11 BTs (approximately -1°C) at 0000 UTC on the 23rd were nearly identical. Yet, as seen with channel 12, the channel 11 comparisons of 1°C

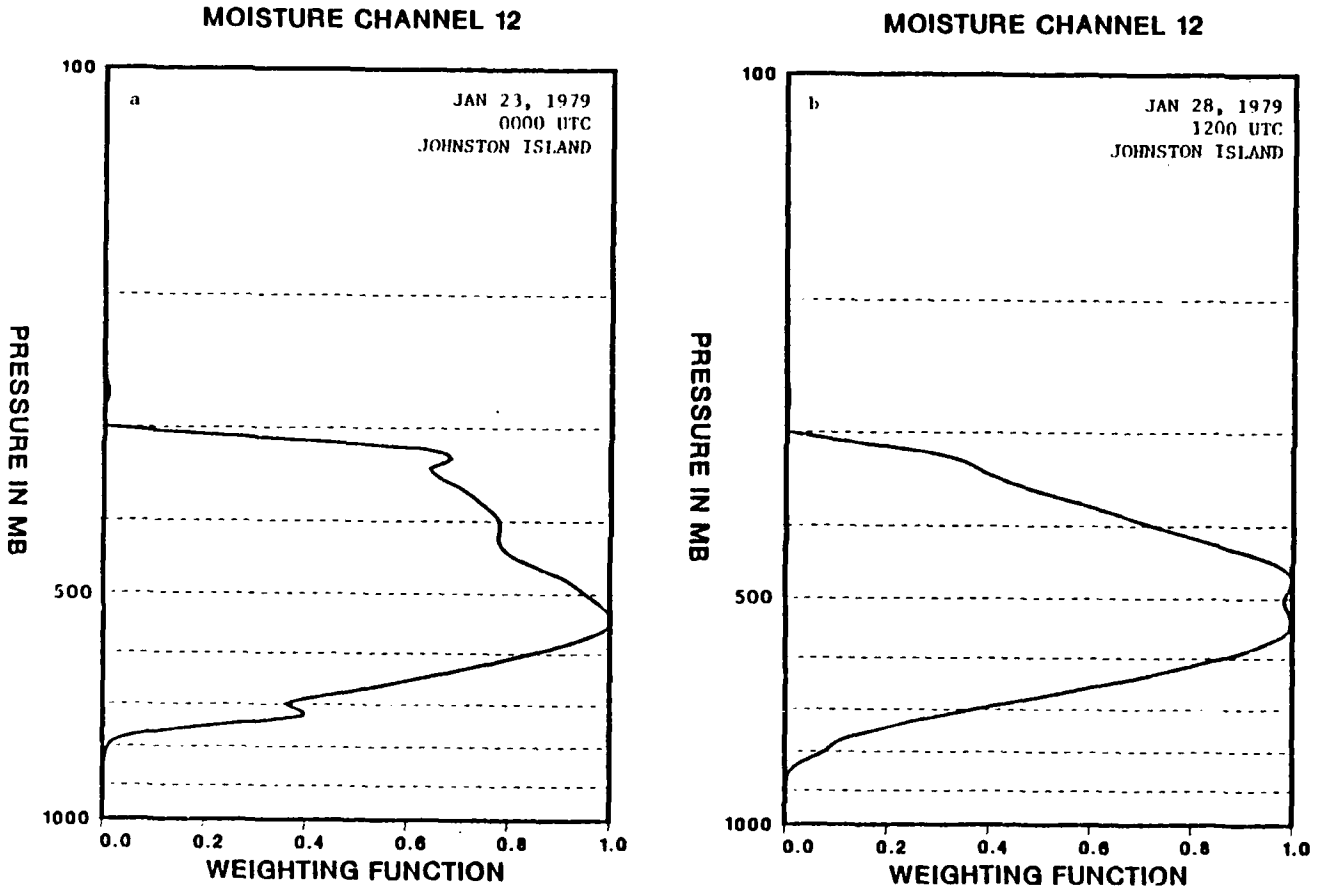

Figure 27. RTM channel 12 weighting function profiles for the Johnston Island soundings at 0000 UTC 23 January 1979 (a) and 1200 UTC 28 January 1979 (b). Moisture has been deleted at heights above 300 mb. The slight weighting above 300 mb is not due to the influence of moisture on the RTM.

versus -5°C at 1200 UTC on the 28th differed considerably.

Channel 12 weighting function curves (Fig. 29) for the two Lihue soundings at 0000 UTC on 22 January and 1200 UTC on 24 January (Fig. 30) once again displayed a great deal of similitude. The dry middle tropospheres in both soundings at 0000 UTC on the 22nd and 1200 UTC on the 24th helped produce RTM BTs of -12°C and -11°C, respectively; however, there was considerable variation in the respective observed BTs. The observed BT collocated with the earlier Lihue sounding was 3°C less than the RTM BT while the observed BT over the later sounding was lower than the RTM BT by 11°C.

Channel 11 Lihue BT comparisons presented a very informative illustration of radiative intervention from heights above the 300-mb level. The channel 11 weighting function curve (Fig. 31a) associated with the Lihue sounding at 0000 UTC on the 22nd showed a sharp peak near the 700 mb level which corresponded to the well-defined top of the lower tropospheric moist layer (see Fig. 30a). This profile produced a high RTM BT of -4°C which compared nicely to the observed BT of -5°C. A sharp peak in the weighting function curve (Fig. 31b) also was noted in the Lihue sounding at 1200 UTC on the 24th (see Fig. 30b). Again, this channel 11 peak corresponded with the top of the lower tropospheric moist layer; however, instead of the maximum occurring at 700 mb, it had lowered in height by the 24th to the 850-mb level (see Fig. 30b). Thus, clearly any collocated channel 11 BTs which originated totally from mid and lower tropospheric radiative emissions would be higher at 1200 UTC on the 24th than at 0000 UTC on the 22nd. Indeed this was the case for the RTM BTs; they

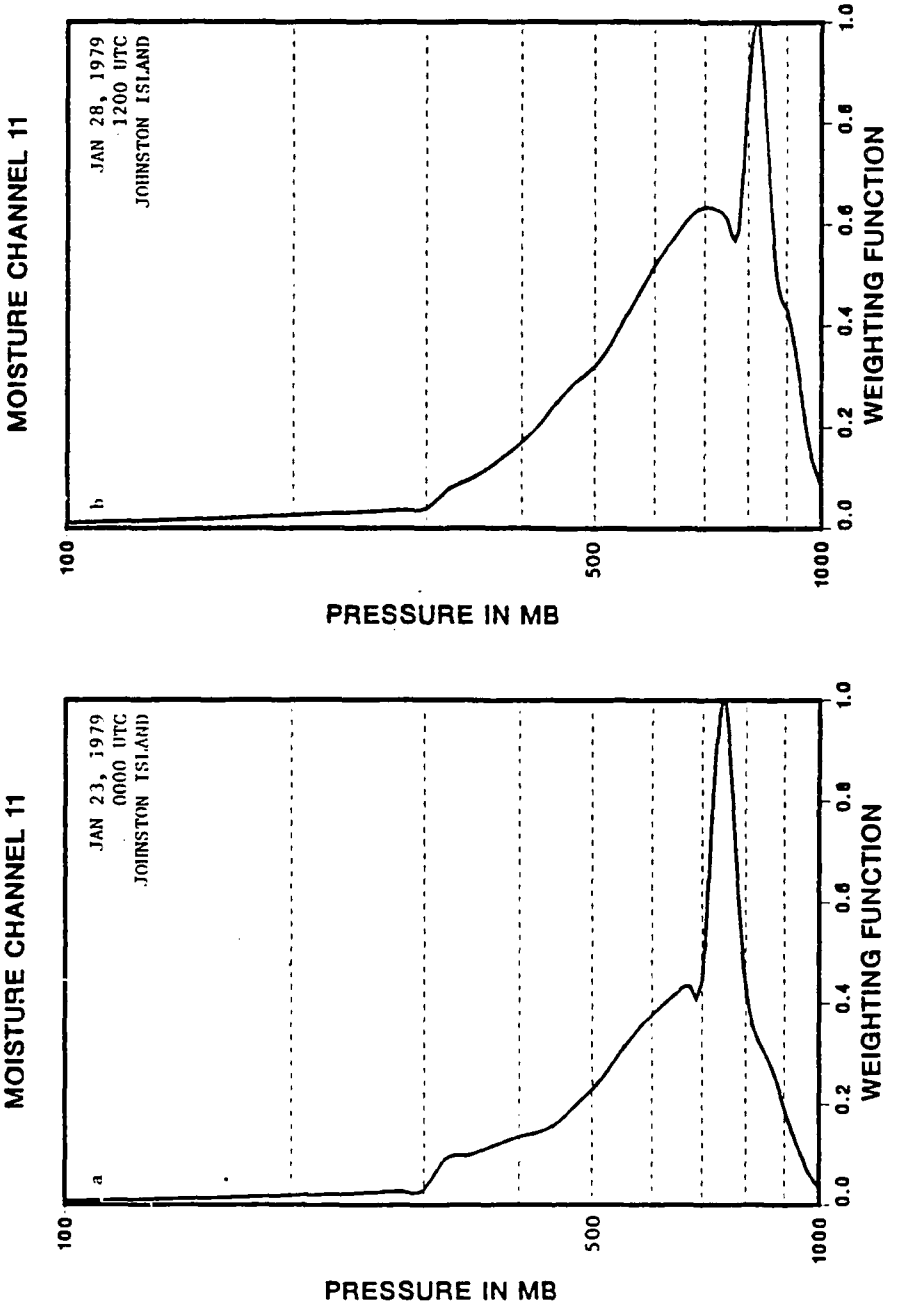

Figure 28. As in Fig. 27 except for channel 11.

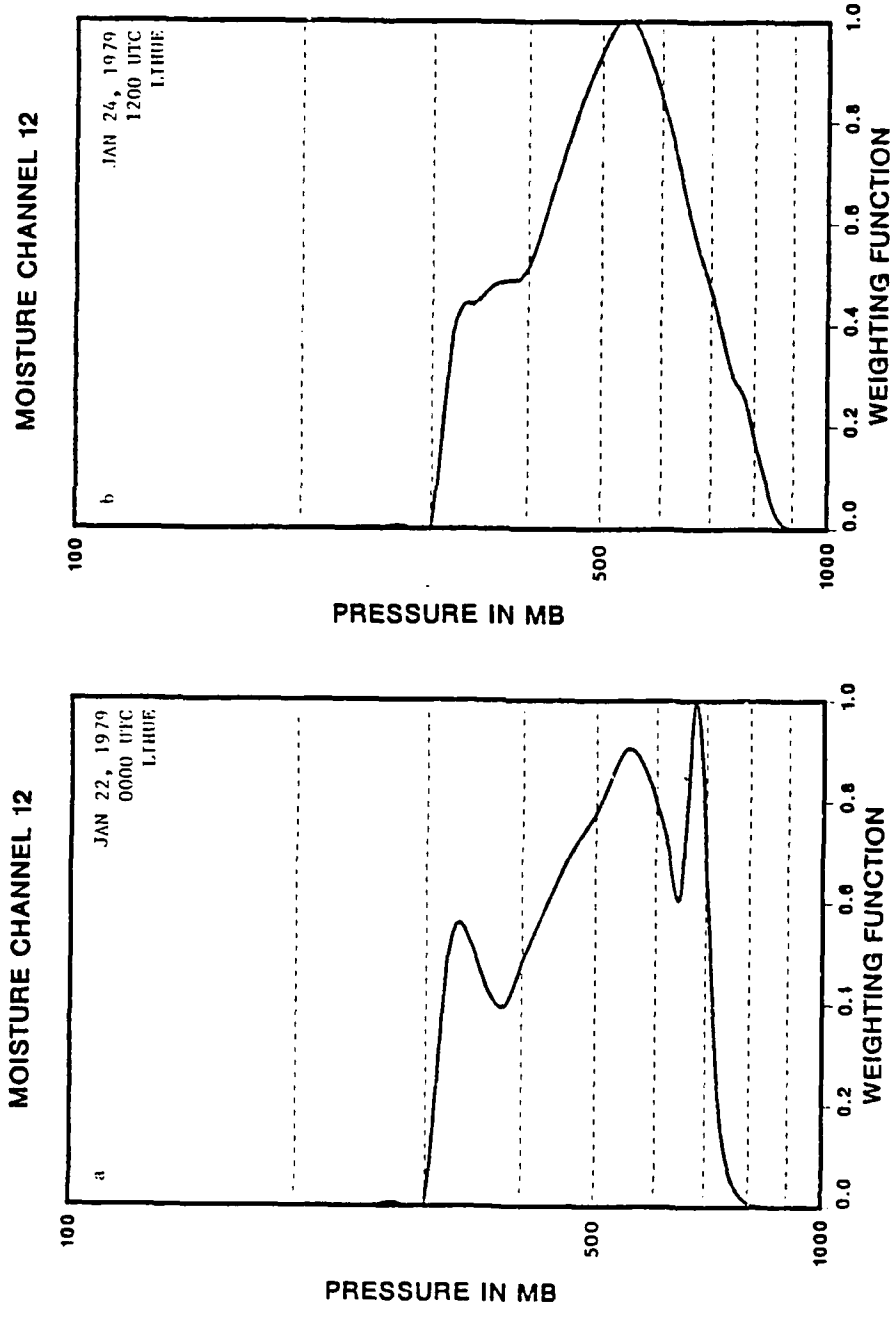

Figure 29. Same as Fig. 27 except for Lihue, Hawaii at 0000 UTC 22 January 1979 (a) and 1200 UTC 24 January 1979 (b).

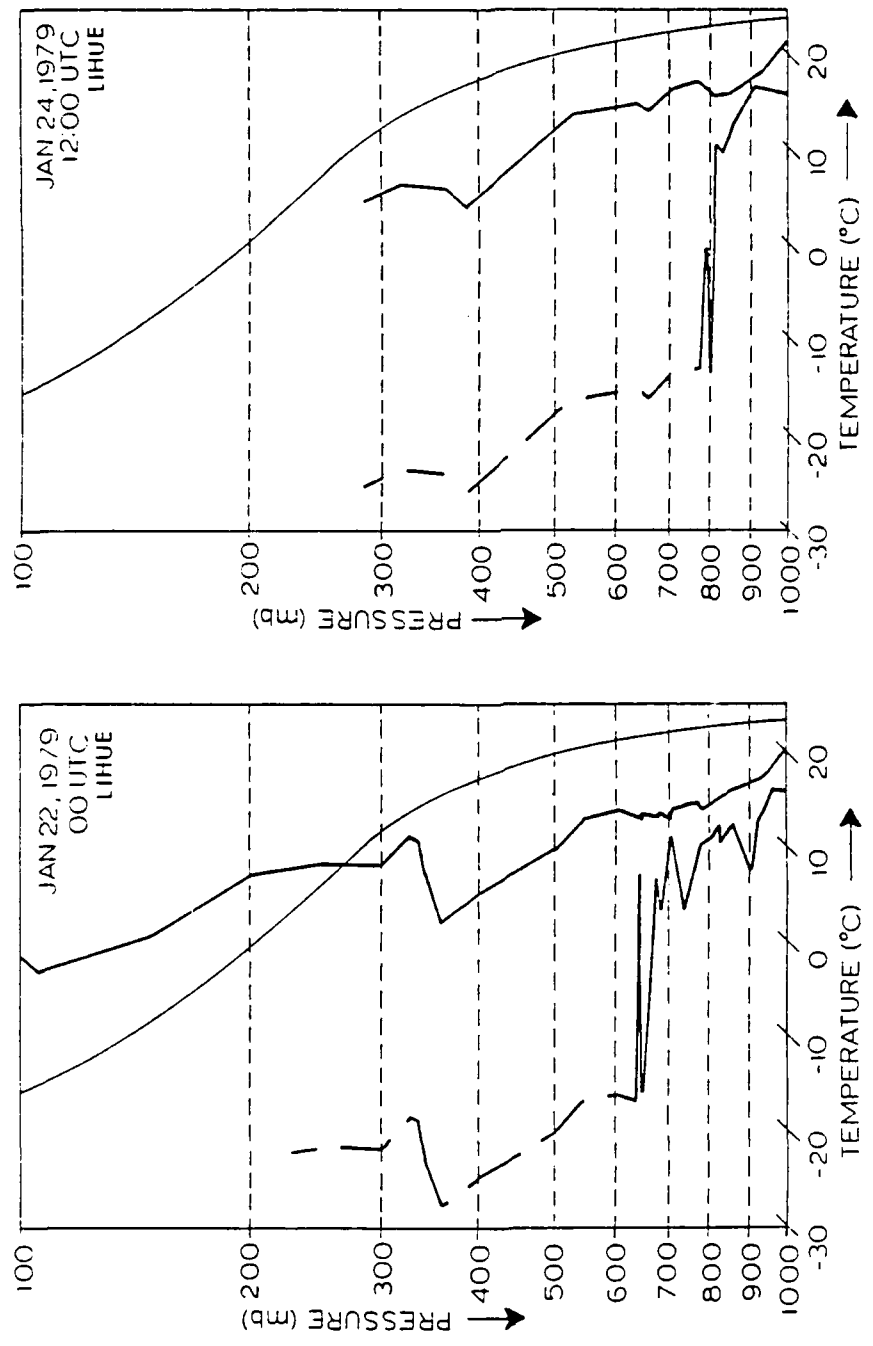

Figure 30. As in Fig. 5 except for Lihue, Hawaii for 0000 UTC 22 January 1979 (a) and 1200 UTC 24 January 1979 (b).

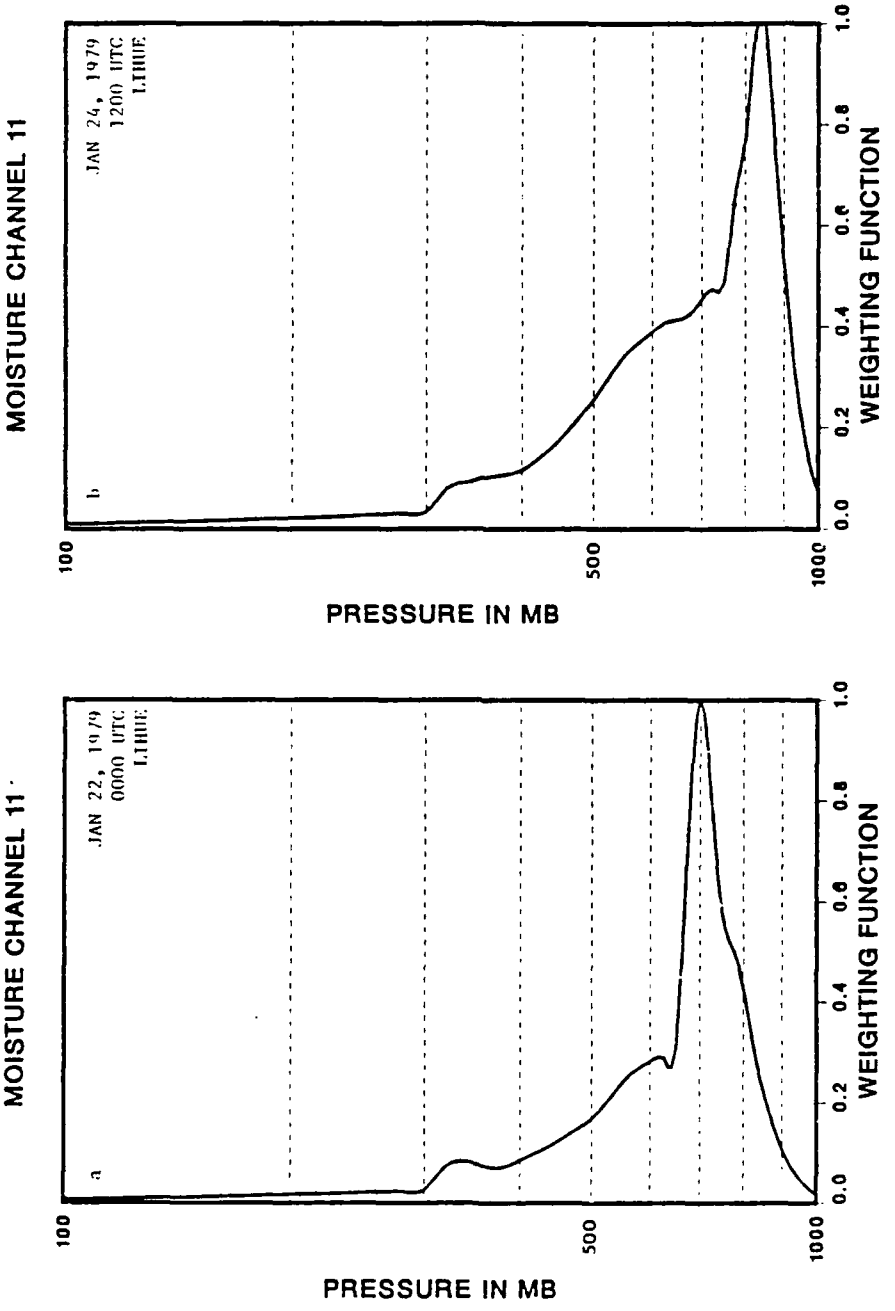

Figure 31. As in Fig. 29 except for channel 11.

rose by nearly 3°C. However, in stark contrast, the observed channel 11 BT actually fell from -5°C to -7°C. Thus, the Johnston Island and Lihue RTM/observed BT comparisons displayed discrepancies which were not explainable by changes in lower and mid-tropospheric rawinsonde moisture profiles.

A more conclusive BT/sounding test was constructed using the detailed moisture information available from the limited number of special rawinsondes launched from scientific ships in the eastern Pacific. As with conventional land-launched rawinsondes, RTM channel 12 and channel 11 BTs were first computed from 1000-300 mb moisture profiles obtained from the ship-launched rawinsondes and these RTM BTs were compared to observed BTs. However, an additional step was introduced whereby observed BTs also were compared to the RTM BTs calculated from the 1000-100 mb moisture profile available from the special soundings. As mentioned in Section A, moisture measurements from these soundings were recorded to the 100 mb level. This type of comparison gave a much more quantitative determination of the possible influence of high tropospheric moisture on channel 12 and 11 BTs.

The Matamoros sounding from 2100 UTC on 26 January (see Fig. 6) was used to compute a 1000-300 mb weighting function curve (Fig. 32a) for channel 12 which yielded a large RTM BT of -8°C. When this RTM BT was compared to the observed channel 12 BT of -19°C, it was evident that the lower and mid troposphere as depicted by the rawinsonde could not account for this BT discrepancy. However, when the 300-100 mb layer, which contained only 0.038 mm of PW, was added

to this 1000-300 mb profile, the RTM BT cooled seven degrees to -15°C. When the 1000-100 mb weighting function curve (Fig. 32b) was compared to the 1000-300 mb curve, a significant amount of weighting area existed in the 300-100 mb layer, especially between 300 and 200 mb.

Similarly, channel 11's 1000-300 mb RTM BT of 0°C was compared to the observed BT of -3°C over Matamoros at 2100 UTC on the 26th. This BT difference was much less than for channel 12. A BT of -1°C was calculated for the 1000-100 mb layer. This reduced upper tropospheric influence on the channel 11 BT is displayed by the nearly insignificant 300-100 mb layer difference between channel 11 weighting function curve profiles for the 1000-300 mb layer (Fig. 33a) and the 1000-100 mb layer (Fig. 33b), respectively.

The special sounding from 2100 UTC on 26 January (Fig. 34) from the ship Pariz provided another graphic example of the influence of the upper tropospheric moisture on channel 12 BTs. Although the total PW contained in the 300-100 mb layer was a seemingly insignificant 0.187 mm, the channel 12 weighting function curves for the 1000-300 mb (Fig. 35a) and 1000-100 mb moisture (Fig. 35b) profiles were extremely different. The profile with moisture extending to the 100-mb level indicated nearly half of the total area encompassed by this weighting curve occurred at heights above the 300-mb level. This large discrepancy in weighting function profiles produced correspondingly large difference in the RTM BTs. The 1000-300 mb layer BT of -15°C was profoundly higher than the 1000-100 mb layer BT of -31°C; yet this latter BT was much closer to the -35°C

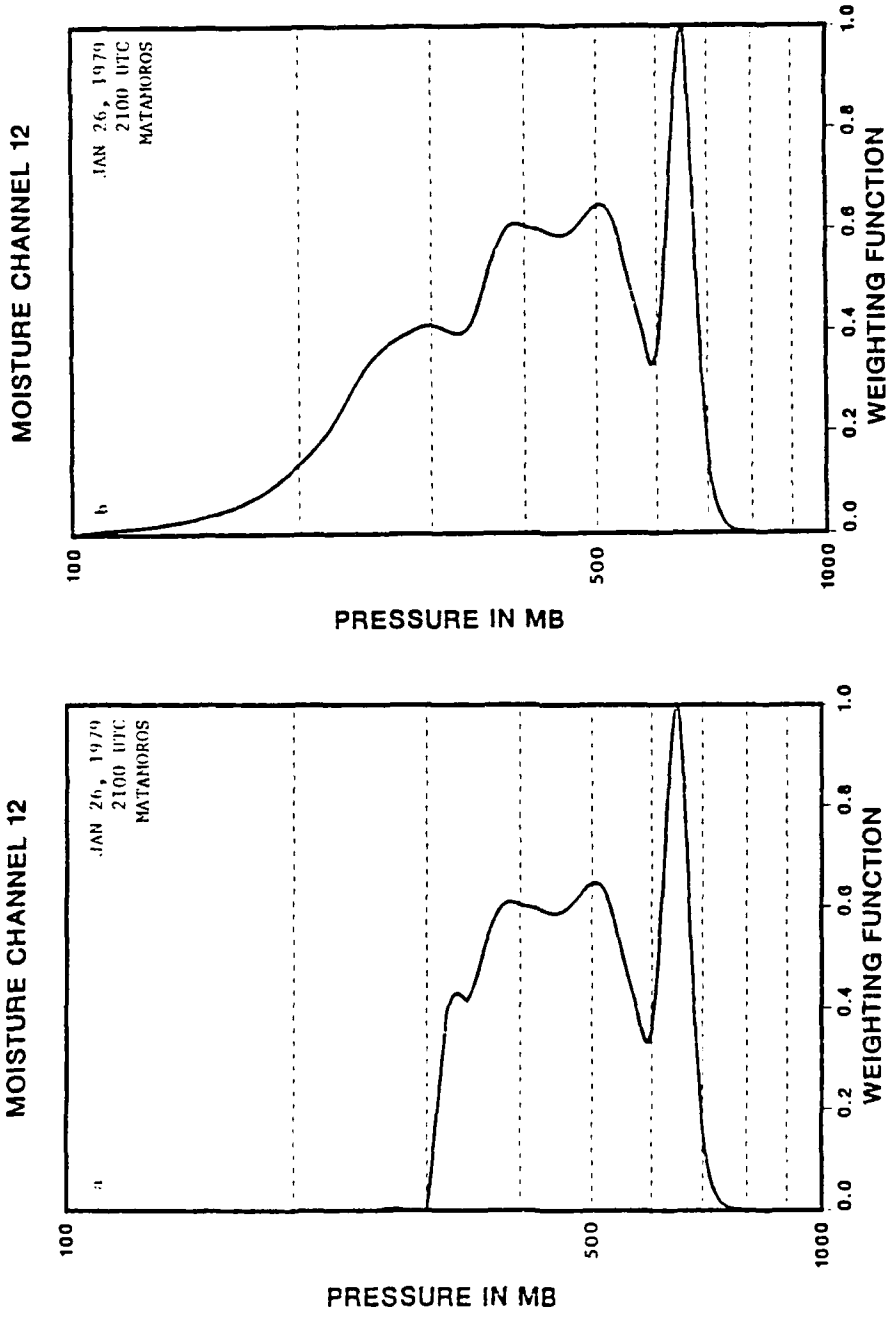

Figure 32. RTM channel 12 weighting function profiles for the Matamoros ship sounding at 2100 UTC 26 January 1979. Moisture deleted at heights above the 300 mb level (a) and moisture deleted at heights above the 100 mb level (b). The slight weighting above 300 mb in (a) is not due to the influence of moisture on the RTM.

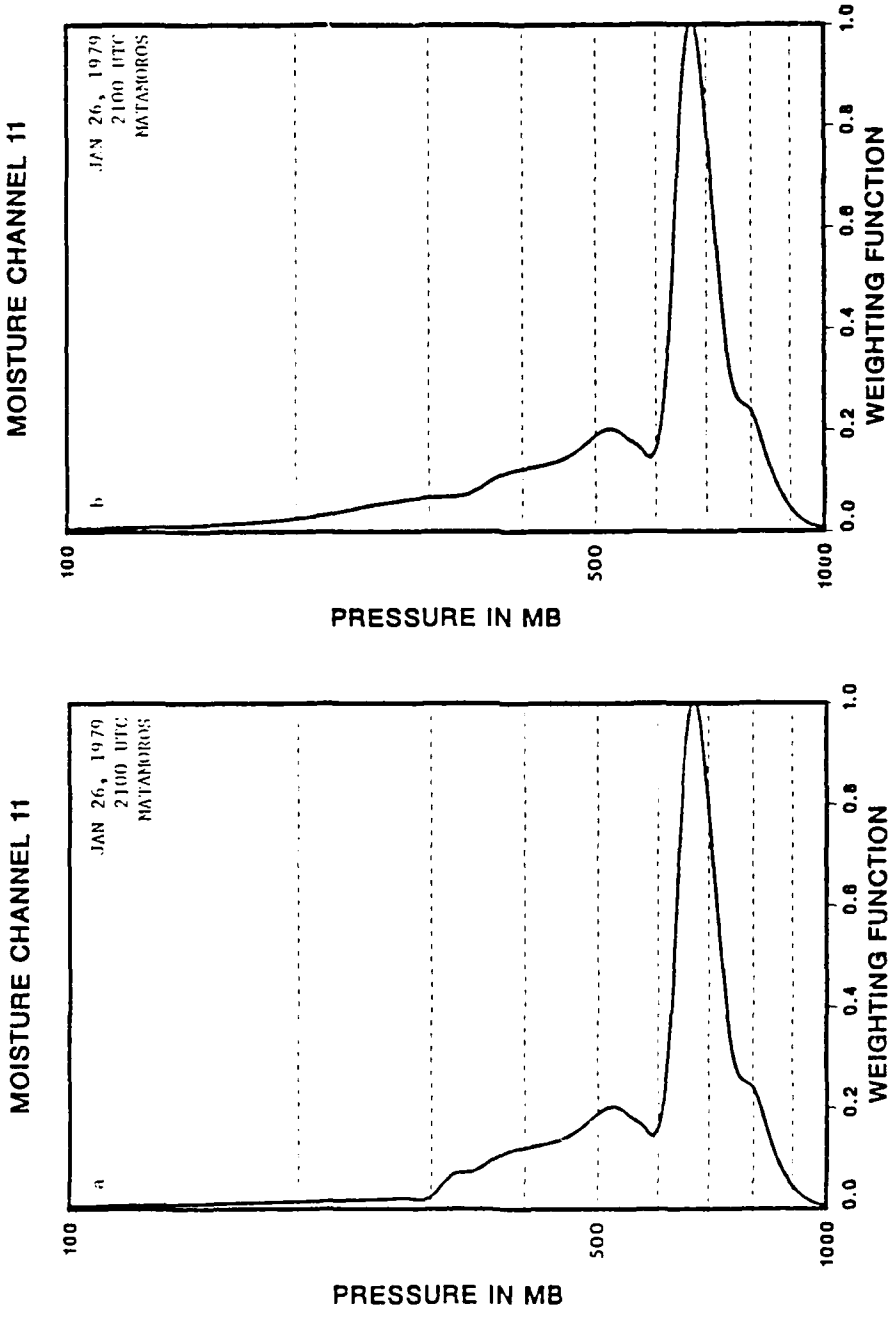

Figure 33. As in Fig. 32 except for channel 11.

channel 12 BT observed over Pariz.

Channel 11 weighting curves (Fig. 36) presented a similar, but less drastic change in their profiles at heights above 300 mb. Although the RTM BT calculated for the 1000-100 mb layer fell within 4°C of the observed channel 11 BT, the 1000-300 mb layer RTM BT originally differed from the observed BT only by 6°C. Thus, this two degree improvement in the channel 11 BT was not nearly as significant as that observed with channel 12.

Finally, RTM BTs, without moisture above 300 mb, were calculated from all 111 rawinsondes which were collocated with observed BTs. These RTM BTs were compared to the collocated BTs and the differences for channel 12 and 11 were analyzed on the scatter plots shown in Figs. 37 and 38, respectively. A trend emerges in the channel 12 comparison. Generally, the drier soundings which were associated with higher channel 12 BTs produced better agreement with the RTM, while the wetter soundings coupled with lower BTs produced poorer agreement. Special significance was given to the BTs in the upper right corner of the plot. Without exception, BTs higher than -14°C closely matched the BTs produced by the RTM. These were the same BTs encompassed within the very high channel 12 BT region observed in the subtropical Pacific to the northwest of the moisture bursts (see Fig. 4a). These high BTs also fell within the secondary frequency maximum observed in channel 12 BTs (see Fig. 2).

A less defined pattern was displayed in the channel 11 analysis. The trend noted in the channel 12 analysis was much less evident in channel 11. In addition, the magnitudes of the differences between

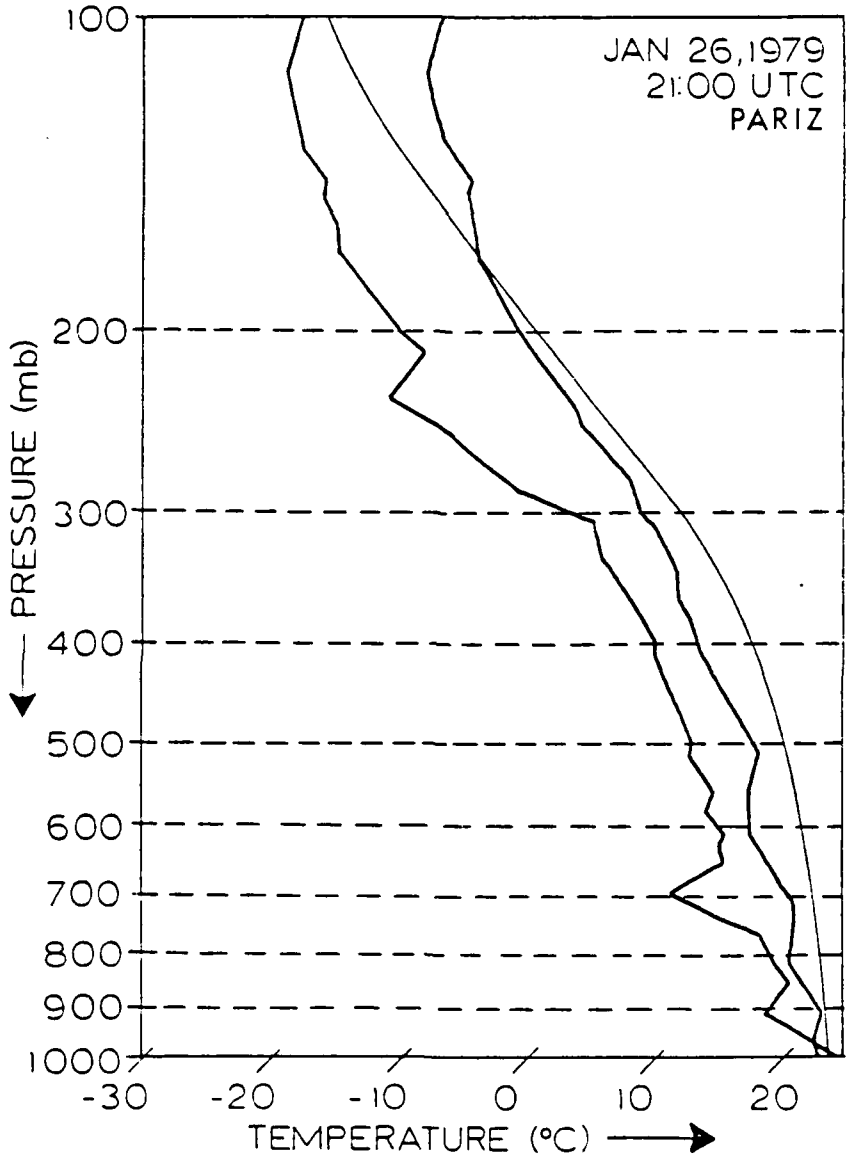

Figure 34. As in Fig. 5 except for Pariz ship for 2100 UTC 26 January 1979 at 1°N/150°W.

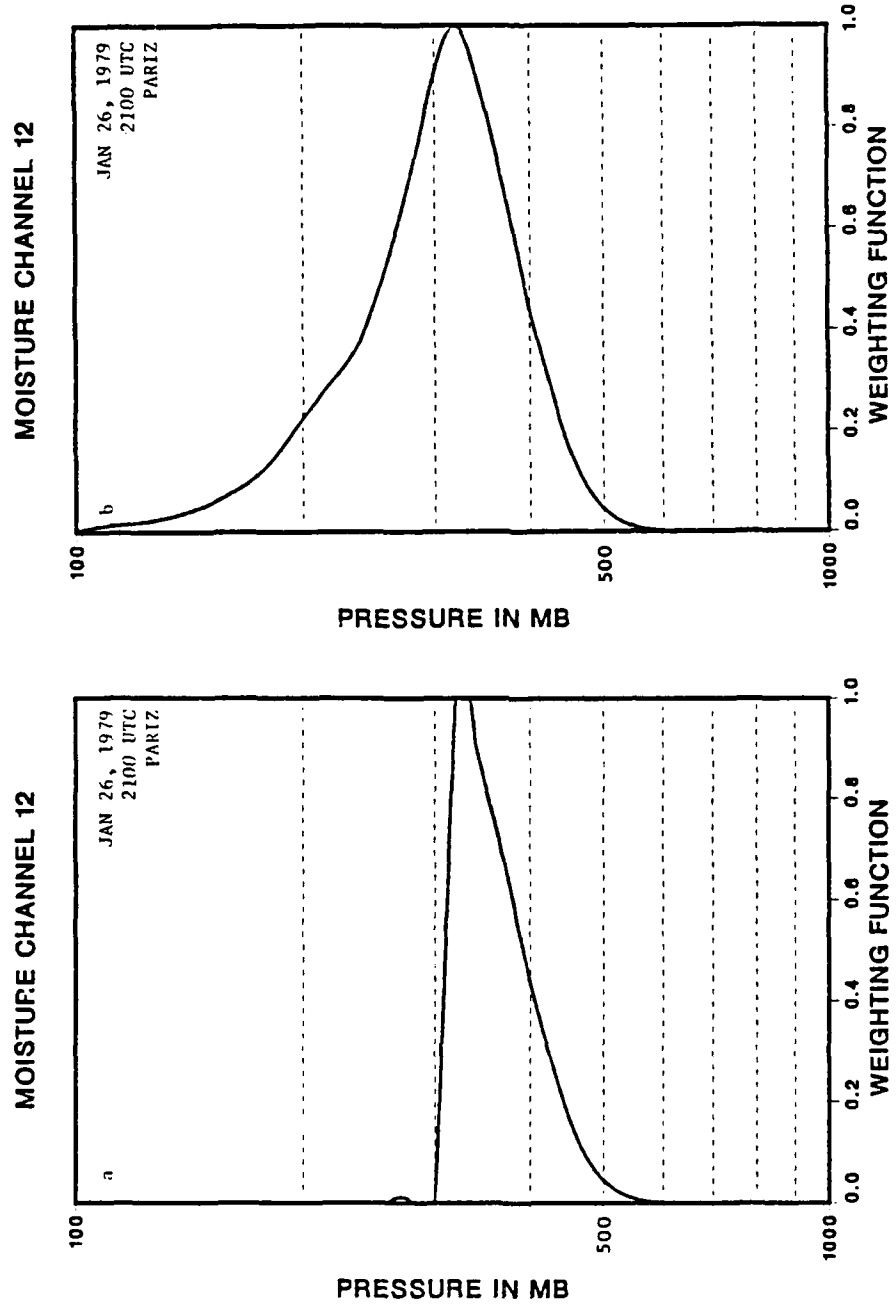

Figure 35. As in Fig. 32 except for the Pariz ship sounding.

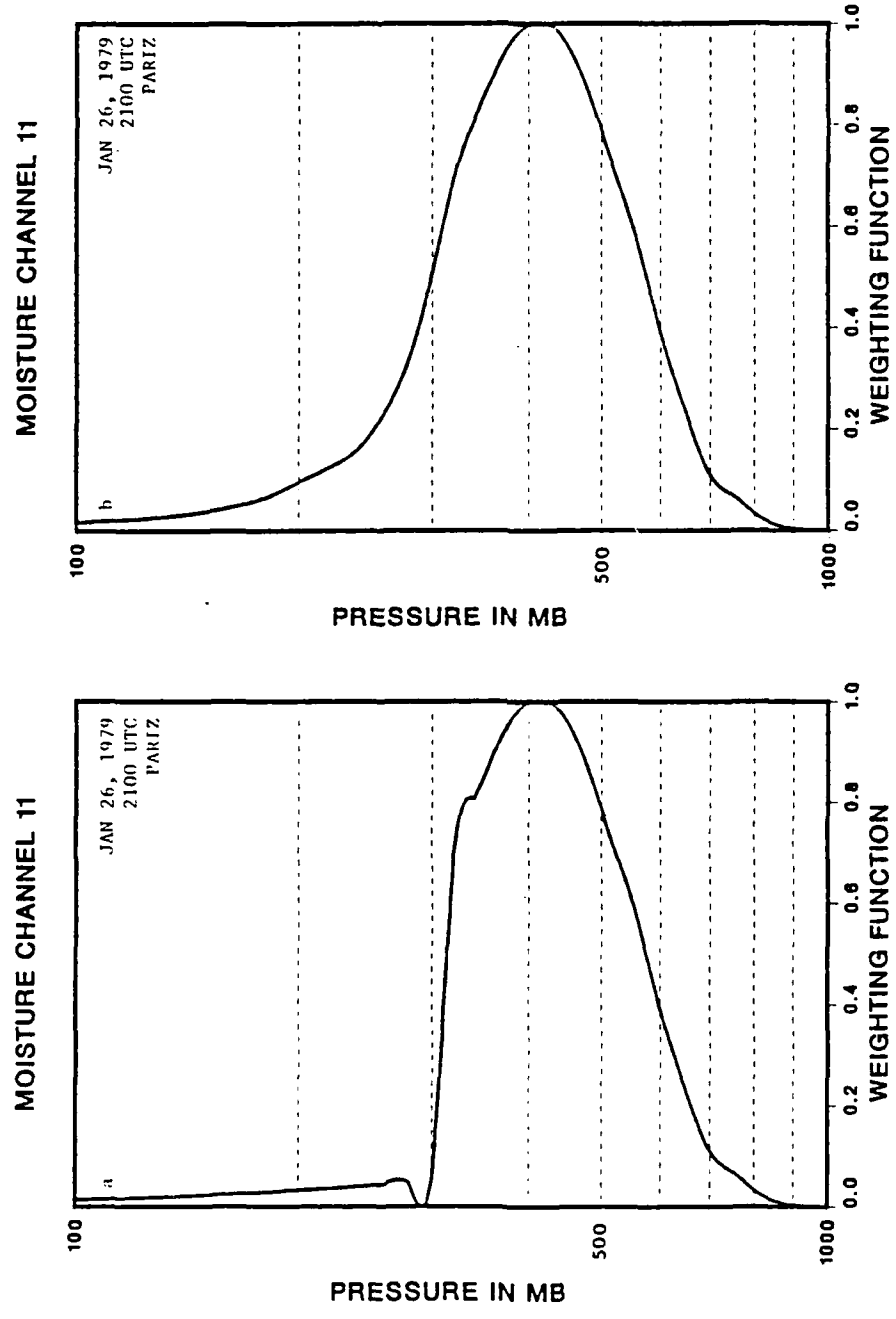

Figure 36. As in Fig. 33 except for the Pariz ship sounding.

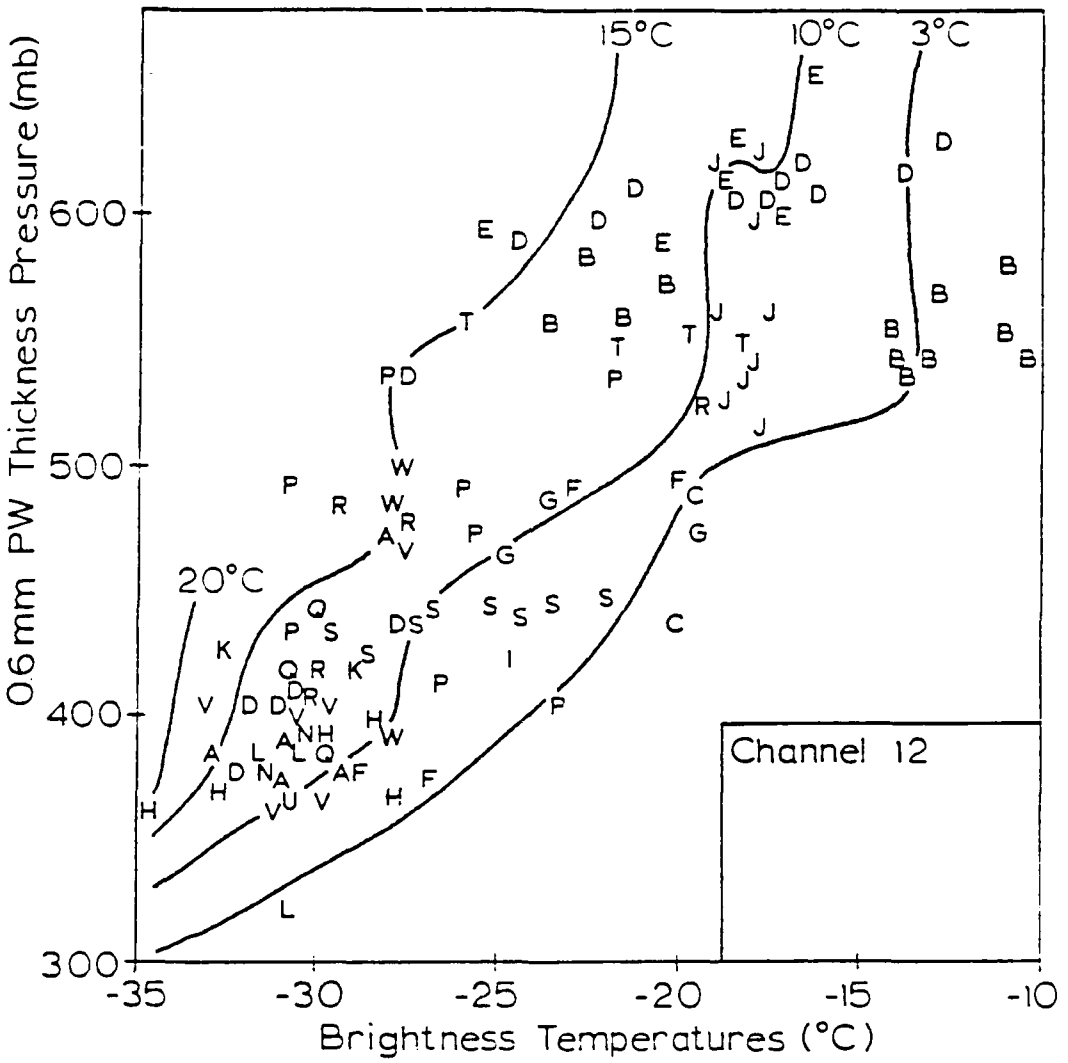

Figure 37. As in Fig. 20a except for overlaid observed-BT/RTM-BT difference contours.

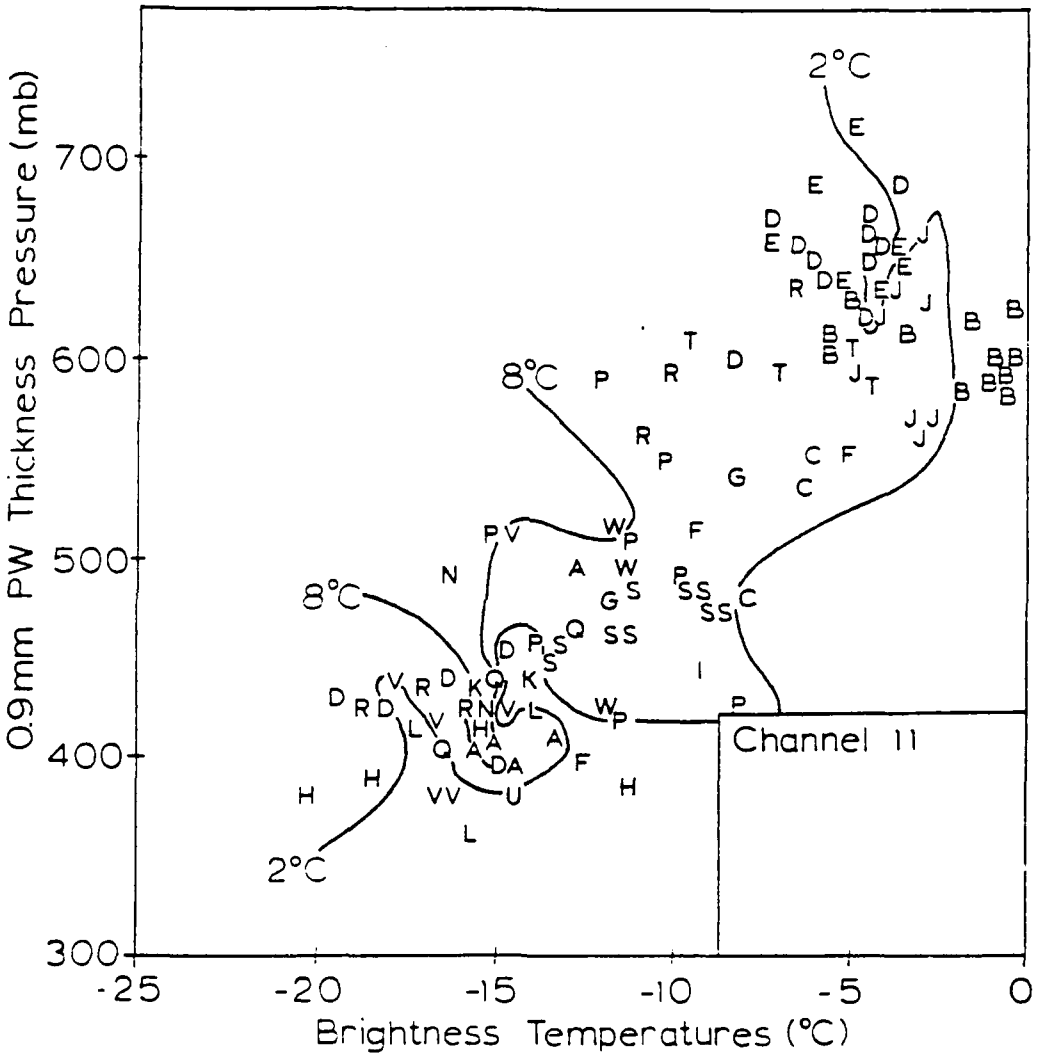

Figure 38. As in Fig. 20b except for overlaid observed-BT/RTM-BT difference contours.

observed BTs and RTM BTs for channel 11 were significantly smaller than those for channel 12. Channel 11 seemed to be much less sensitive to the contaminating influence of upper tropospheric moisture than channel 12. Thus, regardless of the atmospheric profile, channel 11 does not appear to be particularly sensitive to upper tropospheric conditions.

CHAPTER VIII

SUMMARY AND DISCUSSION

Although data were more abundant than normal because of the FGGE SOP 1, reliable satellite and rawinsonde data nonetheless were limited over the eastern Pacific during the 9-day period of interest in the latter half of January, 1979. However, enough information was available for a fairly detailed investigation into the relationship between moisture profiles indirectly obtained from satellite and "ground truth" profiles directly measured by rawinsonde.

Initially, the high correlations obtained between moisture sensitive BTs (derived by satellite) and the upper few tenths of a millimeter of PW (derived by rawinsonde) measured at heights below the 300-mb level implied that the moist layers sensed by satellite were nearly identical to the ones measured by rawinsonde. Thus, it was hypothesized in Chapter V that the WV upper layer (boundary) could be inferred using WV satellite data. However, the large RMS errors obtained when linear and polynomial curves were fitted to the satellite/rawinsonde comparisons suggested a more complex relationship. As shown in Chapter VII, there is significant evidence that minute quantities of upper tropospheric moisture, not detectable by conventional rawinsondes, significantly modulate the radiation signature emanating from lower levels where more abundant moisture at higher temperatures can be measured by rawinsondes. Thus, this upper moisture acts to mask the true moisture profile in the middle and lower troposphere. Channel 11 was less affected by this upper

tropospheric moisture than channel 12; yet, both channels were significantly influenced. Thus, evidence in this study indicates that satellites significantly sense the upper moist layer in the tropical troposphere while, in most situations, rawinsondes do not.

This discrepancy in sensing capability was observed over the vast majority of the eastern Pacific Ocean; therefore, an extensive layer of high tropospheric moisture, possibly concentrated just beneath the tropical tropopause, may be the rule rather than the exception. Indeed, all measurements reported by Kley et al. (1982) indicated saturated conditions in the vicinity of the tropical tropopause. Riehl (1979), Reed and Recker (1971), and Holton (1979) indicated the maximum divergence in tropical convection occurs between 150 and 200 mb. In addition, Reed and Recker (1971) stated that saturation can be achieved over vast areas in the upper tropical troposphere near 175 mb coinciding with the level of maximum divergence from tropical convection.

The concentrated area of very high BTs in the subtropical Pacific (Chapter IV) appears to have been the only region observed during this study where both satellite and rawinsonde consistently and correctly evaluated the top layer of tropospheric moisture actually present. Therefore, through some process, this upper moist layer must have been eliminated. As mentioned in Chapter II, very high channel 12 BTs have been associated with deep tropospheric subsidence; yet, as shown in Chapter IV, these high BTs occurred in the tropical eastern Pacific only in a localized, nearly cloudless region south of Hawaii. From IR satellite pictures, a subsidence-

dominated troposphere is also expected in the cloudless eastern Pacific dry zone to the south of Mexico; however, very few of the high channel 12 BTs were found there, and certainly not the highest. This discrepancy appears to be associated with the presence of upper tropospheric moisture over the eastern Pacific dry zone; whereas, the upper troposphere in the region of high BTs found primarily to the south and southwest of Hawaii appears to be quite dry.

As stated in Chapter II, Ramond et al. (1981) found that very high BTs in METEOSAT WV imagery in the mid-latitudes were associated with tropopause folding where a large amount of stratosphere-troposphere exchange takes place. Palmen and Newton (1969) stated that tropopause folding is associated with the subsidence of stratospheric air into the troposphere. Tropopause folding was implied to be associated with the strong jet located along the northwest flank of developing moisture bursts (Schaefer, 1985; McGuirk et al., 1987). No such folding was likely south of Mexico due to the lack of a significant jet in this region. Furthermore, Stewart and Fuelberg (1986) asserted that satellite-derived ozone concentrations were greatest in the region of a developing jet streak which suggested the downward intrusion of dry stratospheric air into the troposphere.

Thus, analogous to the midlatitude jet streaks, this localized anomalous region of very high BTs in the subtropical Pacific may indicate subsidence of dry stratospheric air into the troposphere. This subsidence would eliminate any layer of upper tropospheric moisture previously existing, therefore allowing the satellite to

sense radiation which has traveled nearly unimpeded from the moist layers in the lower or middle troposphere. In addition, if this subsidence was confined strictly to the troposphere, the necessity of upper-tropospheric convergence over this subsidence also would produce convergence of upper level moisture partially originating from strongly diverging convective tops. Yet, the probable absence of tropopause folding in the region south of Mexico implies that moisture in the upper troposphere (100-300 mb layer) would not be eliminated. Therefore, this upper tropospheric moisture would influence upwelling radiation such that observed BTs would be lower to the south of Mexico than in the region southwest of Hawaii.

The observed closeness of this high BT region to the western flank of a moisture burst, the eastward movement of this BT region as the moisture burst moved eastward, and the areal shrinking of these high BTs concurrent with the weakening of the moisture burst indicate these BTs may be the descending branch of an intense, direct, synoptic-scale circulation. Furthermore, as discussed above, this deep subsidence may originate in the stratosphere and extend into the mid or lower troposphere. More research, including detailed, short-term analyses of stratospheric ozone concentrations over the subtropical Pacific, needs to be performed to investigate this possibility.

The high correlations between rawinsonde PW and satellite BTs (Chapter V) appeared to indicate that the height of the top of the moist layer in the mid or lower troposphere could be estimated strictly from satellite BTs. Thus, using changes in this estimated

height over a 12-h period and neglecting horizontal moisture advection, vertical motion estimates were obtained. The comparison of these BT-derived vertical motion estimates to the adiabatic vertical velocity estimates, OLR satellite signatures, and Snyder's velocity potential fields confirmed that these BT vertical motion estimates where highly inconsistent. Results from Chapters VI and VII indicate that significant errors occurred primarily from BTs which were contaminated to various degrees by upper tropospheric moisture at heights above 300 mb. Other errors occurred from:

1. horizontal advection of mid and/or upper tropospheric moisture; and
2. temporal and spatial collocation error between satellite BTs and rawinsonde or grid point locations.

REFERENCES

Barnes, S.L., 1973: Mesoscale objective map analysis using weighted time-series observations. *Tech. Memo. ERL NSSL-62*, NOAA, U.S. Dept. of Commerce, Washington, DC 20233, 60 pp (NTIS Accession No. COM-7310781).

Chesters, D., L.W. Uccellini, and A. Mostek, 1982: VISSR Atmospheric Sounder (VAS) simulation experiment for a severe storm environment. *Mon. Wea. Rev.*, *110*, 198-216.

Federal Meteorological Handbook No. 3, 2nd Ed., 1981: Radiosonde observations. U.S. Dept. of Commerce, U.S. Dept. of Defense, Washington, DC 20233, 236 pp.

Gerald, C.F., and P.O. Weatley, 1984: *Applied Numerical Analysis*, 3rd Ed. Addison-Wesley Publishing Company, 579 pp (see pp 198-205).

Holton, J.R., 1979: *An Introduction to Dynamic Meteorology*, 2nd Ed. Academic Press, 391 pp (see p 318, 349).

Julian, P.R., 1984: Objective analysis in the tropics: a proposed scheme. *Mon. Wea. Rev.*, *112*, 1752-1767.

Kley, D., A.L. Schmeltekopf, K. Kelly, R.H. Winkler, T.L. Thompson, and M. McFarland, 1982: Transport of water through the tropical tropopause. *Geophys. Res. Lett.*, *9*, 617-620

Lee, T.H., D., Chesters, and A. Mostek, 1983: The impact of conventional surface data upon VAS regression retrievals in the lower troposphere. *J. Climate Appl. Meteor.*, *22*, 1853-1874.

Lin, R.Q., and D.R. Mock, 1986: A test of the ECMWF model in tropical synoptic-scale diagnosis. *Mon. Wea. Rev.*, *114*, 1519-1538.

McGuirk, J.P., A.H. Thompson, and N.R. Smith, 1987: Moisture bursts over the tropical Pacific Ocean. *Mon. Wea. Rev.*, *115*, 787-798.

Palmen, E., and C.W. Newton, 1969: *Atmospheric Circulation Systems*, Academic Press, Inc, 603 pp (see p 257).

Parmenter, F.C., 1972: Comparison of visible, infrared, and moisture channel data. *Mon. Wea. Rev.*, *100*, 318-321.

Petersen, R.A., L.W. Uccellini, A. Mostek, and D.A. Keyser, 1984: Delineating mid- and low-level water vapor patterns in pre-convective environments using VAS moisture channels. *Mon. Wea. Rev.*, *112*, 2178- 2198.

Petterssen, S., 1956: *Weather Analysis and Forecasting, Vol. 1*, 2nd Ed. McGraw-Hill ook Company, Inc, 429 pp (see pp 295-299).

Poc, M.M., M. Roulleau, N.A. Scott, and A. Chedin, 1980: Quantitative studies of Meteosat water-vapor channel data. *J. Appl. Meteor.*, *19*, 868-876.

Ramond, D., H. Corbin, M. Desbois, G. Szejwach, and P. Waldteufel, 1981: The dynamics of polar jet streams as depicted by the Meteosat WV channel radiance field. *Mon. Wea. Rev.*, *109*, 2164-2176.

Reed, R.J., and E.E. Recker, 1971: Structure and properties of synopticscale wave disturbances in the equatorial western Pacific. *J. Atmos. Sci.*, *28*, 1117-1133.

Remsberg, E.E., J.M. Russell III, L.L. Gordley, J.C. Gille, and P.L. Bailey, 1984: Implications of the stratospheric water vapor distribution as determined from the Nimbus 7 LIMS experiment. *J. Atmos. Sci.*, *41*, 2934-2945.

Riehl, H., 1979: *Climate and Weather in the Tropics*. Academic Press, Inc., 611 pp (see p 189).

Rodgers, E.B., V.V. Salmonson, and H.L. Kyle, 1976: Upper tropospheric dynamics as reflected in Nimbus 4 THIR 6.7 μm data. *J. Geophys. Res., 81*, 5749-5758.

Roulleau, M., 1978: *Remote Sensing of the Atmosphere: Inversion Methods and Applications*. Elsevier, 149-159.

Schaefer, J.R., 1985: Observing the synoptic structure of two moisture bursts. Masters Thesis, Texas A&M University, College Station, TX 77843, 145 pp (see pp 38-66).

Shenk, W.E., and E.B. Rodgers, 1978: Nimbus 3/ATS 3 observations of the evolution of Hurricane Camille. *J. Appl. Meteor., 17*, 458-476.

Smith, W.L., 1983: The retrieval of atmospheric profiles from VAS geostationary radiance observations. *J. Atmos. Sci., 40*, 2025-2035.

_____, H.M. Woolf, C.M. Hayden, D.Q. Wark, and L.M. McMillin, 1979: The TIROS-N Operational Vertical Sounder. *Bull. Amer. Meteor. Soc., 60*, 1177-1187.

Snyder, B.A., 1985: The divergent wind component in data sparse tropical wind fields. Masters Thesis, Texas A&M University, College Station TX 77843, 105 pp (see pp 71-78).

Steranka, J., L.J. Allison, and V.V. Salmonson, 1973: Applications of Nimbus-4 THIR 6.7 μm observations to regional and global moisture and wind field analysis. *J. Appl. Meteor., 12*, 386-395.

Stewart, M.R., and H.E. Fuelberg, 1986: Relationships between 6.7 micrometer imagery and radiosonde-derived parameters. *Preprints, Second Conference on Satellite Meteorology/Remote Sensing and Applications*, Amer. Meteor. Soc., Williamsburg, VA, May 13-16, 1986, 67-72.

Stewart, T.R., C.M. Hayden, and W.L. Smith, 1985: A note on water-vapor wind tracking using VAS data on McIDAS. *Bull. Amer. Meteor. Soc., 66*, 1111-1115.

Stout, J., J. Steranka, and R.A. Petersen, 1984: Vertical displacements of the mid-tropospheric water vapor boundary in the tropics derived from the VISSR Atmospheric Sounder (VAS) 6.7 μm channel. *Preprints, Conference on Satellite/Remote Sensing and Applications*, Amer. Meteor. Soc., Clearwater Beach, FL, Jun. 25-29, 1984, 86-89.

Susskind, J., J. Rosenfield, D. Reuter, and M.T. Chahine, 1982: The GLAS physical inversion method for analysis of HIRS2/MSU sounding data. *Tech. Memo. No. 84936*, NASA, Goddard Space Flight Center, Greenbelt, MD 20771.

Timchalk, A., 1986: Satellite derived moisture profiles. *Preprints, Second Conference on Satellite Meteorology/Remote Sensing and Applications*, Amer. Meteor. Soc., Williamsburg, VA, May 13-16, 1986, 64-66.

U.S. Standard Atmosphere Supplements, 1966. ESSA, NASA, USAF, U.S. Government Printing Office, Washington, DC 20402.

Velden C.S., W.L. Smith, and M. Mayfield, 1984: Application of VAS and TOVS to tropical cyclones. *Bull. Amer. Meteor. Soc., 65,* 1059-1067.

VITA

Keith Gordon Blackwell [redacted]

PII Redacted [redacted] to Mr. and Mrs. Gordon E. Blackwell Jr.. He graduated in June 1974 from Murphy High School in Mobile, Alabama. He attended the University of Alabama from August 1974 to May 1975 and Florida State University from June 1975 to May 1977. As an undergraduate, he was employed from June-August 1979 as a student intern at the National Weather Service Forecast Office in Birmingham, Alabama. He graduated in June 1980 from the University of Wisconsin-Madison with a B.S. in Meteorology.

He was employed from June 1980 to July 1981 as an air pollution meteorologist by the Jefferson County Health Department in Birmingham, Alabama. From July 1981 to January 1983 he was employed as an industrial meteorological consultant, weather forecaster, and broadcast meteorologist by Capital Weather Service in Mobile, Alabama. He joined the U.S. Air Force in January 1983 and was commissioned in August 1983. Subsequently, he was stationed at Little Rock Air Force Base, Arkansas as a weather forecaster and staff weather officer.

Then, beginning in August 1985, he was assigned to Texas A&M University under the Air Force Institute of Technology.

The author's permanent mailing address is:

[redacted]